PROPERTIES AND MICROSTRUCTURE OF LIGHT-WEIGHT WOOD-MAGNESIUM OXYCHLORIDE CEMENT COMPOSITES

HE PINGPING

PhD

The Hong Kong Polytechnic University

2020

THE HONG KONG POLYTECHNIC UNIVERSITY
DEPARTMENT OF CIVIL AND ENVIRONMENTAL ENGINEERING

Properties and Microstructure of Light-weight Wood-Magnesium Oxychloride Cement Composites

HE PINGPING

A thesis submitted in partial fulfilment of the requirement for the degree of Doctor of Philosophy

October 2019

CERTIFICATE OF ORIGINALITY

I hereby declare that this thesis is my own work and that, to the best of my knowledge and belief, it reproduces no materials previously published or written, nor material that has been accepted for the award of any other degree or diploma, except where due acknowledgement has been made in the text.

HE Pingping

Abstract of thesis entitled ‘Properties and Microstructure of Light-weight Wood-Magnesium Oxychloride Cement Composites’

Submitted by HE Pingping

for the degree of Doctor of Philosophy

at The Hong Kong Polytechnic University in 2020

ABSTRACT

This work developed a novel way to recycle timber waste in magnesium oxychloride cement (MOC). MOC has many superior properties compared to Ordinary Portland cement (OPC), but it shows poor water resistance due to the decomposition of hydration products (e.g. Phase 3 and Phase 5)

In the first part, CO_2 curing and various supplementary cementitious materials (SCMs) were used to improve the water resistance of MOC paste. The experimental results demonstrated that the water resistance was enhanced when CO_2 curing method was adopted due to the formation of a certain amount of amorphous phase which was stable in water and protect the hydration product from decomposition.

The addition of SCMs, pulverized fuel ash (PFA), glass powder (GP) and incinerated sewage sludge ash (ISSA), could significantly improve the water resistance and volume stability of MOC pastes in water. The active phases in PFA or ISSA could react with MgO and produce an amorphous phase (amorphous magnesium aluminosilicate gel), which was interspersed with Phase 5 and changed the morphology of Phase 5 to fibroid or lath-like phases. These fibroid or lath-like phases interlocked with each other and connected with the amorphous phase in the

matrix to form a stable compact structure.

In the second part, waste timber was added in MOC paste as fibre. The properties and microstructure of wood-MOC board was investigated. It was found that the flexural strength of wood-MOC paste was similar to that of MOC paste after 28 days of water immersion. And wood fibre could enhance the volume stability of MOC paste matrix after 28 days of water immersion due to the high porosity that accommodated the expansion of MOC paste. ATR-FTIR showed new bonding were formed between the wood fibre and the MOC paste matrix. XRD results showed the formation of dashkovaite ($Mg(HCOO)_2 \cdot 2H_2O$), which was in agreement with the ATR-FTIR results. The flexural strength of the wood cement paste increased with the increasing fibre length due to the higher crack bridge function of the longer fibre. And the expansion in air decreased with the increasing fibre length. There is no clear trend about the effect of fibre length on the water resistance of wood-cement paste after 28 days of water immersion. Adding supplementary cementitious materials, especially incineration sewage sludge ash (ISSA), could improve the water resistance and volume stability of the wood-cement paste. In terms of fibre content, the result showed that the wood-MOC composites prepared with a higher content of wood fibre had a lower thermal conductivity, higher flexural strength, higher residual flexural strength after exposure to high temperatures and water immersion, and better noise reduction effect. Even though the water absorption was increased with the increase of wood fibre content, it can still be considered low. The wood - MOC composites incorporating ISSA showed higher flexural strength, better high temperature resistance and better water resistance than other composites. Besides, greenhouse gases (GHGs) emission for the production of different types of composite boards was assessed and compared by using lifecycle assessment (LCA) technique. The ‘cradle-to-gate’ system boundary with 1 kg of board production was considered as the functional unit in this assessment. The results showed that the production of the wood MOC board induces lower GHGs emission than

plywood and lower human toxicity than conventional resin-based particleboards.

PUBLICATIONS ARISING FROM THE THESIS

The thesis is submitted for the degree of Doctor of Philosophy at the Hong Kong Polytechnic University. The work described in this thesis was carried out by the candidate during the years from 2014 to 2019 in the Department of Civil and Environmental Engineering under the supervision of Professor Poon Chi Sun, the chief supervisor, and Prof. Daniel C.W. Tsang, the co-supervisor.

Eight papers were written by the candidate based on the work presented in this thesis.

Academic Journal Papers:

1. **He Pingping**, Poon Chi Sun*, Daniel C.W. Tsang, Effect of pulverized fuel ash and CO_2 curing on the water resistance of magnesium oxychloride cement (MOC). *Cement and Concrete Research*, 2017. **97**: p. 115-122.

2. **He Pingping**, Poon Chi Sun*, Daniel C.W. Tsang, Comparison of glass powder and pulverized fuel ash for improving the water resistance of magnesium oxychloride cement. *Cement and Concrete Composites*, 2017.**86**:p.98-109.

3. **He Pingping**, Poon Chi Sun*, Daniel C.W. Tsang, Using incinerated sewage sludge ash to improve the water resistance of magnesium oxychloride cement (MOC). *Construction and Building Materials*, 2017. **147**: p. 519-524.

4. **He Pingping**, Poon Chi Sun*, Daniel C.W. Tsang, Mechanical, durability and environmental aspects of magnesium oxychloride cement boards incorporating waste wood. *Journal of Cleaner Production*, 2018. **207**: p. 391-399.

5. **He Pingping**, Poon Chi Sun*, Daniel C.W. Tsang, Water resistance of magnesium oxychloride cement wood board with the incorporation of supplementary cementitious materials. *Construction and Building Materials*, 2020. **255**.

6. **He Pingping**, Poon Chi Sun*, Daniel C.W. Tsang, The mechanism of supplementary cementitious materials enhancing the water resistance of magnesium oxychloride cement (MOC): a comparison between pulverized fuel ash and incinerated sewage sludge ash. *Cement and Concrete Composites*, 2020, **109**.

Conference Papers:

7. **He Pingping**, Poon Chi Sun*, Daniel C.W. Tsang, Mechanism of pulverized fuel ash and CO_2 curing to improve the water resistance of magnesium oxychloride cement. *Proceedings of 14th International Conference on Durability of Building Materials and Components*, May 29-31, 2017, Ghent, Belgium.

8. **He Pingping**, Poon Chi Sun*, Daniel C.W. Tsang, Improvement of the water resistance of magnesium oxychloride cement: comparison of PFA and ISSA. *Proceedings of 9th International Symposium on Cement & Concrete,* November 1-3, Wuhan, China.

ACKNOWLEDGEMENT

First, I would like to express my sincere gratitude to my chief supervisor, Prof. Poon Chi Sun, for the continuous support of my PhD study and related research, for his patience, motivation, and immense knowledge. His guidance helped me in all the time of research and writing of this thesis. I could not have imagined having a better advisor and mentor for my PhD study. Besides my chief supervisor, I would like to thank my co-supervisor, Prof. Daniel C.W. Tsang, for his support and valuable advice.

My sincere thanks also go to Prof. Caijun Shi for giving me the opportunity to start my research career and pursue PhD in Hong Kong. Without his precious support it would not be possible to conduct this research.

A very special gratitude goes out to Prof. Ian Richardson of the University of Leeds. It was fantastic to have the opportunity to work on my research in Leeds. What a wonderful and colorful four months!

I am also grateful to the following university staff: Mr. K.H. Wong, Mr. John Chan, Mr.Lai, Y.M., Harry, Mr. C.S..Liu, for their unfailing support and assistance and the Construction Industry Council for funding the PhD research.

I would also like to thank my group members who supported me to strive towards my goal.

And finally, last but by no means least, I would like to thank my family: my parents and my brother. This dissertation would not have been possible without their warm love, continued patience, and endless support.

TABLE OF CONTENTS

LIST OF FIGURES

LIST OF TABLES

LIST OF ABBREVIATIONS

BSE	Back-scattering scanning electron microscopy
CSH	Calcium silicate hydrates
EDX	Energy dispersive X-ray spectroscopy
FA	Fly ash
FTIR	Fourier-transformed infrared spectroscopy
GGBS	Ground granulated blast-furnace
GHGs	Greenhouse gases
GP	Glass powder
ISSA	Incinerated sewage sludge ash
LCA	Lifecycle assessment
MAS-NMR	Magic angle spinning nuclear magnetic resonance
M-A-S-H	Magnesium alumina silicate hydrate
M-A-S-P-H	Magnesium alumina silica phosphate hydroxide
M-S-H	Magnesium silica hydroxide
MKPC	Magnesium potassium phosphate cement
MOC	Magnesium oxychloride cement
MPC	Magnesium phosphate cement

OPC	Ordinary Portland cement
PFA	Pulverized fuel ash
Q-XRD	Quantitative X-ray diffraction
SAED	Selected area electron diffraction
SCMs	Supplementary cementitious materials
SEM	Scanning Electron Microscope
TG	Thermogravimetry
TEM	Transmission electron microscope
TS	Thickness swelling
WA	Water absorption

Chapter 1. Introduction

This chapter will firstly give a brief introduction to the motivation of the current research topic; then the research objectives will be presented; and finally, the layout of the thesis will be outlined.

1.1 Overview

In Hong Kong, the quantity of construction waste being disposed of at landfills in 2017 was 1.49 million tonnes according to the Hong Kong Environment Protection Department (EPD 2017). Among the construction waste, timber wastes from timber formworking is a significant waste type as it cannot be reused in reclamation works or recycled as construction materials and has to be disposed of at municipal solid waste landfills (Poon et al. 2004). According to the EPD, Hong Kong's landfills might be full in recent years, which indicates the importance of reusing the waste construction materials. Therefore, it is necessary to develop green approaches to recycle the waste timber wastes.

The utilisation of timber boards in making cement-bonded construction materials offers an attractive alternative route of recycling(Elinwa and Mahmood 2002, Wang et al. 2017). But the chemical constitutes in wood could react with Portland cement and retard Portland cement hydration(Hachmi and Moslemi 1989, Jorge et al. 2004). The typical cement-hardening inhibitory components can be classified into two groups. One group is comprised of carbohydrates of sucrose in beech and arabinogalactan in larch, and the other are phenolic compounds with a catechol unit of plicatic acid in western red cedar, teracacidin in acacia mangium, and sequirin C in sugi.(Na et al. 2014) When using magnesium oxychloride cement (MOC) composites, on the other hand, there is much lower incompatibility between the chemical contents in wood and the cement matrix(Simatupang and Geimer 1990). Besides, the

MOC cement has a yellowish color which is similar to the color of natural wood. And the MOC cement demonstrates higher fire resistance than Ordinary Portland cement (OPC) (Montle and Mayhan 1974, Li et al. 2003). So MOC cement is more suitable for producing light-weight, high-fire-resistance cement boards than Portland cement.

MOC has many superior properties compared to Portland cement, such as high early strength(Li and Chau 2007, Misra and Mathur 2007), good resistance to abrasion(Ozturk and Timucin 2011), and low thermal conductivity(Yunsong 2001). However, the water resistance of MOC is poor due to the decomposition of the reaction products in water(Lu et al. 1994, Xu et al. 2012). It has been shown that adding fly ash could improve the water resistance of MOC paste, but the mechanism is not clear. It has also been reported that during natural carbonation of MOC, the reaction product Phase 5 ($5MgO\bullet MgCl_2\bullet 8H_2O$) would be transformed into Phase 3 ($3MgO\bullet MgCl_2\bullet 8H_2O$). When Phase 3 is further carbonated, a new phase ($Mg(OH)_2\bullet MgCl_2\bullet 2MgCO_3\bullet 6H_2O$) would be formed (De Castellar et al. 1996, Maravelaki-Kalaitzaki and Moraitou 1999). This new phase is much less soluble in water than either of Phase 5 and Phase 3, which means the carbonation may improve the water resistance of MOC. Carbon dioxide curing of concrete is different from natural carbonation, because the carbonation reaction occurs at an early age and is used to accelerate the strength gain and to reduce the early drying shrinkage of cement products(Berger et al. 1972, Zhan et al. 2014).

Wood fibres offer several potential advantages over other synthetic fibres such as glass fibres and carbon fibres. They are light, sourced from a renewable resource and low cost (Almgren et al. 2009, Yu et al. 2018). However, little previous work has provided insight into the influence of wood fibres on the water resistance of MOC paste.

1.2 Research objectives

This study aims to recycle the waste timber formwork into MOC based material with high

water resistance. The specific objectives of this study are:

- To explore the feasibility of using a CO_2 curing technique for improving the water resistance of MOC paste;
- To investigate the effect of SCMs on the water resistance of MOC paste;
- To understand the mechanism of CO_2 curing and SCMs improving the water resistance of MOC paste;
- To explore the water resistance of wood fibre reinforced MOC boards;
- To investigate the effect of fibre content and fibre length on the properties of wood MOC paste.

1.3 Thesis outline

The flowcharts of the thesis structure and the experimental work are shown in Figure 1-1 and Figure 1-2 respectively.

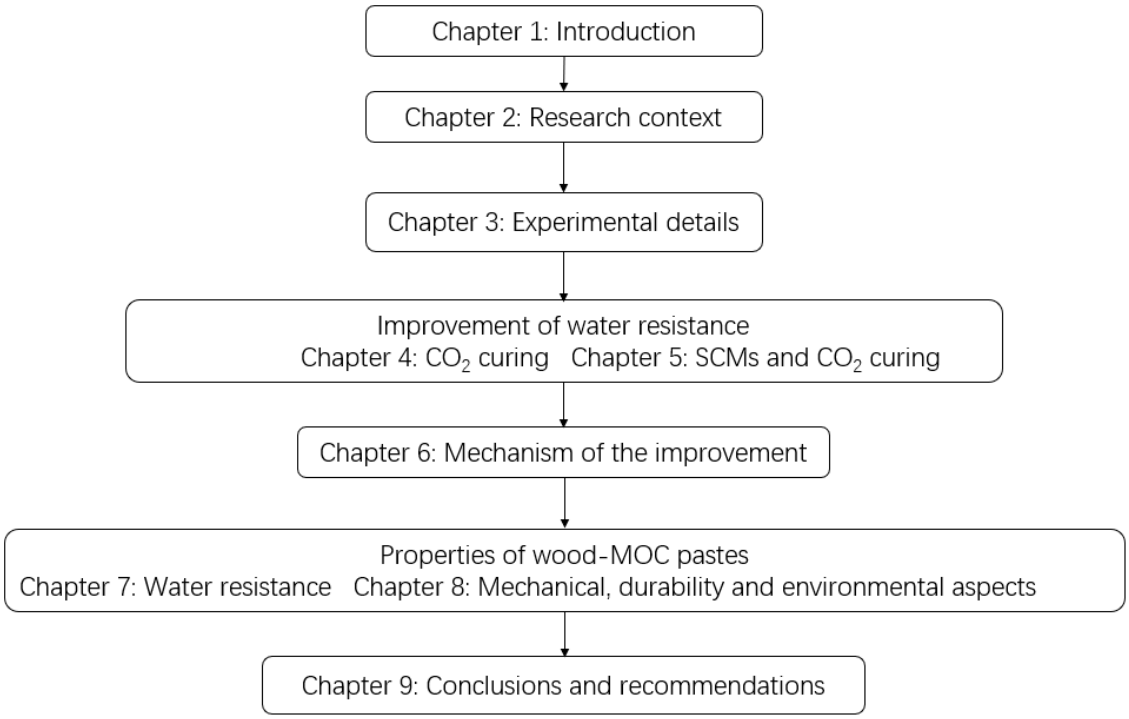

Figure 1-1 Flowchart of the thesis

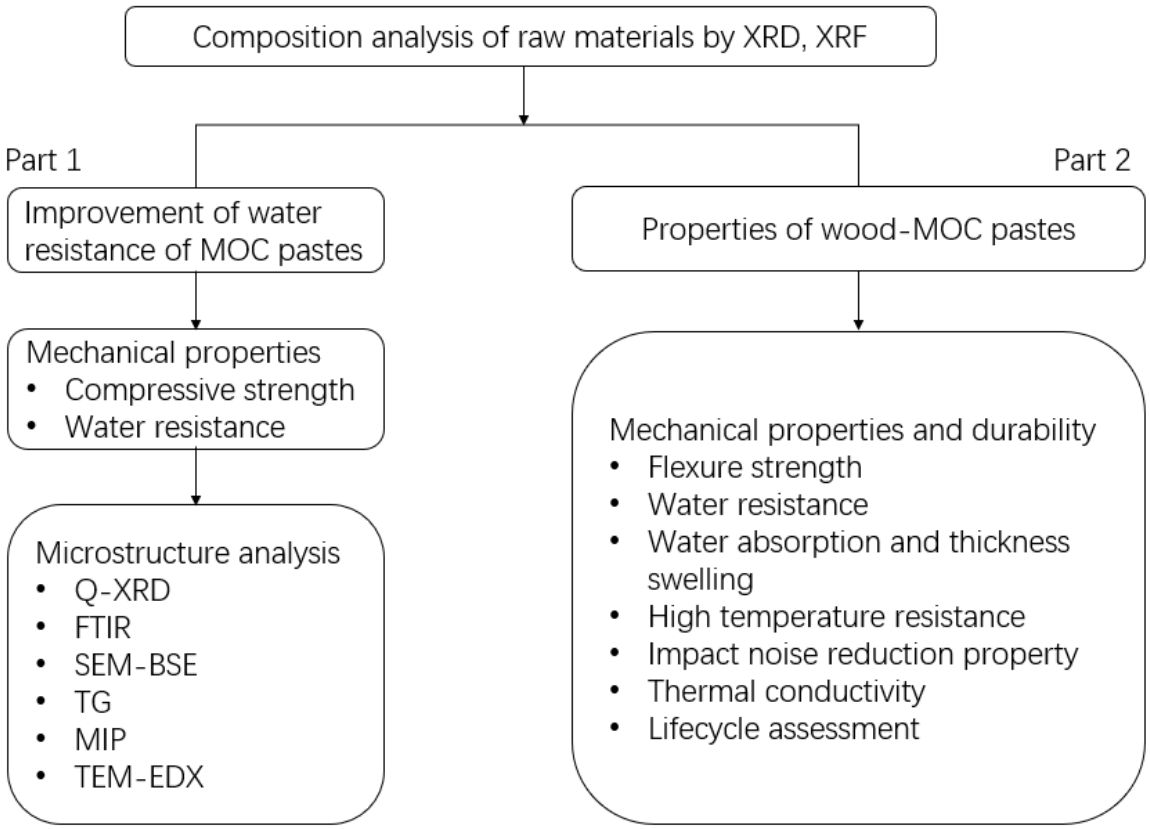

Figure 1-2 Flowchart of the experimental work

The thesis structure is briefly presented below:

Chapter 1 provides an introduction of the proposed research in terms of background and objectives.

Chapter 2 reviews the current situation of recycling wood waste into construction materials and compares the inorganic binder bonded wood composites. Moreover, it compares several common magnesia-based cements and explained why MOC was used to recycle waste timber.

Chapter 3 gives an overall introduction to the common properties of the materials used and experimental methodologies.

Chapter 4 exploits the effect of CO_2 curing on the water resistance of MOC paste and the volume stability of MOC mortar.

Chapter 5 presents the combined influence of PFA, GP, ISSA and CO_2 curing on the water

resistance of MOC paste.

Chapter 6 shows the investigation of mechanism of CO_2 curing and SCMs improving the water resistance of MOC paste via transmission electron microscopy (TEM) techniques.

Chapter 7 presents the water resistance behavior of wood-MOC paste incorporating different lengths of wood fibre.

Chapter 8 shows the effect of wood fibre content on the properties of wood-MOC paste.

Chapter 9 draws the conclusions from the research work. Recommendations for future investigation are provided.

References

Environmental Protection Department (2018). Monitoring of Solid Waste in Hong Kong, Waste Statistics for 2018, available at **https://www.wastereduction.gov.hk/sites/default/files/msw2018.pdf.**

Almgren, K. M., E. K. Gamstedt, P. Nygård, F. Malmberg, J. Lindblad and M. Lindström (2009). Role of fibre–fibre and fibre–matrix adhesion in stress transfer in composites made from resin-impregnated paper sheets. International Journal of Adhesion and Adhesives **29**(5): 551-557.

Berger, R., J. Young and K. Leung (1972). Acceleration of hydration of calcium silicates by carbon dioxide treatment. Nature **240**(97): 16-18.

De Castellar, M., J. Lorente, A. Traveria and J. Tura (1996). Cracks in Sorel's cement polishing bricks as a result of magnesium oxychloride carbonatation. Cement and Concrete Research **26**(8): 1199-1202.

Elinwa, A. U. and Y. A. Mahmood (2002). Ash from timber waste as cement replacement material. Cement and Concrete Composites **24**(2): 219-222.

Hachmi, M. H. and A. Moslemi (1989). Correlation between wood-cement compatibility and wood extractives. Forest products journal (USA).

Jorge, F., C. Pereira and J. Ferreira (2004). Wood-cement composites: a review. Holz als Roh- und Werkstoff **62**(5): 370-377.

Li, G., Y. Yu, J. Li, Y. Wang and H. Liu (2003). Experimental study on urban refuse/magnesium oxychloride cement compound floor tile. Cement and Concrete Research **33**(10): 1663-1668.

Li, Z. and C. Chau (2007). Influence of molar ratios on properties of magnesium oxychloride cement. Cement and Concrete Research **37**(6): 866-870.

Lu, H., P. Wang and N. Jiang (1994). Design of additives for water-resistant magnesium oxychloride cement using pattern recognition. Materials Letters **20**(3): 217-223.

Maravelaki-Kalaitzaki, P. and G. Moraitou (1999). Sorel's cement mortars: Decay susceptibility and effect on Pentelic marble. Cement and Concrete Research **29**(12): 1929-1935.

Misra, A. and R. Mathur (2007). Magnesium oxychloride cement concrete. Bulletin of Materials Science **30**(3): 239-246.

Montle, J. and K. Mayhan (1974). The role of magnesium oxychloride as a fire-resistive material. Fire Technology **10**(3): 201-210.

Na, B., Z. Wang, H. Wang and X. Lu (2014). Wood-cement compatibility review. Wood Research **59**(5): 813-826.

Ozturk, A. and M. Timucin (2011). Silicon carbide particle embedded magnesium oxychloride cement composite bricks for polishing of porcelain stoneware tiles. Advances in Applied Ceramics **110**(7): 400-408.

Poon, C. S., A. T. W. Yu, S. W. Wong and E. Cheung (2004). Management of construction waste in public housing projects in Hong Kong. Construction Management and Economics **22**(7): 675-689.

Simatupang, M. H. and R. L. Geimer (1990). Inorganic binder for wood composites: feasibility and limitations. Proceedings of Wood Adhesive Symposium, Forest Product Resources Society.

Wang, L., S. S. Chen, D. C. Tsang, C.-S. Poon and J.-G. Dai (2017). CO 2 curing and fibre reinforcement for green recycling of contaminated wood into high-performance cement-bonded particleboards. Journal of CO2 Utilization **18**: 107-116.

Xu, K., J. Xi, Y. Guo and S. Dong (2012). Effects of a new modifier on the water-resistance of magnesite cement tiles. Solid State Sciences **14**(1): 10-14.

Yu, K.-Q., J.-T. Yu, J.-G. Dai, Z.-D. Lu and S. P. Shah (2018). Development of ultra-high performance engineered cementitious composites using polyethylene (PE) fibers. Construction and Building Materials **158**: 217-227.

Yunsong, J. (2001). Study of the new type of light magnesium cement foamed material. Materials Letters **50**(1): 28-31.

Zhan, B., C. S. Poon, Q. Liu, S. Kou and C. Shi (2014). Experimental study on CO 2 curing for enhancement of recycled aggregate properties. Construction and Building Materials **67**: 3-7.

Chapter 2. Literature Review

2.1 Introduction

Waste timber is a significant waste type in Hong Kong. Many researchers focused on recycling wood in cement to produce wood cement composite. Wood cement composite has many advantages over conventional wood materials, such as better fire performance, better resistance to bacteria. Besides, it can reuse waste wood and has higher thermal insulation properties and lower density. Normally, it can be incorporated in Ordinary Portland cement (OPC) and magnesia-based cement.

2.2 Recycling of wood in building materials

In recent years, more and more researchers have been working on the utilizing wood for making building materials to enhance the properties of the construction (Karade 2010, Ashori et al. 2012). There are many advantages using wood as composites such as low processing cost, low energy consumption, low density etc. However, increasing demand for wood requires new resources apart from traditional forest to alleviate the rapid decreasing of forest area. As mentioned above, most of the waste timbers are either burnt or landfilled due to most of them have been treated with chemical preservatives containing toxic or polymeric substances which are not easily biodegradable. These disposal methods result in a serious of environmental problems such as emissions of greenhouse gases and occupation of useful land resources. In addition, these approaches are a wastage of natural building materials (Solo - gabriele and Townsend 1999). In view of these environmental concerns, there has been an increasing interest in utilizing waste timber for making low-cost building materials (Soroushian et al. 1994, Franek et al. 2011).

Wood fibre cement composites provide many advantages like lightweight, high tensile strength, high modulus of elasticity, and low thermal conductivity compared to neat cement products. Moreover, they have high resistance to fire and insects compared to traditional particle boards. The bonding between the wood fibre and the matrix includes physical bonds and chemical bonds. Physical bonds are formed during the hydration process when the hydration products formed and interlocked with each other. Chemically, the metal hydroxyl groups in the matrix could react with the carboxylic groups in the wood fibre (Coutts and Kightly 1984). The bonding is formed after three-stage process (Hachmi 1989). The first stage is the formation of chemical bonding corresponds to early wood fibre-cement hydration reactions followed by the combination of physical and chemical bonding when the cement begins to crystallize and form a matrix around the wood. The final stage is further physical bonding which continues for many years. It was found that the hydration products grew into cell lumens and the bond between the wood fiber and cement increased as the cement matrix got stronger (Ahn and Moslemi 1980, Lin et al. 1994). A dense layer consisting a great amount of portlandite calcium hydroxide, calcium silicate hydrate gel (CSH) formed on the surface of the wood fibre. The content of calcium hydroxide decreased with increasing distance from the fibre surface (Coutts 1987). Many parameters affect the strength of the bond between wood fiber and cement matrix, including matrix composition, fiber geometry, and fibre type etc (Bentur and Mindess 2014).

The fibre content affects the flexural strength of wood-cement composites as shown in Figure 2-1(a) (Coutts 1984, Coutts and Warden 1985). The strengthening effect of the fibre is evident and the maximum improvement is achieved when optimum fibre contents is adopted. The decrease of flexural strength at high fibre content can be explained on the basis of inefficient compaction and lower density of the mix as shown in Figure 2-1(b).

In terms of fibre length, the wood fibre-cement composite prepared with the longer had higher flexural strength. This was related to the crack bridging function of wood fibre. Wood-fibre

reinforced composites fail by cracking when loaded in flexure. The short fibre limited the width of crack that can be bridged and would slip from the paste matrix. The wood-cement composites prepared with the shorter fibre and the longer fibre failed by fibre pull-out (Figure 2-2(a)) and fibre fracture (Figure 2-2(b)) respectively (Coutts and Kightly 1982).

Besides, the matrix property is an important key affecting the properties of wood-fibre composites as well. It was found the autoclaved composites had much higher flexural strength than that cured at room temperature (Akers and Studinka 1989). This may be due to the density of the matrix (Bentur and Akers 1989). It was found the transition zone around the fibres in the room temperature cured composites were more open than that in the autoclaved cement composites. Meanwhile, much more fibres in the former composites failed by pull-out than that in the latter composites. Therefore, they concluded that a denser matrix had positive effects on composites properties.

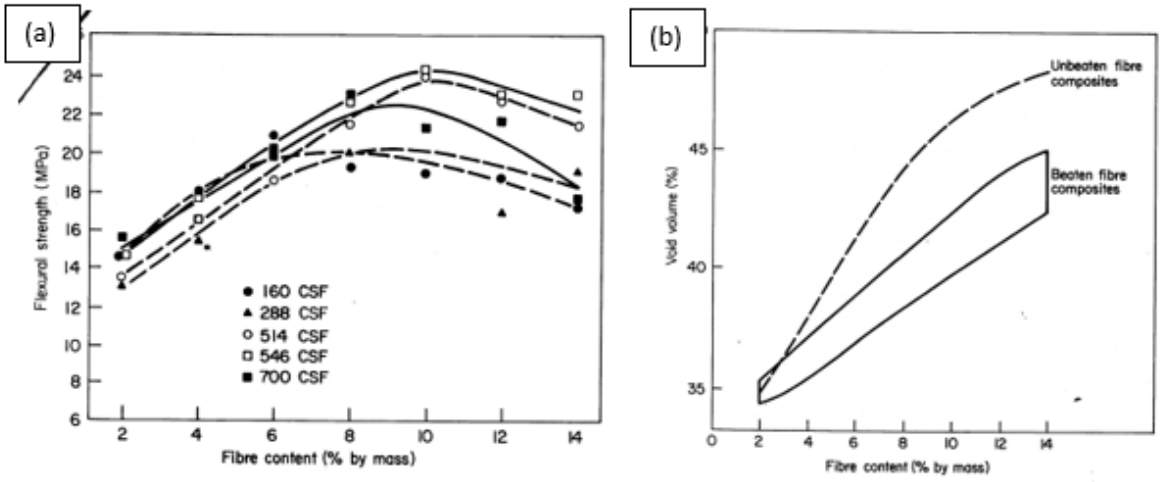

Figure 2-1 Effect of fibre content on (a)flexural strength (b) void volume at various freeness values (Coutts 1984, Coutts and Warden 1985)

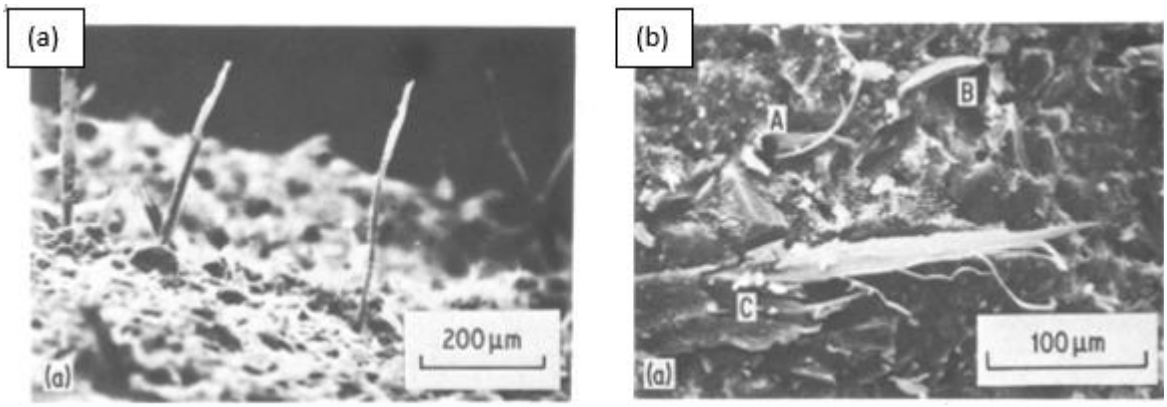

Figure 2-2 Scanning electron microscope (SEM) images of the fracture surface of wood-cement composite (a) pull-out fibres (b) fractured fibres (Coutts and Kightly 1982)

2.3 Comparison of inorganic binder bonded wood composites

Inorganic binders are either gypsum, magnesia cement, Portland cement or a mixture of at least two of these compounds. In this section, the properties and environmental effects of wood-Portland cement and wood-magnesia cement are compared.

2.3.1 Compatibility between inorganic binders and wood

The interaction between the inorganic binders and wood is the key factor determining the mechanical properties of the wood-cement composites. When water and wood are added to cement, hydration reactions occur and the pH of the mixture increases, which facilitates the dissolution of the extractives of certain woods. It was found that the extractives retard the hydration of cements and the inhibiting reaction varies with the type of wood species. The typical cement-hardening inhibitory components can be classified into two groups. One group is comprised of carbohydrates of sucrose in beech and arabinogalactan in larch, and the other are phenolic compounds with a catechol unit of plicatic acid in western red cedar, teracacidin in acacia mangium, and sequirin C in sugi (Na et al. 2014). It was reported that the relative hydration time of wood-Portland cement was much longer than that of wood-magnesia cement for most wood species (Simatupang and Geimer 1990). So MOC could significantly reduce

this problem and be used to produce building components such as windows, door panels and partition walls (Zhou and Li 2012). The addition of chemicals that act as cement curing accelerators like $SnCl_2$, $FeCl_3$ and $AlCl_3$ can also accelerate the hydration reaction of the wood-cement composites(Zhengtian and Moslemi 1985, Lee and Hong 1986).. Therefore, wood-magnesia cement bonded board is easy to be manufactured and requires lower cost and energy.

Shear strength, internal bond strength and bending strength can be used to quantify the compatibility between the cements and wood. The strength and other mechanical properties of the cement composites may decrease after adding wood, but they still may meet requirement of certain structure. Some researchers described the use of waste wood from a mattress manufacturer as an aggregate for lightweight concrete masonry(Stahl et al. 2002). It was noted that despite their relative low strength compared to the requirements of ASTM C90 for loadbearing concrete masonry unit (CMU) , the composites had sufficient strength and moisture cycling to meet the requirements of ASTM C129 for non-loadbearing CMU. Spruce veneer was used to prepare wood-cement pastes and it was found the shear strength of the wood-Portland cement pastes (1.8MPa) is half of that of wood- MOC cement (3.6MPa) (Simatupang and Geimer 1990). So the strength of the wood-MOC composite is higher than the wood-OPC composite though both of them reached only 25 to 30 percent of the strength of the pure binders.

Both the wood/cement ratio and the characteristic of the wood affect the strength and durability of the wood-binder composites(Wolfe and Gjinolli 1999). It was found that a cement excelsior board with cement/wood ratios of 2.0, 2.3, and 2.6 met the requirements of commercial standards. While the bonding strength decrease with the increase of cement/wood ratio (Lee 1985). The results from a cement-bonded composite panel developed to characterize the effect of the cement/wood ratio on the flexural and dimensional stability properties showed that the modulus of rupture increased as the cement/wood ratio declined. However, modulus of

elasticity increased linearly with the rise of cement/wood ratio(Moslemi and Pfister 1987) . Some researchers (Zhou and Kamdem 2002) found that the bending strength of particles from wood treated with chromated copper arsenate increased with the cement/wood ratio , but decreased when the cement/wood ratio was above 3.0. An investigation on wood-MOC and wood-MOP particle boards revealed that the physical and mechanical properties of these two composites were similar and vary directly with the binder/wood ratio. Besides, the bending strength, internal bond, thickness swelling of wood-MOP bonded particleboards decreased gradually with the increase of binder/wood ratio from 1.5 to 4.5(Zhou and Kamdem 2002). Therefore, choosing an optimum binder/wood ratio could meet the requirement of strength and suitability of wood-cements composites. It was reported the binder/wood ratio of cement-bonded particleboards was almost twice of that of magnesia-bonded particleboards to obtain the same bending strength and internal bending, which means that the magnesia-wood composite is more environmentally friendly in view of the higher wood content (Simatupang and Geimer 1990).

2.3.2 Physical properties and durability

The physical properties of wood-magnesia cement board are superior to wood-OPC including: lower density, higher abrasion resistance, lower thermal conductivity(Plekhanova et al. 2007), and better thermal insulation. The density of magnesia cement-bonded particleboard is 20%-30% lower than that of OPC. Thus magnesia cement- bonded products suit to used in light-weight construction(Laufenberg et al. 2004). When testing for abrasion, it was found that the strength loss of MOC concrete was between 0.11-0.20% (Misra and Mathur 2007) , which was much lower than that of OPC concrete(10%) after 100 rotations(Fernando and Said 2011). The higher abrasion resistance of wood-magnesia cement board was due to the superior properties of magnesia cement.

As regards fire-resistance, it was found that the sawdust-MOC cement composites could not sustain a high temperature of 500°C, while partially replacing sawdust by perlite could increase the high-temperature resistant performance of the wood-MOC cement composites(Zhou and Li 2012). The addition of boric acid and borax was attempted to improve the fire resistance of cement-wood composite as borax tends to decrease flame-spread and boric acid can suppress smoldering. Cement-wood pretreated with boric acid and borax mixtures may have excellent fire resistance(LeVan and Winandy 1990, Yalinkilic et al. 1999).

2.3.3 Environmental considerations

The price of MgO is almost twice as that of Portland cement. Therefore, the use of magnesia cement-wood bonded materials faces market resistance because of high raw materials and production costs. However, MOC and magnesium phosphate cement (MPC) set rapidly at ambient temperature, thus leading to less energy consumption than conventional OPC, which requires a humid environment or heating curing. Besides, the production of one ton of Portland cement generates approximately one ton of carbon dioxide, including the decalcination of calcium carbonate (Duxson and Provis 2008). The production of one ton of MgO generates approximately 1.1 ton of carbon dioxide due to the decompose of $MgCO_3$. However, a lower calcination temperature is required when producing MgO, which saves fossil fuels. So, reuse the waste timber into magnesia cement may be a method to decrease energy cost and CO_2 emission.

2.4 Magnesia based cement

OPC is the most widely used cement for construction. About 4 billion tonnes of OPC was produced in 2014 (Walling and Provis 2016). However, more and more researchers have focused on alternatives to OPC due to its large CO_2 emission footprint (Juenger et al. 2011). Magnesia-based cement was one class of materials that has been identified as a potential low-

CO_2 alternative due to the lower production temperature of MgO compared to that of OPC and the ability of MgO to absorb CO_2 from the atmosphere. Magnesia-based cement, by definition, uses MgO as a building block which is generally obtained either by a dry rout from the calcination of mined magnesite deposits ($MgCO_3$) or by a wet rout from solutions of magnesium-bearing brines or seawater. Due to the higher energy requirements for production through the wet route (Walling and Provis 2016, Canterford 1985), the bulk of MgO production worldwide is mainly obtained by calcination of mined magnesite $MgCO_3$ as follows:

$$MgCO_3 \xrightarrow{>600^0C} MgO+CO_2 \quad (2\text{-}1)$$

According to the calcination temperature, the MgO can be defined as light burned MgO (700-1000°C), hard burned MgO (1000-1500°C) , dead burned MgO (1500-2000°C) and fused MgO ($\geqslant$ 2800 °C). The increase of calcination temperature reduces the reactivity of MgO. Magnesium oxide cement, MPC, MOC are widely used magnesia-based cements.

2.4.1 Magnesium oxide cement

Magnesium oxide cement refer to conventional OPC system incorporation fine reactive MgO. Brucite is generated during hydration process and followed by the subsequent carbonation to from hydrated magnesium carbonate as follows:

$$MgO+H_2O \longrightarrow Mg(OH)_2 \quad (2\text{-}2)$$

$$Mg(OH)_2 +CO_2 +2H_2O \longrightarrow MgCO_3 \cdot 3H_2O \quad (2\text{-}3)$$

It is important that the cementitious materials shall not undergo considerable volume change in moisture environment for the long-term stability. Therefore, the use of MgO in PC needs careful attention as it may cause delayed excessive expansion, which was first noted in 1884 in France (Chatterji 1995). Even though small quantities of reactive MgO can be used as

expansive additive in cement binders to compensate slight natural shrinkage of PC during hydration (Du 2005, Jin et al. 2008)or shrinkage in large structural applications due to the cooling after the initial exothermic hydration reaction (Riding et al. 2006), the calcination, fineness and dosage of MgO need to be controlled to avoid long-term dimensional stability issues (Zheng et al. 1991, Mo et al. 2010, Lu et al. 2011).

Some researchers (Vandeperre et al. 2008a, Vandeperre et al. 2008b) studied the hydration and microstructure of cement mixtures of fly ash, MgO and OPC. They found the main hydration products due to the hydration of MgO was mainly brucite and a small quantity of hydrotalcite. There was no unhydrated MgO left after 64 days of curing, therefore there should be no risk for cracking due to late hydration if sufficiently active MgO was used. The compressive strength decreased due to the replacement of OPC by MgO as shown in Figure 2-3(Vandeperre et al. 2008b). Other researchers (Cwirzen and Habermehl-Cwirzen 2012) also found the increase of capillary porosity resulted in the decrease of freeze-thaw resistance, flexural strength and compressive strength when MgO was incorporated in the OPC system.

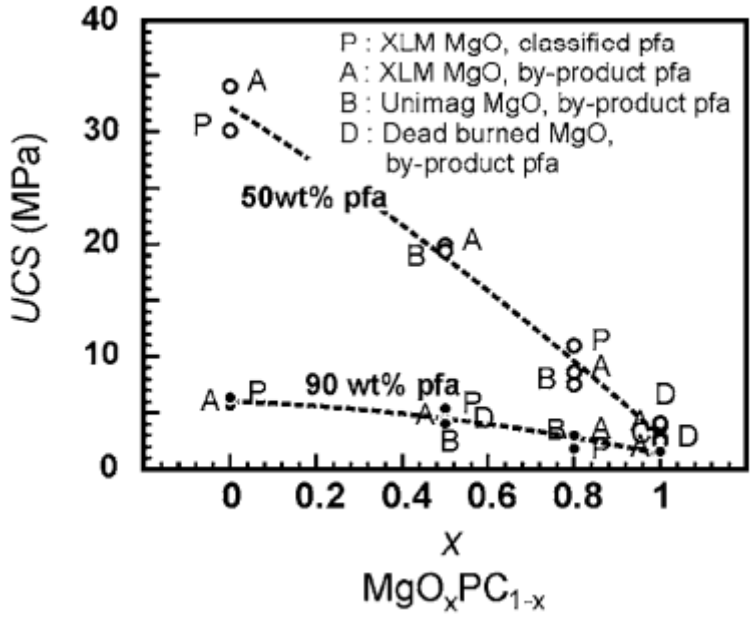

Figure 2-3 Compressive strength of cement paste incorporating MgO as a function of composition of mix (Vandeperre et al. 2008b).

Even though the most thermodynamically stable carbonate for magnesium is the anhydrous form, formation of magnesite at the ambient condition is not common. Instead, formation of hydrated magnesium carbonates (HMCs) prevails as Mg^{2+} ions in the solution are highly hydrated. HCMs are a class of magnesium compounds that form in MgO-CO_2-H_2O systems, including dypingite ($Mg_5(CO_3)_4(OH)_2 \cdot 5H_2O$), hydromagnesite ($Mg_5(CO_3)_4(OH)_2 \cdot 4H_2O$) and nesquehonite ($MgCO_3 \cdot 3H_2O$)(Dong et al. 2019). The formation of different phases of HMCs with different morphologies is influenced by temperature, pH, CO_2 partial pressure and the molar ratio between $Mg(OH)_2$ and CO_2. Some researchers (Vandeperre et al. 2008a) did not found magnesium carbonate in MgO-OPC blended cement after 1 month of conventional curing, indicating these cements do not take up a measurable quantity of CO_2. Recent studies showed that the common product of the carbonation of MgO was nesuehonite with needle-like morphology under ambient conditions(Botha and Strydom 2001, Vandeperre and Al-Tabbaa 2007, Wang et al. 2008, Ferrini et al. 2009). It was found that approximately 11.7-30% CO_2 by

mass of raw mixes was sequestered after 7 days of accelerated carbonation due to the formation of calcium and/or magnesium carbonates as shown below(Mo and Panesar 2013):

$$Ca^{2+}(aq)+CO_3^{2-}(aq) \longrightarrow CaCO_3\ (s) \quad (2\text{-}4)$$

$$Ca^{2+}(aq)+Mg^{2+}(aq)+CO_3^{2-}(aq) \longrightarrow Ca_xMg_{1-x}CO_3(s) \quad (2\text{-}5)$$

$$Mg^{2+}(aq)+CO_3^{2-}(aq)+H_2O(aq) \longrightarrow MgCO_3 \cdot 3H_2O(s) \quad (2\text{-}6)$$

They suggested the enhancement of microstructure and compressive strength of accelerated carbonation product compared to the atmosphere cured sample was due to the intergrowth of round-shaped magnesium calcite ($CaMg(CO_3)_2$) and agglomeration of carbonates as shown in Figure 2-4.

Some researchers focused on the thermodynamic stability of nesquehonite ($MgCO_3 \cdot 3H_2O$), which is the main hydrous magnesium carbonate phase in reactive MgO cements. It was reported that it was stable up to around 100℃ (Ferrini et al. 2009, Ballirano et al. 2010), while others stated that it is a metastable phase(Swanson et al. 2014). Recent research highlighted the effect of analytical conditions on the dehydration of $MgCO_3 \cdot 3H_2O$. It was found that dehydration began at around 55 °C under an atmosphere of flowing nitrogen (Hales et al. 2008), whereas decomposition in water occurred at around 50°C (Dong et al. 2008) . Hydromagnesite ($Mg_5(CO_3)4(OH)_2 \cdot 4H_2O$) was more stable than nesquehonite under conditions of $PCO_2 \leq 1$ atm (Königsberger et al. 1999). The pH could also affect the morphologies of HMCs. It was found the needle-like nesquehonite was replaced by hydromagnesite with sheet-like morphology as the reaction temperature and pH values increased (Zhang et al. 2006). Therefore, more attention should be paid on the dehydration or phase conversion of nesquehonite in application of MgO cement, which may weaken the structure.

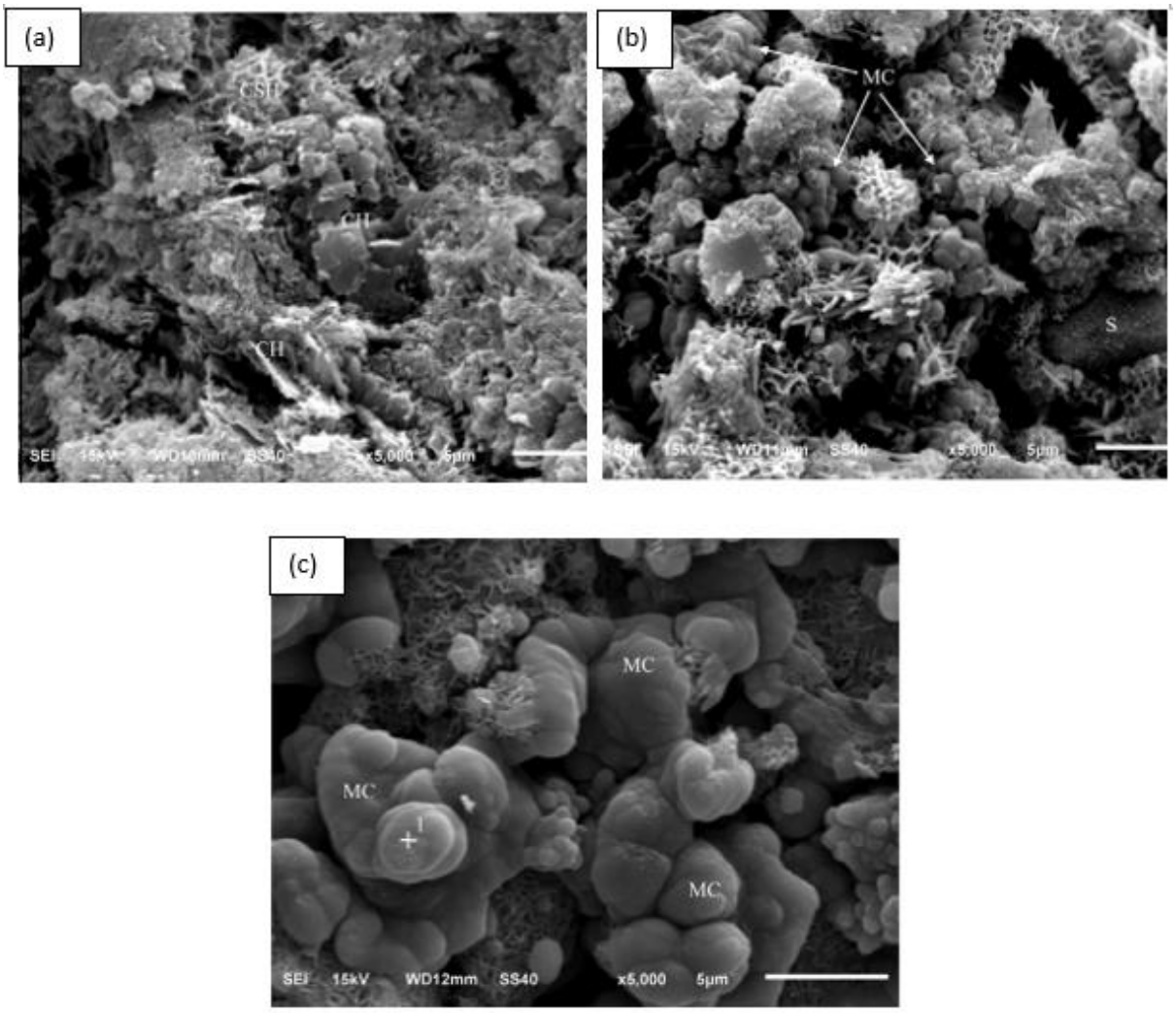

Figure 2-4 SEM images of OPC-ground granulated blast-furnace (GGBS) based cement incorporating 0%, 20% and 40% of active MgO as cement replacement by weight (CH: portlandite, CSH: calcium silicate hydrate, MC: magnesium calcite, S: GGBS) (Mo and Panesar 2013)

2.4.2 Magnesium phosphate cement

Magnesium phosphate cements are formed based on aqueous reaction between MgO and a soluble acid phosphate like phosphoric acid, monoammonium dihydrogen phosphate or diammonium phosphate. It was accepted that the main hydration product was struvite ($NH_4MgPO_4 \cdot 6H_2O$) as follows:

$$MgO + NH_4H_2PO_4 + 5H_2O \longrightarrow NH_4MgPO_4 \cdot 6H_2O \quad (2\text{-}7)$$

These cements were firstly used as dental cements from the late 19th century (Servais and Cartz 1971, Wilson et al. 1979, Oilo 1991). However, it sets too rapidly to be used in construction. The use of dead-burned MgO, which has a lower reactivity than light-burned MgO, has provided the possibility for the production of MPC cement for construction purposes. This cement has been used as repair materials since early 1970s as it produces high early strength, low permeability and good durability under ambient temperature (Seehra et al. 1993, Yang et al. 2002). It was revealed that highway or airfield pavement repaired by using MPC could be open to traffic within a few hours.

Traditional MPC used ammonium phosphate as the reactant. However, the release of unavoidable by-product, ammonium gas limits the application of this cement. Recently, researchers attempted to use monopotassium phosphate as the replacement of ammonium phosphate to form magnesium potassium phosphate cement (MKPC) as shown below (Wagh et al. 1999, Lide 2007):

$$MgO + KH_2PO_4 + 5H_2O \longrightarrow MgKPO_4 \cdot 6H_2O \quad (2\text{-}8)$$

Many methods have been used to retard the reaction rate of MPC. Sodium tripolyphospate ($Na_5P_3O_{10}$) was an early retarder used in MPC and the setting time increased from 4-7 min to 15 min (Abdelrazig et al. 1988, Hall et al. 2001). However, the limited solubility of $Na_5P_3O_{10}$ restricted its application. Borates have been generally used as retarders in recent years. The widely used retarders include $Na_2B_4O_7 \cdot 10\ H_2O$ and H_3BO_3, which show higher effectiveness compared to $Na_5P_3O_{10}$. The setting time of MPC incorporating borates could be up to 30 min, which meets the requirement of commercial applications (Seehra et al. 1993). The retarding mechanism of borates in MPC is currently unclear. It was suggested that the Mg^{2+} ions were chelated by $B_4O_7^{2-}$ ions, forming a colloidal precipitate around MgO grains, thus reducing further dissolution of MgO as shown below (Sugama and Kukacka 1983, Arora 2005):

$Mg^{2+}(aq) + B_4O_7^{2-}(aq) \longrightarrow MgB_4O_7(s)$ (2-9)

However, Other researchers argued that $B_4O_7^{2-}$ was unlikely to form in this system. They suggested that $B(OH)_3$ or $B(OH)_4^-$ reduced the dissolution of MgO grains (Hall et al. 2001). Even though borates are the widely used retarder, more attention is required due to its reproductive toxicity.

2.4.3 Magnesium oxysulfate cement

Magnesium oxysulfate cement (MOS), which is obtained by mixing a light-burnt magnesium oxide with magnesium sulfate solution, has many excellent engineering properties such as good fire resistance, rapid hardening, low thermal conductivity, good abrasion resistance and low metal corrosion potential. It can be used to produce wood wool boards and fire protection materials(Shand 2020). In general, four primary hydration products are possible generated when the temperature was between 30°C to 120°C (Wu et al. 2018): 513 phase ($5Mg(OH)_2 \bullet MgSO_4 \bullet 3H_2O$), 318 phase ($3Mg(OH)_2 \bullet MgSO_4 \bullet 8H_2O$), 123 phase ($Mg(OH)_2 \bullet 2MgSO_4 \bullet 3H_2O$), and 115 phase ($Mg(OH)_2 \bullet MgSO_4 \bullet 5H_2O$). 513 phase and 318 phase are generally formed in MOS cement. 513 phase phase showed needle-like morphology and had higher strength compared to the 318 phase which showed flaky like morphology (Shand 2020).

MOS cement had poor water resistance as the contact of this cement with water results in the breakdown of the hydration products into magnesium hydroxide. Numerous studies focused on improving the water resistance of MOS cement. The incorporation of phosphoric acid and potassium phosphates could improve the water resistance of MOS cement as a new phase was formed, $5Mg(OH)_2 \bullet MgSO_4 \bullet 7H_2O$(517 phase) which had low solubility in water (Wu et al. 2015). The addition of citric acid, boric acid and trisodium citrate could also improve the water resistance of MOS cement due to the formation of 517 phase (Qin et al. 2018).

2.4.4 Magnesium oxychloride cement

2.4.4.1 Phase composition

Discovered in a 1866 patent (Sorel 1866), MOC was described as a production generated from the reaction between MgO and magnesium chloride solution. When MgO is dissolved in an aqueous solution of $MgCl_2$, basic magnesium chloride salts precipitate, which can be expressed as $xMg(OH)_2 \cdot yMgCl_2 \cdot zH_2O$ or $xMgO \cdot yMgCl_2 \cdot (z+x)H_2O$(Walling and Provis 2016).

The composition of magnesium oxychloride has been a subject of a number of study began with the study of Bender, who prepared magnesium oxychloride by using magnesia and magnesium chloride solution and found the composition was $5MgO \cdot MgCl_2 \cdot 17H_2O$ (i.e. Phase 5) (Bender 1871). Some researchers doubted the result of Bender in consideration of carbon dioxide in air and found the product of reaction between magnesium oxide and magnesium chloride solution was $10MgO \cdot MgCl_2 \cdot 14H_2O$(Krause 1873). But this result was not accurate as the crystals decomposed when washed with water. In 1909, it was found the composition of the basic magnesium chloride cement was $3MgO \cdot MgCl_2 \cdot 10H_2O$ (i.e. Phase 3) (Robinson and Waggaman 1909). After that, $3MgO \cdot MgCl_2 \cdot xH_2O$ and $5MgO \cdot MgCl_2 \cdot xH_2O$ were accepted to be the main hydration products in basic magnesium chloride cement (Lukens 1932), but the amount of combined water was not a constant as the products were prepared in water. An agreement was subsequently reached that $3MgO \cdot MgCl_2 \cdot 8H_2O$ (Phase3) and $5MgO \cdot MgCl_2 \cdot 8H_2O$ (Phase 5) were the main hydration products in MOC paste (Matković et al. 1977).

Apart from phase 3 and phase 5, phase 2 ($2MgO \cdot MgCl_2 \cdot 4H_2O$, $2MgO \cdot MgCl_2 \cdot 2H_2O$) and phase 9 ($9MgO \cdot MgCl_2 \cdot 4H_2O$) were observed during the hydration process of MOC pastes. The formation of phase 2 and phase 5 was found at high temperature when the hardening of MOC paste released a great amount of heat (Newman et al. 1952, Demediuk et al. 1955). But

these phases are metastable and transformed to phase 3 after cooling down to room temperature according to the following equations (Dinnebier et al. 2010):

$$3MgO+MgCl_2+11H_2O \rightarrow 1/3[9Mg(OH)_2 \bullet \ MgCl_2 \ \bullet 4H_2O]+2/3MgCl_2+20/3H_2O \rightarrow 3Mg(OH)_2 \bullet MgCl_2 \bullet 8H_2O \quad (2\text{-}10)$$

Limited study have been focused on the formation mechanism of hydration products in MOC paste (i.e. Phase 3 and Phase 5). Some researchers reported it involved gel formation and crystallization (Robinson and Waggaman 1909). It was found that the formation of phase 3 and phase 5 occur though $[HO\text{-}Mg\text{-}O]^-$, $[Mg(H_2O)_{6-X} \bullet OH]^+$, OH^-, Cl^-, H^+, and $[MgOH]^+$, etc. (Ved et al. 1976). By comparing the system of $MgO\text{-}MgCl_2\text{-}H_2O$ and $NaOH\text{-}MgCl_2\text{-}H_2O$, some researchers proposed that phase 3 and phase 5 were formed through Mg^{2+}, OH^-, and Cl^- ions instead complicated ions (Bilinski et al. 1984). However, other researchers concluded there were three steps for the formation of phase 3 and phase 5: neutralizing-hydrolyzing-crystallizing. The first step is the neutralizing of MgO by the free H^+ formed in $MgCl_2$ solution. The second step is the hydrolysing-bridging reaction of Mg^{2+} ions and the production of some polynuclear complexes $[Mg_x\text{-}(OH)_y(H_2O)_z]^{2x-y}$. Then these complexes and Cl^- ions, H_2O condensed to form amorphous phase followed by the crystallization process (Dehua and Chuanmei 1999).

Phase 3, phase 5, phase 2 and phase 9 present similar needle like morphology as shown in Figure 2-5. It was believed that the obtain of high strength of MOC paste was due to the bonding of these strong needle like crystals, with additional bonding derived from the interpenetration of crystals together with enhanced growth where they touch each other (Tooper and Cartz 1966). However, some researchers argued that well developed needles formed in regions of high porosity which did not contribute to strength development(Matković et al. 1977). Once the free space between MgO grains were filled with crystals, the crystals

intergrowth into a denser structure which contributed to strength (Chau and Li 2008). The crystal structure of phase 3 and phase 5 was found from high-quality laboratory powder diffraction data (Sugimoto et al. 2007). Later, the crystal structure of phase 9 was derived as shown in Figure 2-6. The crystal structure of the phase 3, double chains of $Mg(OH)_4(OH_2)$ octahedra run along the b-axis, parallel to alternately ordered chains of intercalating chlorine atoms and water molecules. In the crystal structure of phase 5, triple chains of MgO_6 octahedra run along b axis, intercalating disordered chlorine ions and water molecules. The structure of phase 9 consists of infinite triple chains of the MgO_6 octahedra linked by double chains of the MgO_6 octahedra (Dinnebier et al. 2010).

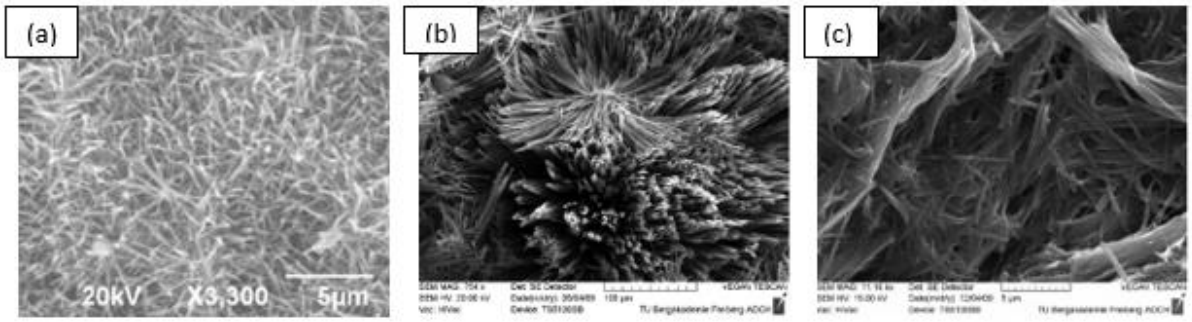

Figure 2-5 SEM pictures of the hydration products in MOC paste, (a) phase 5 (b) phase 2 (Dinnebier et al. 2012) (c) phase 9 (Dinnebier et al. 2010)

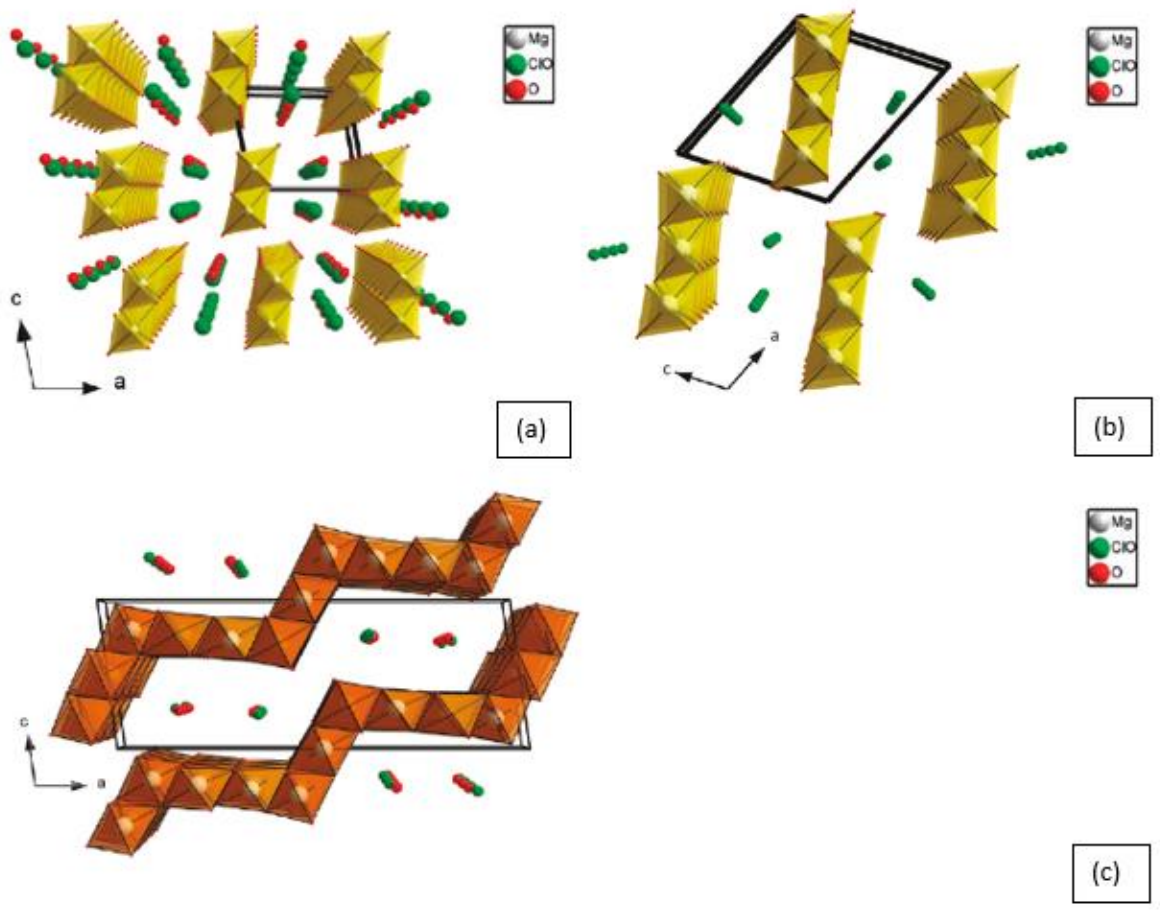

Figure 2-6 Packing diagram of (a) phase 3 (b) phase 5 (c) phase 9 in perspective views along the b-axis (Dinnebier et al. 2010)

The activity of MgO affects the hydration rate and products in system MgO-$MgCl_2$-H_2O at room temperature. By using MgO with different activity and $MgCl_2$ solutions with different concentration, a phase diagram was developed to show the hydration products under different conditions in MOC paste (Figure 2-7) (Sorre and Armstrong 1976). It was suggested that if a 5-1-8 bulk composition (i.e. the molar ratio of MgO:$MgCl_2$:H_2O was 5:1:8) was prepared in a closed container, the product would be phase 5 theoretically. However, the water could be evaporated from an open container, thus the hydration products formed were dependent on the

reactivity of MgO. The MgO calcined under lower temperature presents a higher reactivity and dissolves in water rapidly, which will not affect the evaporation of water and the hydration products. On the contrary, a MgO calcined under higher temperature presents lower reactivity, allowing water to evaporate over a longer period. The products would be phase 3 rather than phase 5. Some researchers investigated the effect of calcination temperature of MgO on the MOC paste and found the calcination temperature influenced the reaction rate and the reaction products. They found the major product was phase 3 instead of phase 5 in a 5-1-8 bulk composition when using very active MgO(calcination temperature was below 700 ℃), which showed divergence with the phase diagram in Figure 2-7. They thought MgO dissolved in water rapidly and $Mg(OH)_2$ was generated. The reaction products of $Mg(OH)_2$ and $MgCl_2$ was phase 3. Later, a new phase diagram (Figure 2-8) was established taking into account of equilibria as the diagram in Figure 2-7 only presented the system with rich MgO and excluded the system rich in $MgCl_2$ and H_2O.

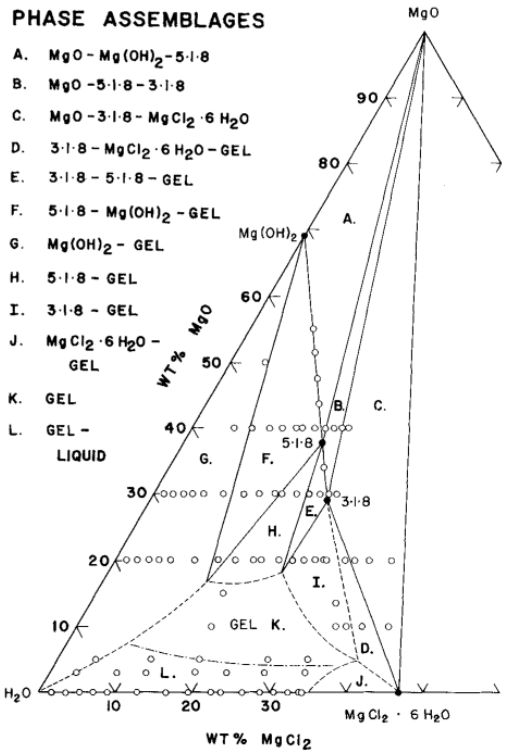

Figure 2-7 Phase diagram in system MgO-$MgCl_2$-H_2O at room temperature. Points indicate compositions prepared; dot-dash line shows approximate limits of homogeneous gel formation. (Matković et al. 1977)

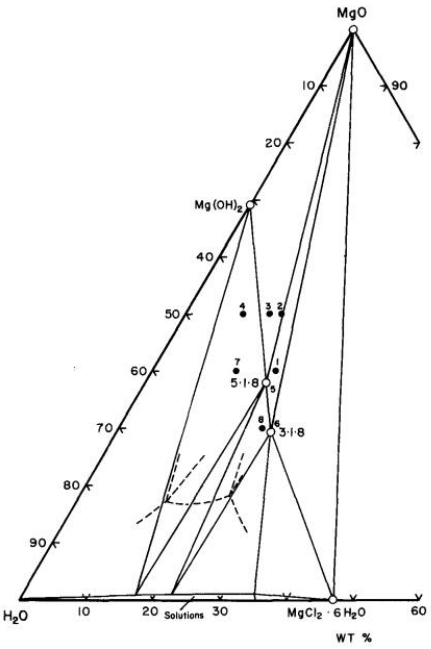

Figure 2-8 Isothermal section in system MgO-$MgCl_2$-H_2O at room temperature. Dashed lines indicate phase boundaries proposed in Figure 2-7. (Urwongse and Sorrell 1980)

Apart from the reactivity of MgO, the molar ratio between raw materials influences the formation of hydration products of the MOC paste as well. Most researchers only investigated the 3-1-8 and 5-1-8 bulk composition or the weight ratio between raw materials. In 2007, some researchers conducted an experiment to investigate the hydration product in the system with different molar ratios of MgO/$MgCl_2$ and H_2O/$MgCl_2$ (Li and Chau 2007). They found the molar ratio between MgO/$MgCl_2$ was critical and the adoption choice of molar ratio between H_2O/$MgCl_2$ was dependent on workability. To obtain more phase 5 which provides the best mechanical properties, the molar ratios of MgO/$MgCl_2$ of 11-17 and H_2O/$MgCl_2$ of 12-18 are found to be optimal.

2.4.4.2 Properties of MOC based materials

MOC is a special cement with a lower carbon footprint compared with OPC. Most commercially available MgO is produced through the calcination of magnesite (Eq 2-11). The

calcination temperature is lower than that of $CaCO_3$ (Eq 2-12) and the temperature to convert limestone and silica to the tricalcium silicate (Eq 2-13) for the production of OPC. Besides, humidity curing is necessary for the hydration of OPC based materials, while the MOC based composites only air curing is required. Therefore, MOC is considered as an environmentally friendly cement.

$$MgCO_3 \xrightarrow[\sim 900^0\,C]{>600\text{-}1000\,^0\,C} MgO + CO_2 \quad (2\text{-}11)$$

$$CaCO_3 \xrightarrow[\sim 1450^0\,C]{} CaO + CO_2 \quad (2\text{-}12)$$

$$3CaO + SiO_2 \longrightarrow CaSiO_5 \quad (2\text{-}13)$$

MOC shows much higher compressive strength compared to OPC. It was found the MOC concrete exhibited approximately 2.5 times the compressive strength of Portland cement concrete(Biel and Lee 1996). The molar ratio of raw materials significantly influences the development of compressive strength (Figure 2-9) and the strength of the MOC paste sample (40*40*40mm) was around 150MPa after 7 days of air curing when the molar ratio of $MgO/MgCl_2$ was 13 and $H_2O/MgCl_2$ was 12(Li and Chau 2007). Apart from the mix proportion of the raw materials, the activity of MgO affect the compressive strength of MOC paste as well as shown in Figure 2-10. Cement paste prepared with the most reactive MgO (batch A) had a higher strength development rate (Chau and Li 2008).

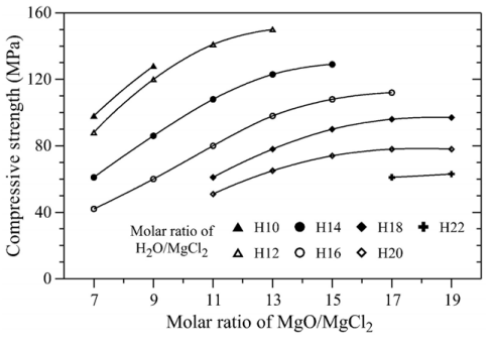

Figure 2-9 Compressive strength of MOC paste with different molar ratio of raw materials after 7 days of air curing (Li and Chau 2007)

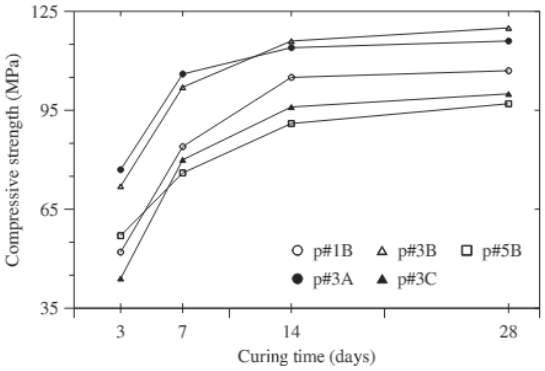

Figure 2-10 Strength development of MOC paste. (The activity of MgO is A>B>C) (Chau and Li 2008)

MOC could be used as grinding wheel due to the high abrasion resistance. It was found the abrasion of MOC concrete was around 2% (Misra and Mathur 2007), which indicated the high resistant towards abrasion. Besides, MOC has been used as fire-resistant material, which is due to the presence of a large amount of crystalline water in MOC requiring a large amount of energy to liberate, and the ability of MgO to effectively reflect heat (Montle and Mayhan 1974). Phase 3 and Phase 5 lose crystalline water and consume a large amount of heat when exposed to high temperature as shown in Eq 2-14 to 2-18 and Eq 2-19 to 2-23 respectively (Xia et al. 1991) and the TG curves of MOC paste as compared to an epoxy resin are shown in Figure 2-11(Qin et al. 2009):

$$3Mg(OH)_2 \cdot MgCl_2 \cdot 8H_2O \xrightarrow{75\text{-}120\ ^0C} 3Mg(OH)_2 \cdot MgCl_2 \cdot 6H_2O + 2H_2O \quad (2\text{-}14)$$

$$3Mg(OH)_2 \cdot MgCl_2 \cdot 6H_2O \xrightarrow{120\text{-}160\ ^0C} 3Mg(OH)_2 \cdot MgCl_2 \cdot 4H_2O + 2H_2O \quad (2\text{-}15)$$

$$3Mg(OH)_2 \cdot MgCl_2 \cdot 4H_2O \xrightarrow{180\text{-}230\ ^0C} 3Mg(OH)_2 \cdot MgCl_2 + 4H_2O \quad (2\text{-}16)$$

$$3Mg(OH)_2 \cdot MgCl_2 \xrightarrow{300\text{-}400\ ^0C} MgCl_2 \cdot H_2O + 2H_2O + 3MgO \quad (2\text{-}17)$$

$$MgCl_2 \cdot H_2O \xrightarrow{400\text{-}600\ ^0C} MgO + 2HCl \quad (2\text{-}18)$$

$$5Mg(OH)_2 \cdot MgCl_2 \cdot 8H_2O \xrightarrow{72\ ^0C} 5Mg(OH)_2 \cdot MgCl_2 \cdot 6H_2O + 2H_2O \quad (2\text{-}19)$$

$$5Mg(OH)_2 \cdot MgCl_2 \cdot 6H_2O \xrightarrow{72\text{-}130\ ^0C} Mg(OH)_2 \cdot MgCl_2 \cdot 4H_2O + 2H_2O \quad (2\text{-}20)$$

$$5Mg(OH)_2 \cdot MgCl_2 \cdot 4H_2O \xrightarrow{140\text{-}200\ ^0C} 5Mg(OH)_2 \cdot MgCl_2 + 4H_2O \quad (2\text{-}21)$$

$$5Mg(OH)_2 \cdot MgCl_2 \xrightarrow{300\text{-}350\ ^0C} MgCl_2 \cdot H_2O + 4H_2O + 5MgO \quad (2\text{-}22)$$

$$MgCl_2 \cdot H_2O \xrightarrow{350\text{-}500\ ^0C} MgO + 2HCl \quad (2\text{-}23)$$

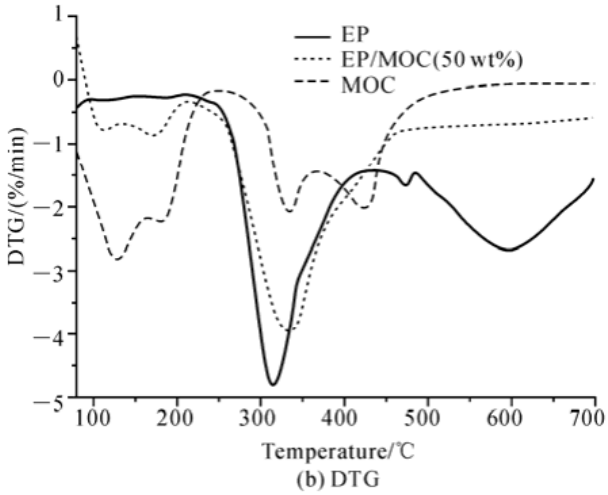

Figure 2-11 TG curves of MOC, EP(epoxy resin) and EP/MOC (50% wt %) (Qin et al. 2009)

As mentioned above, the main hydration products in MOC paste are phase 3 and phase 5. However, phase 5 can be transformed to phase 3, and the cholocarbonate ($Mg(OH)_2$ •$MgCl_2$ •$2MgCO_3$ •$6H_2O$) are formed due to the reaction of phase 3 and carbon dioxide in ambient air as shown in Eq. 2-24 (De Castellar et al. 1996):

$$3Mg(OH)_2 \cdot MgCl_2 \cdot 5H_2O + 2CO_2 \rightarrow Mg(OH)_2 \cdot 2MgCO_3 \cdot MgCl_2 \cdot 6H_2O + H_2O \quad (2\text{-}24)$$

Cholocarbonate can be formed easily at humidity greater than 60%, so it is abundantly present in MOC specimens placed outdoors (Ball 1977). Some researchers stated that the solubility of cholocarbonate was lower than that of phase 3 and phase 5 and a protecting coating was formed on the surface of MOC specimens (Demediuk et al. 1955). However, the carbonation of phase 3 lead to expansion of the specimens and induce cracking , which can cause significant damages as shown in Figure 2-12 (De Castellar et al. 1996, Maravelaki-Kalaitzaki and Moraitou 1999). So the carbonation of MOC could cause compositional gradients to specimens and disruptive effects in adjacent structures.

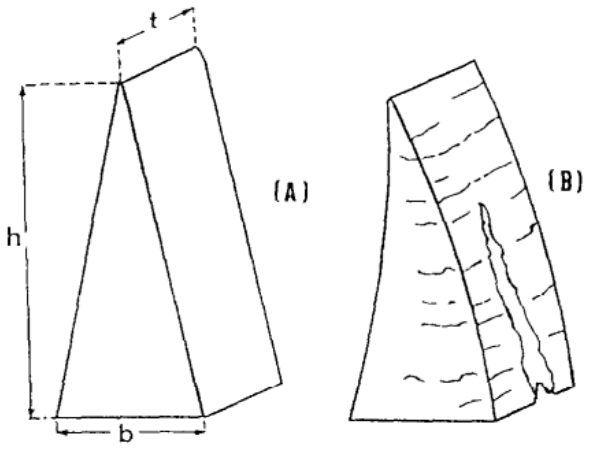

Figure 2-12 (A)Shape of a polishing brick (B)shape of brick after five months (De Castellar et al. 1996)

2.4.4.3 Water resistance

Despite the generally advantages of MOC over OPC mentioned above, the employment of MOC based products has been limited due to its poor water resistance. The hydration products

(i.e. phase 3 and phase 5) are not stable in water and decompose to $Mg(OH)_2$. A solubility model of brucite, phase 3 and phase 5 was as shown in Figure 2-13. It was reported that phase 3 is not stable in solution with m_{Mg}<2.25 mol •kg^{-1} and phase 5 is not stable in solution with m_{Mg}<1.47 mol •kg^{-1}(Zhou et al. 2015).

.

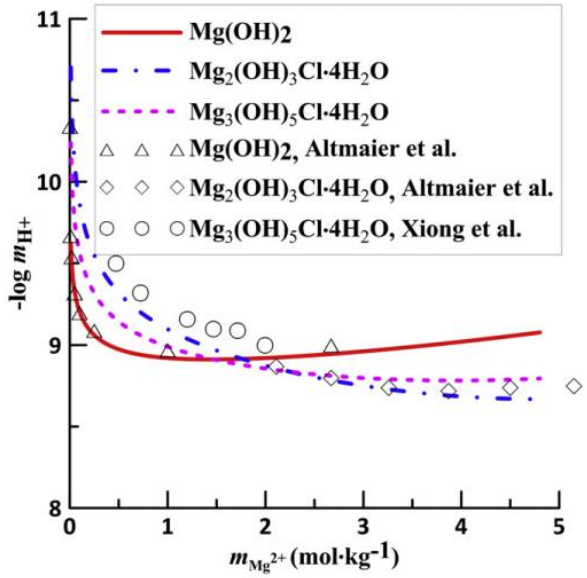

Figure 2-13 Solubility of phase 3 and phase 5 in Mg-Cl binary system at T=25° C, P=0.1MPa (Zhou et al. 2015)

Most researchers used strength retention coefficient (R) to evaluate the water resistance of MOC paste as followed:

$$R=Sx/Sy \quad (2\text{-}25)$$

Where Sx is the residual compressive strength of the sample after soaked in water for a period of time, and Sy is the strength of sample cured in air (Chau et al. 2009).

For neat MOC paste, the strength retention coefficient was only 10% after immersion in water for 28 days due to the decomposition of the hydration products (Deng 2003). There is no phase

3 or phase 5 and brucite is the only phase observed in XRD curve of MOC paste after 28 days of water immersion (Deng 2003).

A promising method to improve the water resistance of MOC is the addition of small amounts of additives (Lu et al. 1994). It was found small quantities of phosphate could significantly improve the water resistance of MOC. The strength retention coefficients could be more than 80% when the dosage of phosphates was 0.5-1% the MOC paste mass(Deng 2003). It was proposed that phosphate could react with magnesium to produce insoluble hydrated products such as magnesium phosphate that protected the magnesium cement crystal from decomposing (Li et al. 2008). However, some researchers argued that there was no new phase observed from the X-ray diffraction (XRD) result and the quantity of insoluble phosphates was not high enough to produce a layer of the insoluble phosphates (Deng 2003). They stated that phosphates reduced the level of free Mg^{2+} ions required in solution for the formation and stable existence of phase 3 and phase 5. This was confirmed in another study which found that the addition of NaH_2OP_4 altered the conditions of phase formation in MOC paste as shown in Figure 2-14 (Zhou et al. 2015). On the other hand, some studies revealed the transformation from the crystalline to gel-like Phase 5 was the main reason for the improved water resistance of MOC when adding phosphate as shown in Figure 2-15. They suggested the decrease of initial thermal decomposition temperature of MOC with the addition of phosphate was due to the formation of gel-like phase 5, which required lower energy for thermal decomposition compared to crystalline phase 5. (Li et al. 2016). The mechanism involved in the improvement of water resistance of MOC by the addition of phosphates required further research.

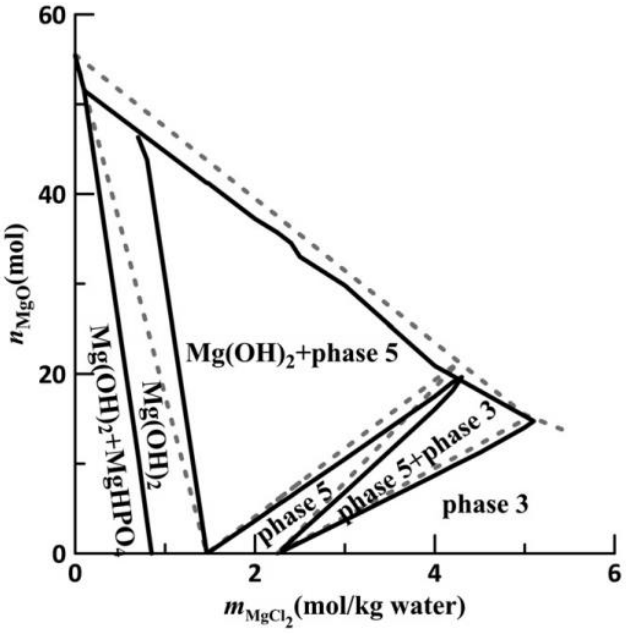

Figure 2-14 The equilibrium phase diagram of solids in the MgO-$MgCl_2$-H_2O system with 0.5% NaH_2PO_4 at T=25 ° C, P=0.1MPa (The dash line refers to the diagram of system without NaH_2PO_4) (Zhou et al. 2015)

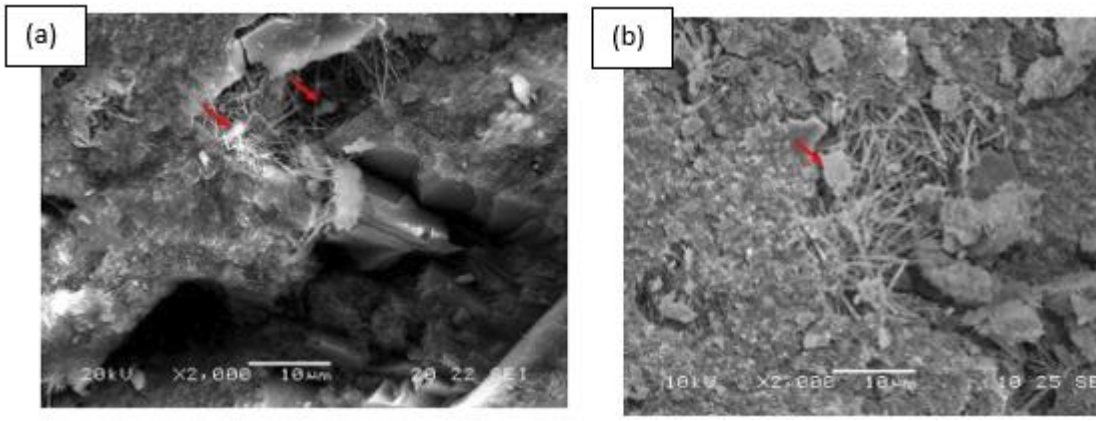

Figure 2-15 SEM images of MOC after air curing for 28 days (a) control MOC paste (b) MOC paste with the addition of 1% of KH_2PO_4. (Li et al. 2016)

Although adding additives is an effective way to improve the water resistance of MOC, it increases the cost of producing the material. Therefore, using waste materials should be considered. Fly ash (FA) was used to improve the water resistance of MOC. It was reported

that the residual compressive strength of MOC mortars incorporating 30% fly ash cured in air for 14 days was about 80% of the initial value even after immersion in water for 28 days. A certain amount of phase 5 was still remained in MOC incorporating 30% of FA after water immersion(Chau et al. 2009). It was suggested that the improvement of water resistance of MOC incorporating fly ash or silica fume was due to the generation of alumino-silicate 5 •1 •8 gel (Li and Yu 2010). However, the mechanism for FA improving the water resistance of MOC was not clear as no new crystalline phase was observed in MOC incorporating FA.

2.4.4.4 M-S-H gel

The mechanism for FA improving the water resistance of MOC remained unclear as no new crystalline phase was observed from X-ray diffraction pattern. So it is possible that some amorphous phase was generated through the reaction between FA and MOC. Some researchers proposed the generation of alumina-silicate gel in MOC paste prepared with FA and silica fume (Li and Yu 2010). Other researchers recognised the possibility that brucite could react with amorphous silica present in FA to form magnesium silicate hydrate (M-S-H) gel (Vandeperre et al. 2008a). However, the multiple crystalline phases present in FA made it difficult to discern changes present in the amorphous phases. Some researchers used silica fume or amorphous silica (SiO_2) and MgO or $Mg(OH)_2$ to prepare M-S-H gel. While some researchers used pure chemicals like Na_2SiO_3 •$5H_2O$ $Mg(NO_3)_2$• $6H_2O$ to synthesize this amorphous gel. The minerals having similar structure to M-S-H gel are summarised in Table 2-1 (Walling and Provis 2016).

Table 2-1 Minerals linked to M-S-H gel (Walling and Provis 2016)

Mineral	Group	Formulation
Lizardite	serpentine	$Mg_3(Si_2O_5)(OH)_4$

Antigorite	serpentine	$Mg_3(Si_2O_5)(OH)_4$
Chrysotile	serpentine	$Mg_3(Si_2O_5)(OH)_4$
Sepiolite	phyllosilicate	$Mg_4(Si_6O1_5)(OH)_2•6H_2O$
Saponite	phyllosilicate	$Ca_{0.25}(Mg,Fe)_3((Si,Al)_4O_{10})(OH)_2•nH_2O$
Talc	phyllosilicate	$Mg_3(Si_4O_{10})(OH)_2$

The synthesis of M-S-H gel began from the early 1950s, when most studies used high pressure and temperature. Both pressure and temperature affect the molar ratio and morphology of M-S-H gel. It was found the Mg/Si molar ratio of the products varied from 0.75 (similar to talc structure as shown in Figure 2-16(a)) to 1.5(similar to chrysotile structure as shown in Figure 2-16(b)) (Tonelli et al. 2016). In 1960, some researchers investigated the ternary system MgO-SiO_2-H_2O over the temperature range 100 ^{0} C to 300 ^{0} C at pressures up to 138MPa. Under 100 ^{0} C to 200^0 C, the molar ratio of the product was 1.5. While the products were two stable phases, $3MgO•2SiO_2•2H_2O$ and $3MgO•4SiO_2•H_2O$, in the range 200 ^{0} C to 300^0 C(YANG 1960). The physical and chemical properties of these two phases were similar to that of serpentine and talc respectively. The effect of time and temperature on properties of M-S-H gel prepared by mixing MgO and SiO_2 was investigated with DTA-TG-EGA and XRD methods as shown in Figure 2-17(Szczerba et al. 2013). The major endothermic peaks at 100 ^{0} C and 400 ^{0} C in the sample aged for 30 days was correlated to the adsorbed water and the decomposition of brucite. A new peak up to 700^0 C in the sample aged for 180 days can be correlated with initial decomposition of the M-S-H gel. It was concluded that the increase of aging time and temperature led to the increase of organization of the internal structures. And a new crystal nucleus may be formed when prolonging the aging time. Some researchers investigated the effect of aging time and temperature on properties of M-S-H gel prepared by using pure

chemicals Na_2SiO_3 •5 H_2O and $Mg(NO_3)_2$ •6H_2O (Brew and Glasser 2005). They found aging of the gels for 6 months at 85 ^{0} C resulted in increased polymerization and enhanced structural development of the crystallinity according to nuclear magnetic resonance (NMR) results. However, the aged products still remained poorly ordered by XRD result.

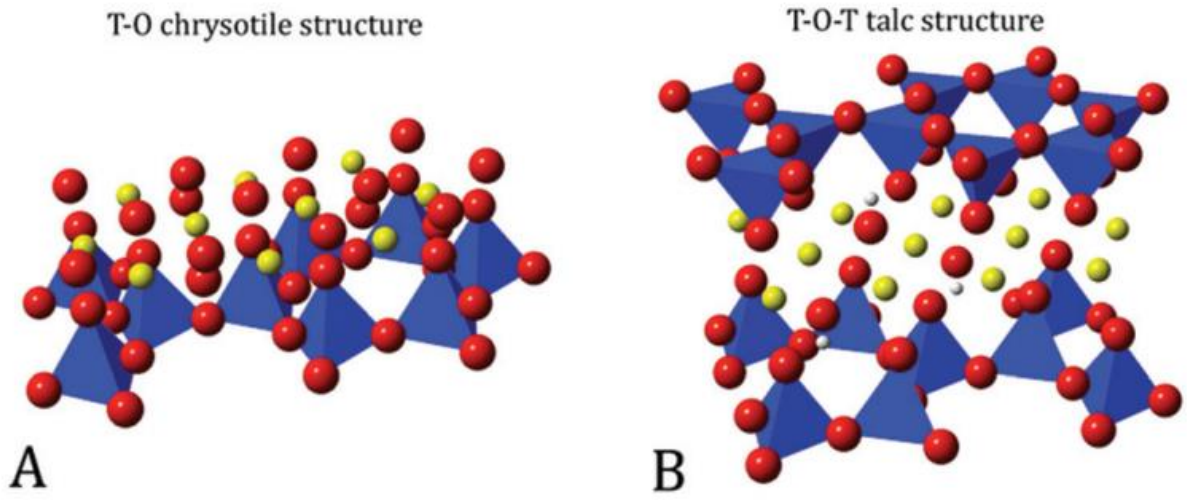

Figure 2-16 Crystal structure of (A) chrysotile (B) talc. Blue tetrahedral represent Si species. Red, yellow and white spheres represent O, Mg and H atoms, respectively(Tonelli et al. 2016)

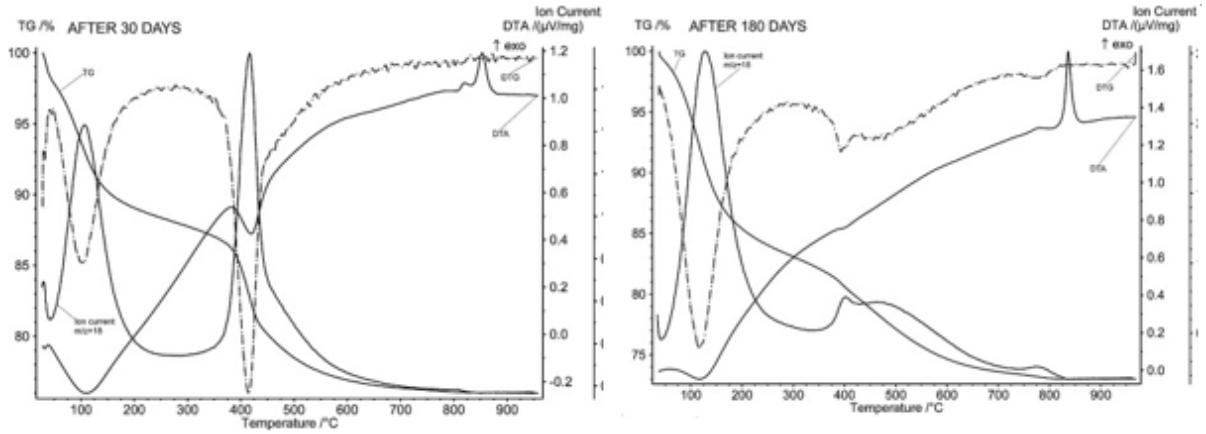

Figure 2-17 Thermal analysis for samples aging at 20 ° C for 30 days and 180 days (Szczerba et al. 2013)

Some researchers prepared M-S-H gel with magnesium hydroxide and hydrated silicic acid via grinding instead of hydrothermal method(Temuujin et al. 1998). New broad peaks appeared at $2\theta=10^{\circ}$-13°, 20°-22°,24°-27°, 35°-39°, and 60°-62° corresponding to the poorly crystalline layered magnesium silicate hydrate phase of talc and chrysotile-like materials by a reaction between $Mg(OH)_2$ and silicic acid as shown in Figure 2-18, which was similar to the product obtained via the hydrothermal method. Water was important for the generation of M-S-H gel as no new phase was observed in the mixture: $Mg(OH)_2$-silica gel (Temuujin et al. 1998).

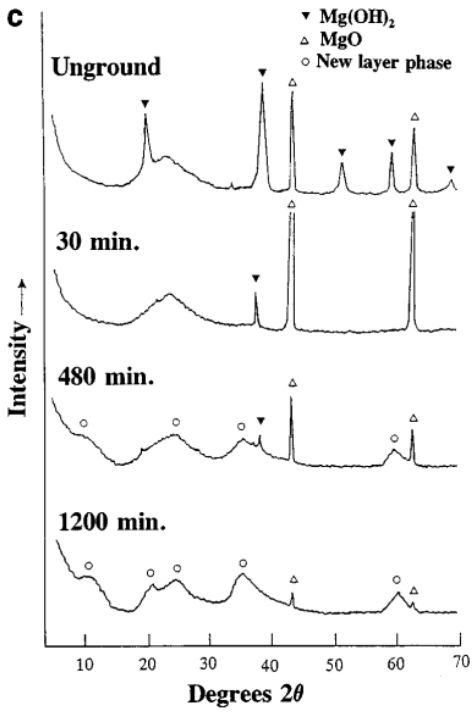

Figure 2-18 XRD patterns of mixtures MgO-silicic acid ground for varying time (Temuujin et al. 1998)

2.5 Summary

Incorporating recycled wood in building materials provides many advantages such as lightweight, high tensile strength, low thermal conductivity compared to neat cement. Many researchers focused on the study of incorporating wood in OPC as it is the most widely used construction material. However, the utilization of wood-OPC composites was limited due to the incompatibility between wood and OPC. On the contrary, wood-magnesia cement composites could significantly reduce this problem. Besides, wood-magnesia cement composites have many superior physical properties than wood-OPC composites such as lower density, higher abrasion resistance and compressive strength etc. Moreover, the production of wood-magnesia composites save energy and reduce CO_2 emissions. So, magnesia cement was selected in this study to incorporate recycled waste timber.

Three types of magnesia cements were reviewed and compared in this chapter: magnesium oxide cement, MPC and MOC. There are many disadvantages of using magnesium oxide cement and MPC. When using magnesium oxide cement, the delayed excessive expansion of the cement due to the hydration reaction of MgO need careful attention as it may cause severe cracking. And more attention should be paid on the stability of the carbonation products of MgO, which may weaken the structure. Traditional MPC uses ammonium phosphate as the reactant, but it releases toxic ammonium gas. Recent researchers used monopotassium phosphate as the replacement of ammonium phosphate, but more attention is required due to the toxicity of borates which are widely used as retarders. Without the need to use any toxic reactant or unstable hydration products, MOC is a promise magnesia cement for the recycling of waste wood.

However, MOC suffers from significant strength reductions when immersed in water due to the decomposition of hydration products. So, it can only be used in indoor environments. Various additives could help to improve the water resistance, but they increase the cost. SCMs were used to improve the water resistance of MOC, but the mechanism is still not clear.

Reference

Abdelrazig, B., J. Sharp and B. El-Jazairi (1988). The chemical composition of mortars made from magnesia-phosphate cement. Cement and Concrete Research **18**(3): 415-425.

Ahn, W. Y. and A. Moslemi (1980). SEM examination of wood-Portland cement bonds. Wood Science **13**(2): 77-82.

Akers, S. and J. Studinka (1989). Ageing behaviour of cellulose fibre cement composites in natural weathering and accelerated tests. International Journal of Cement Composites and Lightweight Concrete **11**(2): 93-97.

Arora, A. (2005). Text book of inorganic chemistry, Discovery Publishing House.

Ashori, A., T. Tabarsa and S. Sepahvand (2012). Cement-bonded composite boards made from poplar strands. Construction and Building Materials **26**(1): 131-134.

Ball, M. C. (1977). Reactions of compounds occurring in sorel's cement. Cement and Concrete Research **7**(5): 575-583.

Ballirano, P., C. De Vito, V. Ferrini and S. Mignardi (2010). The thermal behaviour and structural stability of nesquehonite, MgCO3· 3H2O, evaluated by in situ laboratory parallel-beam X-ray powder diffraction: New constraints on CO2 sequestration within minerals. Journal of hazardous materials **178**(1-3): 522-528.

Bender, C. (1871). Ueber die Hydrate des Magnesiumoxychlorids. European Journal of Organic Chemistry **159**(3): 341-349.

Bentur, A. and S. Akers (1989). The microstructure and ageing of cellulose fibre reinforced cement composites cured in a normal environment. International Journal of Cement Composites and Lightweight Concrete **11**(2): 99-109.

Bentur, A. and S. Mindess (2014). Fibre reinforced cementitious composites, CRC Press.

Biel, T. and H. Lee (1996). Magnesium oxychloride cement concrete with recycled tire rubber. Transportation Research Record: Journal of the Transportation Research Board(1561): 6-12.

Bilinski, H., B. Matković, C. MAŽURANIĆ and T. B. ŽUNIĆ (1984). The Formation of Magnesium Oxychloride Phases in the Systems MgO - MgCl2 - H2O and NaOH - MgCl2 - H2O. Journal of the American Ceramic Society **67**(4): 266-269.

Brew, D. and F. Glasser (2005). Synthesis and characterisation of magnesium silicate hydrate gels. Cement and Concrete Research **35**(1): 85-98.

Botha, A., Strydom, C.A.(2001). Preparation of a magnesium hydroxy carbonate from magnesium hydroxide. Hydrometallurgy. **62**: 175-183.

Canterford J H (1985). Magnesia - an important industrial mineral: A review of processing options and uses. Mineral Procesing and Extractive Metallurgy Review, **2**(1-2): 57-104.

Chatterji, S. (1995). Mechanism of expansion of concrete due to the presence of dead-burnt CaO and MgO. Cement and Concrete Research **25**(1): 51-56.

Chau, C., J. Chan and Z. Li (2009). Influences of fly ash on magnesium oxychloride mortar. Cement and Concrete Composites **31**(4): 250-254.

Chau, C. and Z. Li (2008). Microstructures of magnesium oxychloride. Materials and structures **41**(5): 853-862.

Chau, C. K. and Z. Li (2008). Accelerated reactivity assessment of light burnt magnesium oxide. Journal of the American Ceramic Society **91**(5): 1640-1645.

Coutts, R. (1984). Autoclaved beaten wood fibre-reinforced cement composites. Composites **15**(2): 139-143.

Coutts, R. (1987). Fibre-matrix interface in air-cured wood-pulp fibre-cement composites. Journal of materials science letters **6**(2): 140-142.

Coutts, R. and P. Kightly (1982). Microstructure of autoclaved refined wood-fibre cement mortars. Journal of Materials Science **17**(6): 1801-1806.

Coutts, R. and P. Kightly (1984). Bonding in wood fibre-cement composites. Journal of Materials Science **19**(10): 3355-3359.

Coutts, R. and P. Warden (1985). Air-cured, wood pulp, fibre cement composites. Journal of Materials Science Letters **4**(1): 117-119.

Cwirzen, A. and K. Habermehl-Cwirzen (2012). Effects of reactive magnesia on microstructure and frost durability of Portland cement–based binders. Journal of materials in civil engineering **25**(12): 1941-1950.

De Castellar, M., J. Lorente, A. Traveria and J. Tura (1996). Cracks in Sorel's cement polishing bricks as a result of magnesium oxychloride carbonatation. Cement and Concrete Research **26**(8): 1199-1202.

Dehua, D. and Z. Chuanmei (1999). The formation mechanism of the hydrate phases in magnesium oxychloride cement. Cement and concrete research **29**(9): 1365-1371.

Demediuk, T., W. Cole and H. Hueber (1955). Studies on magnesium and calcium oxychlorides. Australian Journal of Chemistry **8**(2): 215-233.

Deng, D. (2003). The mechanism for soluble phosphates to improve the water resistance of magnesium oxychloride cement. Cement and Concrete Research **33**(9): 1311-1317.

Dinnebier, R. E., D. Freyer, S. Bette and M. Oestreich (2010). 9Mg (OH) 2· MgCl2· 4H2O, a high temperature phase of the magnesia binder system. Inorganic chemistry **49**(21): 9770-9776.

Dinnebier, R. E., M. Oestreich, S. Bette and D. Freyer (2012). 2Mg (OH) 2· MgCl2· 2H2O and 2Mg (OH) 2· MgCl2· 4H2O, two high temperature phases of the magnesia cement system. Zeitschrift für anorganische und allgemeine Chemie **638**(3-4): 628-633.

Dong, H., C. Unluer, E. Yang, F. Jin and A. Al-Tabbaa (2019). Microstructure and carbon storage capacity of hydrated magnesium carbonates synthesized from different sources and conditions. Journal of CO_2 Utilization. **34**: 353-361.

Dong, M., W. Cheng, Z. Li and G. P. Demopoulos (2008). Solubility and stability of nesquehonite (MgCO3· 3H2O) in NaCl, KCl, MgCl2, and NH4Cl solutions. Journal of Chemical & Engineering Data **53**(11): 2586-2593.

Du, C. (2005). A review of magnesium oxide in concrete. Concrete international **27**(12): 45-50.

Duxson, P. and J. Provis (2008). Low CO2 concrete: are we making any progress. BEDP environment design guide. Royal Australian Institute of Architects, Darwin.

Fernando, P.-T. and J. Said (2011). Resistance to acid attack, abrasion and leaching behavior of alkali-activated mine waste binders. Materials and structures **44**(2): 487-498.

Ferrini, V., C. De Vito and S. Mignardi (2009). Synthesis of nesquehonite by reaction of gaseous CO2 with Mg chloride solution: Its potential role in the sequestration of carbon dioxide. Journal of hazardous materials **168**(2-3): 832-837.

Franek, J., M. Kollár and I. Makovíny (2011). Microwave Electromagnetic Filed and Temperature Distribution in a Multilayered Wood-Cement Board. Journal of Electrical Engineering **62**(1): 25-30.

Hachmi, M. (1989). Wood-cement chemical relationships. For Prod Res Soc **1**: 43-47.

Hales, M. C., R. L. Frost and W. N. Martens (2008). Thermo-Raman spectroscopy of synthetic nesquehonite—implication for the geosequestration of greenhouse gases. Journal of Raman Spectroscopy: An International Journal for Original Work in all Aspects of Raman Spectroscopy, Including Higher Order Processes, and also Brillouin and Rayleigh Scattering **39**(9): 1141-1149.

Hall, D. A., R. Stevens and B. El-Jazairi (2001). The effect of retarders on the microstructure and mechanical properties of magnesia–phosphate cement mortar. Cement and Concrete Research **31**(3): 455-465.

Jin, F., G. Zhang, X. Luo and C. Zhang (2008). Modelling autogenous expansion for magnesia concrete in arch dams. Frontiers of Architecture and Civil Engineering in China **2**(3): 211-218.

Juenger, M., F. Winnefeld, J. L. Provis and J. Ideker (2011). Advances in alternative cementitious binders. Cement and concrete research **41**(12): 1232-1243.

Karade, S. (2010). Cement-bonded composites from lignocellulosic wastes. Construction and Building Materials **24**(8): 1323-1330.

Königsberger, E., L.-C. Königsberger and H. Gamsjäger (1999). Low-temperature thermodynamic model for the system Na2CO3− MgCO3− CaCO3− H2O. Geochimica et Cosmochimica Acta **63**(19-20): 3105-3119.

Krause, O. (1873). Ueber Magnesiumoxychlorid. Justus Liebigs Annalen der Chemie **165**(1): 38-44.

Laufenberg, T. L., M. Aro and A. Wagh (2004). Phosphate-bonded ceramic–wood composites: R&D project overview and invitation to participate. Proceedings of Ninth International Conference on Inorganic-Bonded Composite Materials.

Lee, A. W. (1985). Effect of cement/wood ratio on bending properties of cement-bonded southern pine excelsior board. Wood and fiber science **17**(3): 361-364.

Lee, A. W. and Z. Hong (1986). Compressive strength of cylindrical samples as an indicator of wood-cement compatibility. Forest products journal (USA).

LeVan, S. L. and J. E. Winandy (1990). Effects of fire retardant treatments on wood strength: a review. Wood and Fiber Science **22**(1): 113-131.

Li, C. and H. Yu (2010). Influence of fly ash and silica fume on water-resistant property of magnesium oxychloride cement. Journal of Wuhan University of Technology-Mater. Sci. Ed. **25**: 721-724.

Li, J., G. Li and Y. Yu (2008). The influence of compound additive on magnesium oxychloride cement/urban refuse floor tile. Construction and building materials **22**(4): 521-525.

Li, Y., Z. Li, H. Pei and H. Yu (2016). The influence of FeSO 4 and KH 2 PO 4 on the performance of magnesium oxychloride cement. Construction and Building Materials **102**: 233-238.

Li, Z. and C. Chau (2007). Influence of molar ratios on properties of magnesium oxychloride cement. Cement and Concrete Research **37**(6): 866-870.

Lide, D. (2007). Handbook of chemistry and physics. CRC Press, Boca Raton, FL. Handbook of chemistry and physics. 88th ed. CRC Press, Boca Raton, FL.: -.

Lin, X., M. Silsbee, D. Roy, K. Kessler and P. Blankenhorn (1994). Approaches to improve the properties of wood fiber reinforced cementitious composites. Cement and Concrete Research **24**(8): 1558-1566.

Lu, H., P. Wang and N. Jiang (1994). Design of additives for water-resistant magnesium oxychloride cement using pattern recognition. Materials Letters **20**(3): 217-223.

Lu, X., F. Geng, H. Zhang and X. Chen (2011). Influence of MgO-type expansive agent hydration behaviors on expansive properties of concrete. Journal of Wuhan University of Technology-Mater. Sci. Ed. **26**(2): 344-346.

Lukens, H. (1932). The composition of magnesium oxychloride. Journal of the American Chemical Society **54**(6): 2372-2380.

Maravelaki-Kalaitzaki, P. and G. Moraitou (1999). Sorel's cement mortars: Decay susceptibility and effect on Pentelic marble. Cement and Concrete Research **29**(12): 1929-1935.

Matković, B., S. Popović, V. Rogić, T. Žunić and J. F. Young (1977). Reaction Products in Magnesium Oxychloride Cement Pastes. System MgO-MgCl2-H2O. Journal of the American Ceramic Society **60**(11-12): 504-507.

Misra, A. and R. Mathur (2007). Magnesium oxychloride cement concrete. Bulletin of Materials Science **30**(3): 239-246.

Mo, L., M. Deng and M. Tang (2010). Effects of calcination condition on expansion property of MgO-type expansive agent used in cement-based materials. Cement and Concrete Research **40**(3): 437-446.

Mo, L. and D. K. Panesar (2013). Accelerated carbonation–A potential approach to sequester CO2 in cement paste containing slag and reactive MgO. Cement and Concrete Composites **43**: 69-77.

Montle, J. and K. Mayhan (1974). The role of magnesium oxychloride as a fire-resistive material. Fire Technology **10**(3): 201-210.

Moslemi, A. and S. C. Pfister (1987). The influence of cement/wood ratio and cement type on bending strength and dimensional stability of wood-cement composite panels. Wood and fiber science **19**(2): 165-175.

Na, B., Z. Wang, H. Wang and X. Lu (2014). Wood-cement compatibility review. Wood Research **59**(5): 813-826.

Newman, E. S., J. V. Gilfrich and L. S. Wells (1952). Heat generation in the setting of magnesium oxychloride cements. Journal of Research of the National Bureau of Standards **49**(6): 377-383.

Oilo, G. (1991). Luting cements: a review and comparison. International dental journal **41**(2): 81-88.

Plekhanova, T., J. Keriene, A. Gailius and G. Yakovlev (2007). Structural, physical and mechanical properties of modified wood–magnesia composite. Construction and Building Materials **21**(9): 1833-1838.

Qin, L., X. Gao, W. Li and H. Ye (2018). Modification of Magnesium Oxysulfate Cement by Incorporating Weak Acids. Journal of Materials in Civil Engineering. 30(9): 04108209.

Qin, L., Z. Huang, L. Zhang and Y. Wang (2009). Flame-retardant mechanism of magnesium oxychloride in epoxy resin. Journal of Wuhan University of Technology-Mater. Sci. Ed. **24**(1): 127-131.

Riding, K. A., J. L. Poole, A. K. Schindler, M. C. Juenger and K. J. Folliard (2006). Evaluation of temperature prediction methods for mass concrete members. ACI Materials Journal **103**(5): 357-365.

Robinson, W. and W. Waggaman (1909). Basic magnesium chlorides. The Journal of Physical Chemistry **13**(9): 673-678.

Seehra, S., S. Gupta and S. Kumar (1993). Rapid setting magnesium phosphate cement for quick repair of concrete pavements—characterisation and durability aspects. Cement and Concrete Research **23**(2): 254-266.

Servais, G. and L. Cartz (1971). Structure of zinc phosphate dental cement. Journal of dental research **50**(3): 613-620.

Shand, M.K.(2020), Magnesium oxysulfate cement. Magnesia Cements: from Formulation to Application: 75-83

Simatupang, M. H. and R. L. Geimer (1990). Inorganic binder for wood composites: feasibility and limitations. Proceedings of the Wood Adhesive Symposium.

Simatupang, M. H. and R. L. Geimer (1990). Inorganic binder for wood composites: feasibility and limitations. Proceedings of Wood Adhesive Symposium, Forest Product Resources Society.

Solo‐gabriele, H. and T. Townsend (1999). Disposal practices and management alternatives for CCA‐treated wood waste. Waste Management and Research **17**(5): 378-389.

Sorel, S. (1866). Improved composition to be used as a Cement and as a Plastic Material for Molding Various Articles. United States Patent Office. Patent **53**(092): 6.

Soroushian, P., Z. Shah, J.-P. Won and J.-W. Hsu (1994). Durability and moisture sensitivity of recycled wastepaper-fiber-cement composites. Cement and Concrete Composites **16**(2): 115-128.

Sorre, C. A. and C. R. Armstrong (1976). Reactions and Equi ibria in Magnesium Oxych oride Cements. Journal of the American Ceramic Society **59**(1-2): 51-54.

Stahl, D. C., G. Skoraczewski, P. Arena and B. Stempski (2002). Lightweight concrete masonry with recycled wood aggregate. Journal of materials in civil engineering **14**(2): 116-121.

Sugama, T. and L. Kukacka (1983). Characteristics of magnesium polyphosphate cements derived from ammonium polyphosphate solutions. Cement and Concrete Research **13**(4): 499-506.

Sugimoto, K., R. E. Dinnebier and T. Schlecht (2007). Structure determination of Mg3 (OH) 5Cl· 4H2O (F5 phase) from laboratory powder diffraction data and its impact on the analysis of problematic magnesia floors. Acta Crystallographica Section B: Structural Science **63**(6): 805-811.

Swanson, E. J., K. J. Fricker, M. Sun and A.-H. A. Park (2014). Directed precipitation of hydrated and anhydrous magnesium carbonates for carbon storage. Physical Chemistry Chemical Physics **16**(42): 23440-23450.

Szczerba, J., R. Prorok, E. Śnieżek, D. Madej and K. Maślona (2013). Influence of time and temperature on ageing and phases synthesis in the MgO–SiO2–H2O system. Thermochimica acta **567**: 57-64.

Temuujin, J., K. Okada and K. MacKenzie (1998). Role of Water in the Mechanochemical Reactions of MgO-SiO~ 2 Systems. Journal of Solid State Chemistry **138**(1): 169-177.

Temuujin, J., K. Okada and K. J. MacKenzie (1998). Formation of layered magnesium silicate during the aging of magnesium hydroxide–silica mixtures. Journal of the American Ceramic Society **81**(3): 754-756.

Tonelli, M., F. Martini, L. Calucci, E. Fratini, M. Geppi, F. Ridi, S. Borsacchi and P. Baglioni (2016). Structural characterization of magnesium silicate hydrate: towards the design of eco-sustainable cements. Dalton Transactions **45**(8): 3294-3304.

Tooper, B. and L. Cartz (1966). Structure and formation of magnesium oxychloride sorel cements. Nature **211**(5044): 64.

Urwongse, L. and C. A. Sorrell (1980). The System MgO-MgCl2-H2O at 23° C. Journal of the American Ceramic Society **63**(9-10): 501-504.

Vandeperre, L. and A. Al-Tabbaa (2007). Accelerated carbonation of reactive MgO cements. Advances in Cement Research **19**(2): 67-79.

Vandeperre, L., M. Liska and A. Al-Tabbaa (2008a). Microstructures of reactive magnesia cement blends. Cement and Concrete Composites **30**(8): 706-714.

Vandeperre, L., M. Liska and A. Al-Tabbaa (2008b). Hydration and mechanical properties of magnesia, pulverized fuel ash, and portland cement blends. Journal of materials in civil engineering **20**(5): 375-383.

Ved, E., E. Zharov and H. Phong (1976). Mechanism of magnesium oxychloride formation during the hardening of magnesium oxychloride cement. Zh Prikl Khim **49**(10): 2154-2158.

Wagh, A. S., R. Strain, S. Jeong, D. Reed, T. Krause and D. Singh (1999). Stabilization of Rocky Flats Pu-contaminated ash within chemically bonded phosphate ceramics. Journal of Nuclear Materials **265**(3): 295-307.

Walling, S. A. and J. L. Provis (2016). Magnesia-based cements: a journey of 150 years, and cements for the future? Chemical reviews **116**(7): 4170-4204.

Wang, Y., Z. Li, and G.P.Demopoulos (2008). Controlled precipitation of nesquehonite ($MgCO_3 \cdot 3H_2O$) by the reaction of $MgCl_2$ with $(NH_4)_2CO_3$. Journal of Crystal Growth. 310: 1220-1227.

Wilson, A. D., J. M. Paddon and S. Crisp (1979). The hydration of dental cements. Journal of dental research **58**(3): 1065-1071.

Wolfe, R. W. and A. Gjinolli (1999). Durability and strength of cement-bonded wood particle composites made from construction waste. Forest Products Journal **49**: 24-31.

Wu, C., C.Chen, H.Zhang , Y.Tan and H.Yu (2018). Preparation of magnesium oxysulfate cement using magnesium-rich byproducts from the production of lithium carbonate from salt lakes. Construction and Building Materials. **172**: 597-607.

Wu, C., H. Yu, H. Zhang, J. Dong, J, Wen and Y, Tan (2015). Effects of phosphoric acid and phosphates on magnesium oxysulfate cement. Materials and structures. **48**: 907-917.

Xia, S., P. Xing and S. Gao (1991). Studies on the basic compounds of magnesia cement: the thermal behaviour of magnesium oxychlorides. Thermochimica acta **183**: 349-363.

Yalinkilic, M., E. Gezer, M. Takahashi, Z. Demirci, R. Ilhan and Y. Imamura (1999). Boron addition to non-or low-formaldehyde cross-linking reagents to enhance biological resistance and dimensional stability of wood. Holz als Roh-und werkstoff **57**(5): 351-357.

YANG, J. C. S. (1960). The System Magnesia‐Silica‐Water Below 300° C.: I, Low‐Temperature Phases from 100° to 300° C. and Their Properties. Journal of the American Ceramic Society **43**(10): 542-549.

Yang, Q., S. Zhang and X. Wu (2002). Deicer-scaling resistance of phosphate cement-based binder for rapid repair of concrete. Cement and Concrete Research **32**(1): 165-168.

Zhang, Z., Y. Zheng, Y. Ni, Z. Liu, J. Chen, and X. Liang (2006). Temperature-and pH-dependent morphology and FT− IR analysis of magnesium carbonate hydrates. The Journal of Physical Chemistry. **110** (26): 12969-12973.

Zheng, L., C. Xuehua and T. Mingshu (1991). MgO-type delayed expansive cement. Cement and Concrete Research **21**(6): 1049-1057.

Zhengtian, L. and A. Moslemi (1985). Influence of chemical additives on the hydration characteristics of western larch wood-cement-water mixtures. Forest Products Journal **35**(7-8): 37-43.

Zhou, X. and Z. Li (2012). Light-weight wood–magnesium oxychloride cement composite building products made by extrusion. Construction and Building Materials **27**(1): 382-389.

Zhou, Y. and D. P. Kamdem (2002). Effect of cement/wood ratio on the properties of cement-bonded particleboard using CCA-treated wood removed from service. Forest products journal **52**(3): 77-81.

Zhou, Z., H. Chen, Z. Li and H. Li (2015). Simulation of the properties of MgO-MgfCl2-H2O system by thermodynamic method. Cement and concrete research **68**: 105-111.

Chapter 3. Methodology

3.1 Materials

3.1.1 Binders

The light-burned magnesia powder (MgO) was obtained from Liaoning province, China; $MgCl_2$ used in this study was bischofite ($MgCl_2 \cdot 6H_2O$) with a purity of 98 wt%, produced by Qinghai, China. Class F pulverized fuel ash (PFA) used was a pozzolanic waste material generated during the combustion of coal sourced from a local power plant in Hong Kong. The glass powder (GP) was obtained by milling recycled glass cullet produced by a local glass recycler (Laputa Eco-Construction Material Co. Ltd.). The incinerated sewage sludge ash (ISSA) was obtained from the sewage sludge incineration center-T park, HK. The chemical characteristics of MgO, PFA, GP and ISSA are shown in Table 3-1. The particle size distribution curves of MgO, PFA, GP and ISSA are shown in Figure 3-1.

Table 3-1 Chemical compositions of MgO, PFA, GP and ISSA

Composition (% by mass)	MgO	GP	PFA	ISSA
MgO	94.86	1.16	4.10	3.21
SiO_2	2.75	73.29	45.70	28.34
AlO_3	--	1.10	19.55	12.44
Fe_2O_3	0.45	0.30	11.72	18.60
CaO	1.60	12.14	12.27	10.63

Na_2O	--	10.54	1.36	7.43
K_2O	--	0.84	1.71	1.92
SO_4	0.24	0.24	1.82	6.22
P_2O_5	--	--	--	9.92

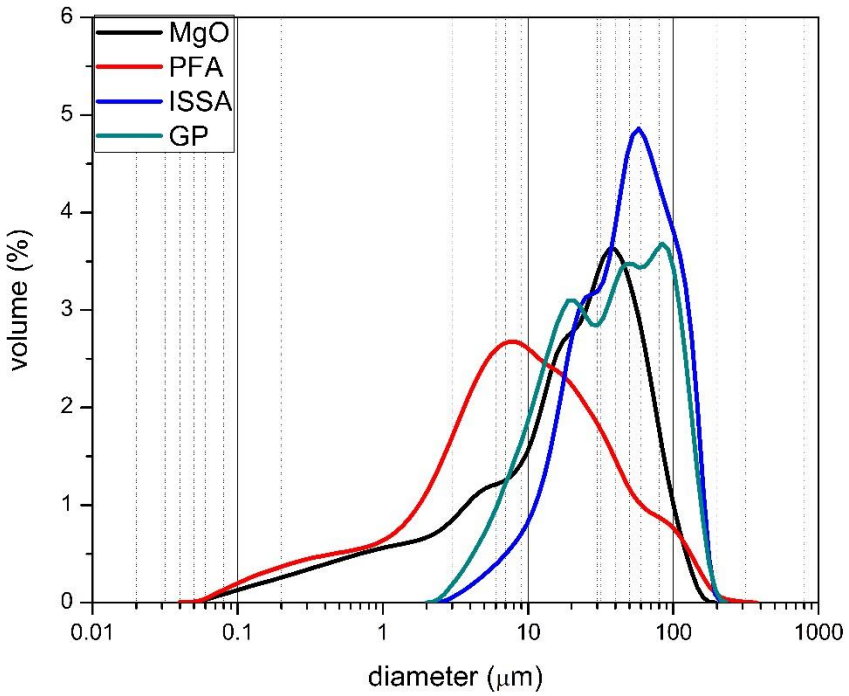

Figure 3-1 Particle size distribution of MgO, PFA, ISSA and GP

3.1.2 Aggregates

Natural aggregates

The fine aggregate used for preparing the wood cement mortar was a standard quartz sand (ISO679:1989) with particle sizes ranging from 0.5 mm to 1 mm.

Waste wood fibre

Wood fibre materials used in this experiment were prepared using waste timber formworks (masson pine) collected from construction sites in Hong Kong. The density and water absorption were 0.45 g/cm^3 and 0.55 g/g respectively.

3.2 Curing process

Two curing methods, CO_2 curing, and air curing were employed in this study.

An airtight steel-cylindrical vessel was used for CO_2 curing and it was vacuumed to 0.5 bar before the CO_2 injection. The CO_2 used was at >99% purity sourced from a commercial manufacturer. The CO_2 pressure in the chamber was kept at 0.1 bar for 24 h curing duration.

For air curing, the specimens were placed in an air curing chamber (25ºC, RH=50%) for different days.

3.3 Test methods

3.3.1 Physical and chemical properties

Compressive strength

The compressive strength of the specimens was determined using a Denison compression machine at a loading rate of 1 kN/s. Six samples were tested for each composition and the average results were reported.

Flexural strength

The flexural strength was determined with the three-point bending flexure test and the strength value was calculated using the following equation as recommended by ASTM C1185.

$$S=\frac{3Pl}{2bd^2} \quad (3\text{-}1)$$

Where P is the breaking load (N); l is the test span (100mm), b is the width of the specimen (100mm); d is the thickness of the specimen (5mm). The testing machine (Testometric CXM 500-50 KN) was used to test the flexural strength and the loading rate was 0.3mm min^{-1}.

Strength retention coefficient

The strength retention coefficient was used to evaluate water resistance and was calculated as follows:

$$SR_n=Sc_n/Sc \quad (3\text{-}2)$$

Where SR_n is the strength retention coefficient of water immersion for n days; Sc_n is the strength of specimens immersed into water for n days; Sc is the strength before immersion into water.

Water absorption and thickness swelling

water absorption and thickness swelling were conducted according to ASTM C1185, 2008(ASTM 2008) and ASTM D 1037, 2012(ASTM 2012) respectively.

High temperature resistance

The high temperature resistance of wood-MOC board was evaluated based on the flexural strength retention after heating for 2h in an electric high temperature furnace at a temperature of 200°C, 300 °C and 400°C. After two hours of heating, the residual flexural strength was tested. The water resistance was evaluated by testing the flexural strength of wood-MOC boards before and after water immersion at room temperature for 28 days.

Impact noise reduction property

As one major application of the wood-MOC boards would be to replace plywood for flooring, it is of interest to study the impact noise reduction ability of the boards. The test was carried

out using a modified standard based on ASTM E1007-90(ASTM 2016). A metal ball was used to generate the impact noise as shown in Figure 3-2.

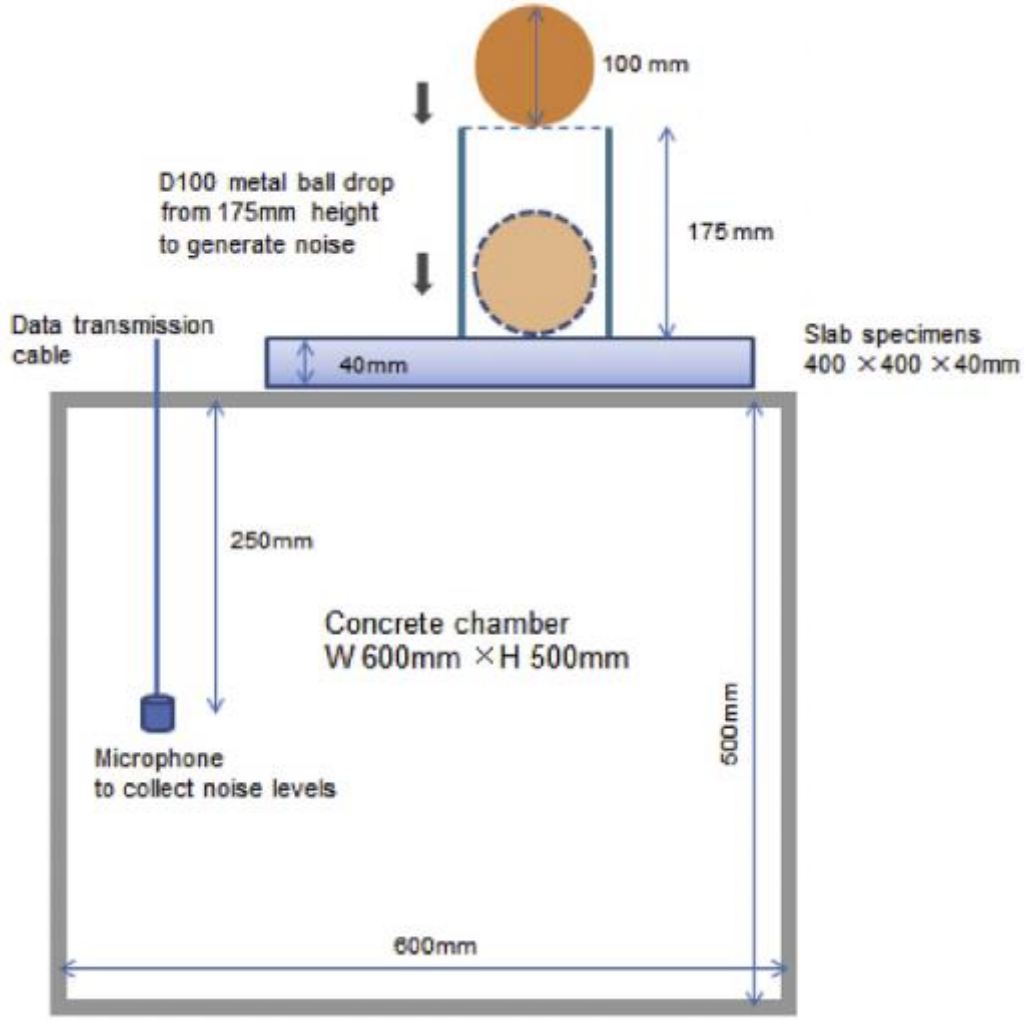

Figure 3-2 Schematic of sound insulation test setup (Zhang and Poon 2018)

Thermal conductivity

A Quick Thermal Conductivity Meter (QTM-500, Kyoto Electronic Manufacturing Co. Ltd. Japan) was employed to examine the thermal conductivity of the wood-MOC boards.

Lifecycle assessment

As the produced wood-MOC would be used for replacing traditional plywood and resin based

particleboards, a lifecycle assessment (LCA) was carried out to compare the environmental performance of the three mentioned materials. For this LCA, the upstream data for MgO was collected from the Ecoinvent database (3.0 2016). As the data for $MgCl_2$ was not available in the databases and the literature, the upstream data for NaCl was used as a proxy due to the similar production process of the two materials (3.0 2016). The assumption is also supported by a recent study (Sinka et al. 2018), where LCA for the unit process of the production of magnesium chloride hexahydrate ($MgCl_2 \cdot 6H_2O$) was assumed to be similar to sodium chloride extracted from brines. In addition, the data for wood chips production from wood waste was based on our previous study (Hossain and Poon 2018). As there is no MOC board manufacturer in Hong Kong, the study assumed that the boards can be potentially manufactured in a nearby location (e.g., Guangdong province in mainland China). Hence, the transportation impacts of the wood chips and ISSA were included using the road transport mode from Hong Kong to the manufacturing site based on CLCD database (Valls and Vazquez 2001). Moreover, the avoided impacts due to the transportation and landfill disposal for both of the waste materials were included. The Ecoinvent database was used for estimating the avoided impact for ISSA (treatment of incineration residues, residual material landfilling)(3.0 2016). Moreover, the transport distance of MgO and $MgCl_2$ from Liaoning province and Qinghai province in mainland China, respectively to the manufacturing site were estimated (about 2750 km and 2162 km, respectively), and the impacts were assessed using the Ecoinvent database for freight train transport (China) (Valls and Vazquez 2001). It is also assumed that impacts due to the industrial production will be similar to the production process of other boards (e.g., resin based particleboard), and hence, the values were included in this study based on our previous study (Hossain and Poon 2018). Finally, GHGs emission was assessed for producing different types of boards by using the IMPACT 2002+ method using SimaPro 8.4 software. The system boundary and processes considered in this assessment are shown in Figure 3-3. The results

were compared with plywood and resin-based particleboard production in southern China.

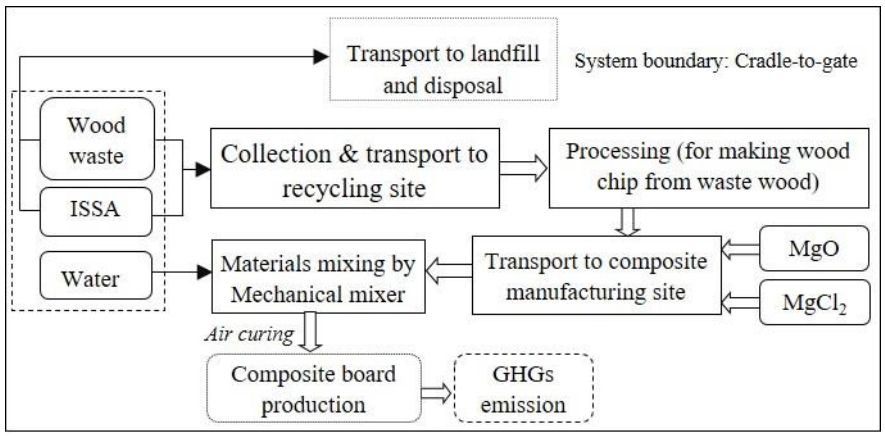

Figure 3-3 System boundary and processes of wood-MOC board production

3.3.2 Microstructures analysis

After the flexural strength test, the crushed chunk samples were immersed in absolute ethyl alcohol for 24 hours to stop reaction. Then they were dried in a vacuum drying oven at 60 ℃ until constant weight. After that, they were stored in a sealed desiccator until the MIP analysis. Powdered samples (less than 75μm), which were used for Q-XRD, FTIR and TG tests, were obtained after crushing and sieving the dried chunk samples.

Q-XRD

The quantitative X-ray powder diffraction (XRD) data were obtained by a SmartLab device manufactured by Rigaku with Cu Kαradiation and 2 θ scanning ranging between 10°to 90°.The scan speed was 0.2°/min. The contents of the crystalline phases in the samples were calculated using Rigaku software by Rietveld refinement of the XRD data. As the sample could contain both crystalline and amorphous phases, all of the samples were mixed with 20wt% of corundum as internal standard to quantify the amorphous content (% Am) as follows:

$$\% Am=(1-W_s/R_s)(100-W_s)^{-1}\times10^4 \quad (3\text{-}3)$$

W_s is the weighted concentration of corundum; R_s is Rietveld analyzed concentration of corundum.

FTIR

A thermo Scientific IS50 spectrometer was used for Fourier-transformed infrared spectroscopy (FTIR). The spectral analysis was performed in the range of 4000-400 cm^{-1}, with a spectral resolution of 1 cm^{-1}.

SEM-BSE

A JEOL Model JSM-6490 with an energy dispersive X-ray spectroscopy (EDX) detector was used for scanning electron microscope (SEM) and back-scattering scanning electron microscopy (BSE) examination. For SEM test, the samples were placed on the sample holders followed by 90s sputter coating of gold. For BSE test, the samples were put into a vacuum chamber followed by impregnation with a low-viscosity epoxy resin (EPO-TEK 301) to remove most of the air in the accessible porosity. After setting of the epoxy, all the samples were polished using a 3000 mesh sand paper, followed by sputtering with a conducting carbon coating.

TG

Thermogravimetry (TG) was performed using a Netzch instrument. Samples were heated at 10 $^oC\ min^{-1}$ from 25 ^oC to 1000 ^oC. Nitrogen was used for cooling.

MIP

Small pieces of samples (less than 3mm) after the flexural strength test were selected for MIP tests, which were performed with a Poresizer9320 mercury porosimeter. Working pressures

covered the range from approximately 0.6 to 30000 p.s.i.a. (corresponding to 300-0.006μm). A contact angle of 120° and a mercury surface tension of 0.483 N/m were assumed.

TEM

MOC pastes were prepared for the TEM test. The samples were first cast in plastic cylindrical tubes, and sections of 2 mm long were cut from the cylinder, polished down to 30 μm, thick and glued between 3 mm diameter nickel grids. Then they were argon ion-beam milled and carbon coated. The bright field images and chemical analyses were collected using a field emission transmission electron microscope (FEI Tecnai TF20 FEGTEM/STEM operating at 200 kV and fitted with an Oxford Instruments INCA 350 EDX system and 80 mm X-Max SDD detector). The test procedures were based on Richardson's study(Richardson and Groves 1993).

Reference

3.0, E. (2016). Magnesium oxide production (RoW), Alloc Def, U. Swiss Centre for Life Cycle Inventories.

3.0, E. (2016). Sodium chloride, brine solution (GLO), Alloc Def, U. Swiss Centre for Life Cycle Inventories.

3.0, E. (2016). Treatment of average incineration residue, residual material landfill (RoW), Alloc Def, U. Swiss Centre for Life Cycle Inventories.

ASTM (2008). Standard test methods for sampling and testing non-asbestos fiber-cement flat sheet, roofing and siding shingles, and clapboards. ASTM standard.

ASTM (2012). Standard test methods for evaluating properties of wood-base fiber and particle panel materials.

ASTM (2016). Standard test method for field measurement of tapping machine impact sound transmission through floor-ceiling assemblies and associated support structures.

Hossain, M. U. and C. S. Poon (2018). Comparative LCA of wood waste management strategies generated from building construction activities. Journal of Cleaner Production **177**: 387-397.

Richardson, I. and G. Groves (1993). Microstructure and microanalysis of hardened ordinary Portland cement pastes. Journal of Materials Science **28**(1): 265-277.

Sinka, M., P. Van den Heede, N. De Belie, D. Bajare, G. Sahmenko and A. Korjakins (2018). Comparative life cycle assessment of magnesium binders as an alternative for hemp concrete. Resources, Conservation and Recycling **133**: 288-299.

Valls, S. and E. Vazquez (2001). Accelerated carbonatation of sewage sludge–cement–sand mortars and its environmental impact. Cement and Concrete Research **31**(9): 1271-1276.

Zhang, B. and C. S. Poon (2018). Sound insulation properties of rubberized lightweight aggregate concrete. Journal of Cleaner Production **172**: 3176-3185.

Chapter 4. Effect of CO_2 Curing on Properties of Cement Pastes

4.1 Introduction

The application of MOC for practical engineering projects has been limited by its poor water resistance. Previous studies found that the compressive strength of MOC decreased significantly when it is immersed in water for 28 days, due to the decomposition of hydration products, Phase 5 ($5Mg(OH)_2•MgCl_2•8H_2O$)and Phase 3 ($3Mg(OH)_2•MgCl_2•8H_2O$), which are the main sources of strength (Chau et al. 2009, Li et al. 2010).

It has been reported that during natural carbonation of MOC, the Phase 5 would be transformed into Phase 3 hydration products. When Phase 3 is further carbonated, new phases would be formed as follows(De Castellar et al. 1996, Maravelaki-Kalaitzaki and Moraitou 1999):

$$5Mg(OH)_2•MgCl_2•8H_2O \rightarrow 3Mg(OH)_2•MgCl_2•8H_2O + 2Mg(OH)_2 \quad (4\text{-}1)$$

$$3Mg(OH)_2•MgCl_2•8H_2O + 2CO_2 \rightarrow Mg(OH)_2•MgCl_2•2MgCO_3•6H_2O + 2\,H_2O \quad (4\text{-}2)$$

This new phase ($Mg(OH)_2•MgCl_2•2MgCO_3•6H_2O$) is much less soluble in water than either of Phase 5 and Phase 3, which means the carbonation may improve the water resistance of MOC. Carbon dioxide curing of concrete is distinct from natural carbonation, because the carbonation reaction occurs at early age and is used to accelerate the strength gain and to reduce the early drying shrinkage of cement products(Berger et al. 1972, Zhan et al. 2014).

Besides, high purity and pressure of CO_2 gas result in rapid reaction between CO_2 and cementitious material(Shi et al. 2011). The positive effects of CO_2 curing on the mechanical properties of cement products have attracted increasing number of studies on accelerated

carbonation of Ordinary Portland cement(Shi et al. 2012, Zhan et al. 2016), cement-solidified wastes(Zhan et al. 2013, Morandeau et al. 2015), aerated lime-based mortars(Cultrone et al. 2005)etc.

In this chapter, CO_2 curing was adopted to accelerate the carbonation reactions aiming to improve the water resistance of MOC paste. The effect of the CO_2 curing on the performance of the MOC paste was assessed in terms of compressive strength, water resistance and volume stability.

4.2 Sample preparation

Previous literatures suggested that the molar ratio of magnesium oxide to magnesium chloride should be more than 5 in order to ensure the complete reaction of magnesium chloride(Li and Chau 2007, Chau and Li 2008). So for MOC paste, the molar ratio of 9 was adopted. The molar ratio of $H_2O/MgCl_2$ was 10 to obtain good workability. The MOC mortar sample was prepared to test volume stability of this cement during air cuing and water immersion. The mix proportion of the mortar was similar to that of the paste except that standard sand was added with a sand/binder ratio of 1.5.

The required amount of magnesium chloride was first dissolved in tap water and thoroughly mixed for about 1 min in a mechanical mixer. Afterwards, magnesium oxide powder and sand (if applicable) were added and the materials were further mixed for about 3 min. The prepared materials were then cast into steel molds. The compressive strength and volume stability of MOC were determined on cubic specimens (20×20×20 mm), cylindrical (25×25×285 mm) specimens, respectively. After casting, the specimens were covered by a plastic sheet and cured initially for 24 h at room temperature (25°C). Then, the specimens were further cured in air for 3, 7 and 14 days, respectively. The other specimens were cured in air for 13 days followed by CO_2 curing for 1 day.

4.3 Test results and discussions

4.3.1 Effect of CO_2 curing on the compressive strength and water resistance

The strength development characteristics of MOC paste are shown in Figure 4-1 (An means air curing for n days; A13C means air curing for 13 days followed by 1 day of CO_2 curing). A rapid strength development can be seen with the prolongation of curing time. After 14 days of air curing, the compressive strength of MOC paste reached around 180MPa. In comparison with the control one, the specimens subjected to CO_2 curing demonstrated slight lower strength.

Figure 4-2 illustrates the compressive strength of MOC in water after soaking different ages. It can be seen that the strength of MOC without CO_2 curing decreased significantly after soaking into water. After 28 days of soaking, the strength was only about 8% of the value before immersed into water. This is in agreement with previous research that the hydration products will decompose to $Mg(OH)_2$ phase and some soluble ions when hardened MOC paste is immersed in water, which results in the significantly decrease of compressive strength(Deng 2003). It also can be found that the CO_2 curing could improve the water resistance of MOC as the strength decreased 58% after 28 days of water soaking, which is much lower than that of mixture without CO_2 curing. And after 28 days of immersing, the decrease of strength tended to plateau.

The effect of CO_2 curing on the strength retention coefficient of MOC is shown in Table 4-1. MOC paste subjected to CO_2 curing exhibited higher strength retention coefficient than the one without CO_2 curing for all the soaking time, which means the CO_2 curing could improve water resistance of MOC. For instance, the strength retention coefficient of paste after 28 days of air curing were only 8.2%, while for the one subjected to CO2 curing, this value increased to 40.4%.

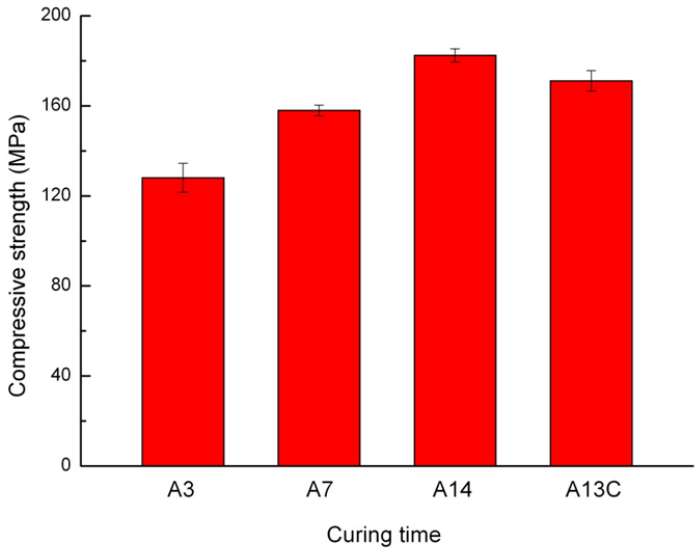

Figure 4-1 Compressive strength of MOC paste with and without CO_2 curing

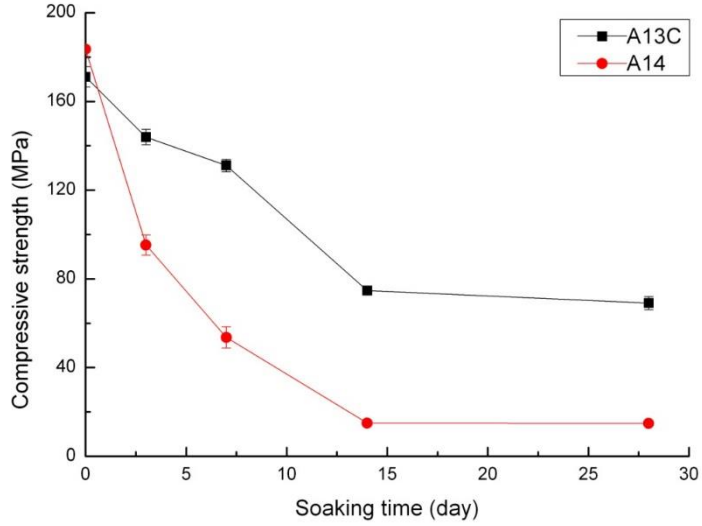

Figure 4-2 Effect of CO_2 curing on the water resistance of MOC paste

Table 4-1 Strength retention coefficient (%)

Curing time	SR_3	SR_7	SR_{14}	SR_{28}
A14	52.2	30.7	11.7	8.2
A13C	83.4	75.5	52.3	40.4

4.3.2 Mechanism of CO_2 curing enhancing water resistance of MOC paste

XRD result

XRD analysis (Figure 4-3) was conducted for specimens with and without CO_2 curing. In XRD diffractogram of cement after 14 days of air curing, typical hydration product (Phase 5) and unreacted MgO were identified. New phase was observed after soaked in water, which was identified as $Mg(OH)_2$. This result was in agreement with previous research that Phase 5 decomposed in water and $Mg(OH)_2$ was generated (Deng 2003). The diffraction peak shows the major phase in the specimens subjected to CO_2 curing was still Phase 5 and no $Mg(OH)_2$ was observed after water soaking for 7 days, which could explain the higher strength retention than the control one. This result confirmed that CO_2 curing could prevent the decomposition of Phase 5 and improve the water resistance of MOC. It is interesting to notice that no new crystalline phase was generated in these samples before and after water soaking, indicating that the product that improved the water resistance of MOC was an amorphous phase. This amorphous phase could be tested in QXRD analysis, which is shown in Table 4-2.

From Table 4-2, it can be seen that the predominant hydration product in the hardened paste of the specimen in air for 14 days was crystalline Phase 5 and its content was 69.5%. After 14 days of air curing, there were about 27.5% of unreacted MgO in MOC paste. When immersed

in water for 7 days, the content of Phase 5 was decreased by 49% and the $Mg(OH)_2$ was identified. After soaking for 14 days, the Phase 5 disappeared and the main phase was $Mg(OH)_2$. No new crystalline phase was observed after CO_2 curing, but the content of Phase 5 decreased and amorphous content increased, indicating that CO_2 reacted with Phase 5 and generated amorphous phase. After soaking in water for 14 days, the content of Phase 5 was 39.1%. This result shows that the amorphous phase could prevent the decomposition of the hydration product and thus improving the water resistance of MOC.

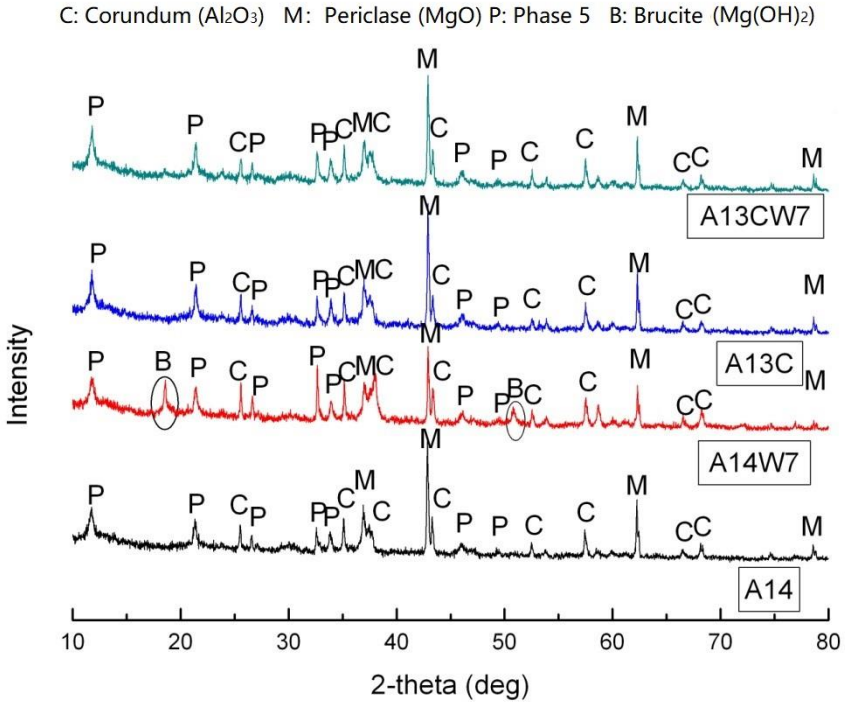

Figure 4-3 XRD patterns of MOC paste subject to different curing regimes

Table 4-2 Phase composition of MOC paste subject to different curing regimes

No.	Phase Contents (wt. %)			
	MgO	Phase 5	$Mg(OH)_2$	Am

A14	27.5	69.5	--	--
A14W7	13.6	35.4	21.3	29.7
A14W14	5.2	--	68.5	25.3
A13C	27.4	35.7	--	26.2
A13CW7	20.4	51.5	--	28.1
A13CW14	12.3	39.1	18.0	21.4

SEM result

The magnification of all the SEM micrographs is 3000x. The typical morphology of the hardened MOC paste is shown in Fig 4-4(a). The needle-like crystals formed in the cement paste were recognized as Phase 5 hydrates by energy spectrum analysis as the molar ratio of Mg to Cl was3.05(Figure 4-4 (b)). After soaking in water for 7 days, Phase 5 was decomposed to flake like $Mg(OH)_2$ (Figure 4-5). The morphologies of the hydration products on the fracture surface of the hardened specimens subjected to CO_2 curing are revealed in Figure 4-6. In addition to the needle-like Phase 5, a gel-like phase with no clear edge could be found in the mixture, which contained Mg, Cl , C and O. It was not identified from XRD spectrum due to the amorphous characteristics. This gel was stable in water and inter grew with Phase 5, thus preventing the decomposition of Phase 5. So the gel and Phase 5 was still present in the specimen after immersing in water for 14 days (Figure 4-7).

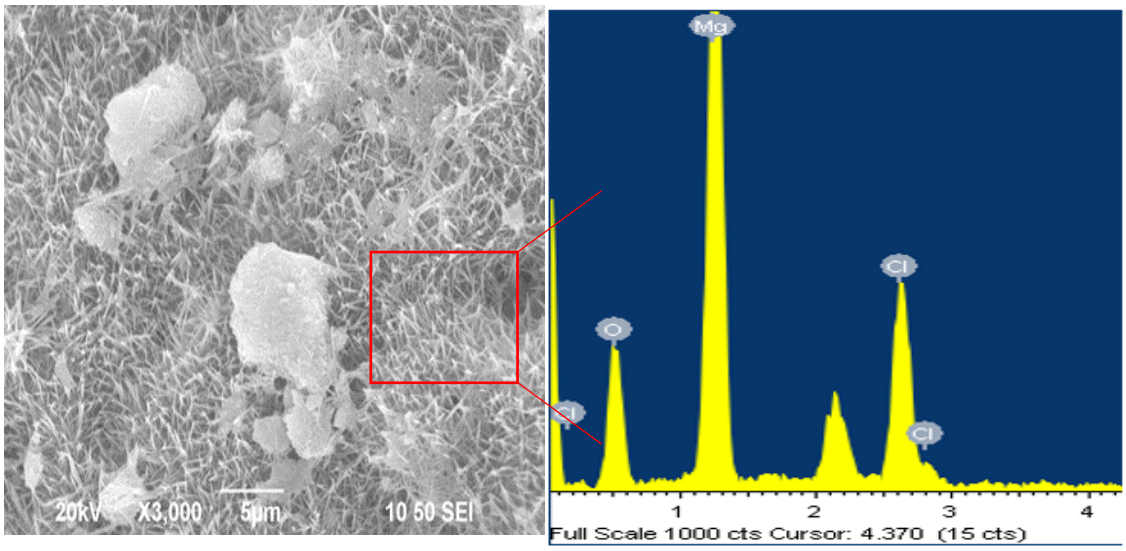

Figure 4-4 SEM-EDXA analysis of MOC paste after 14 days of air curing (a)SEM image (b)EDXA pattern

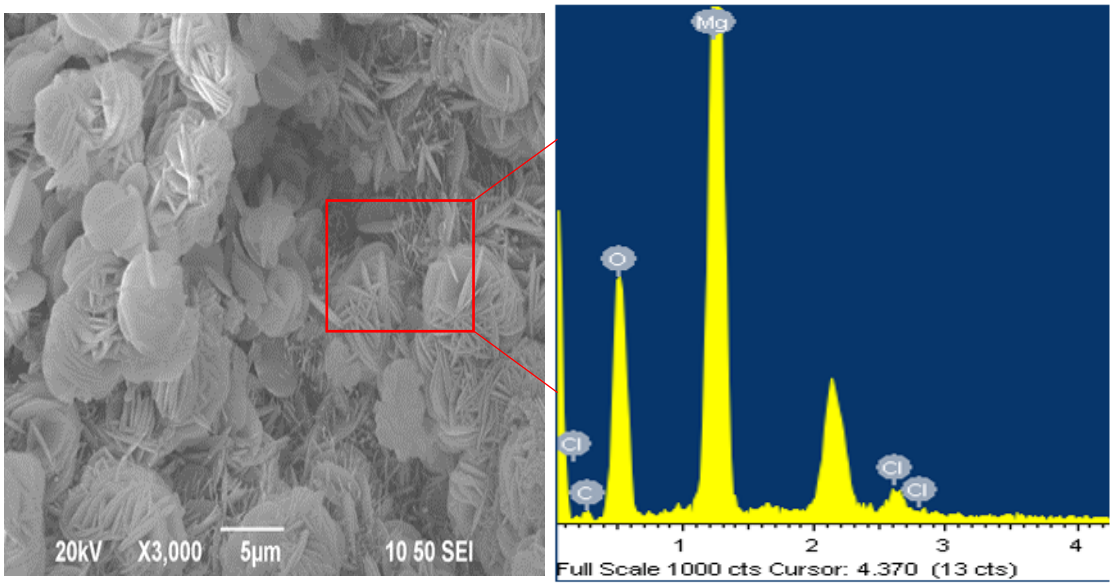

Figure 4-5 SEM-EDXA analysis of MOC paste after immersed in water for 14 days (a)SEM image (b)EDXA pattern

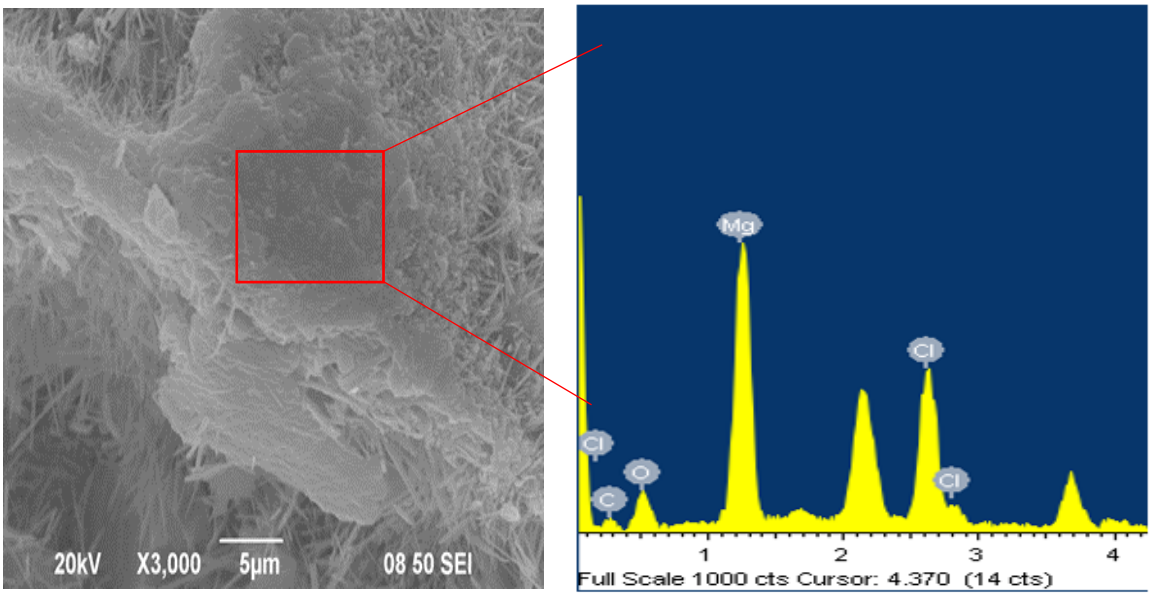

Figure 4-6 SEM-EDXA analysis of MOC paste after CO_2 curing (a)SEM image (b)EDXA pattern

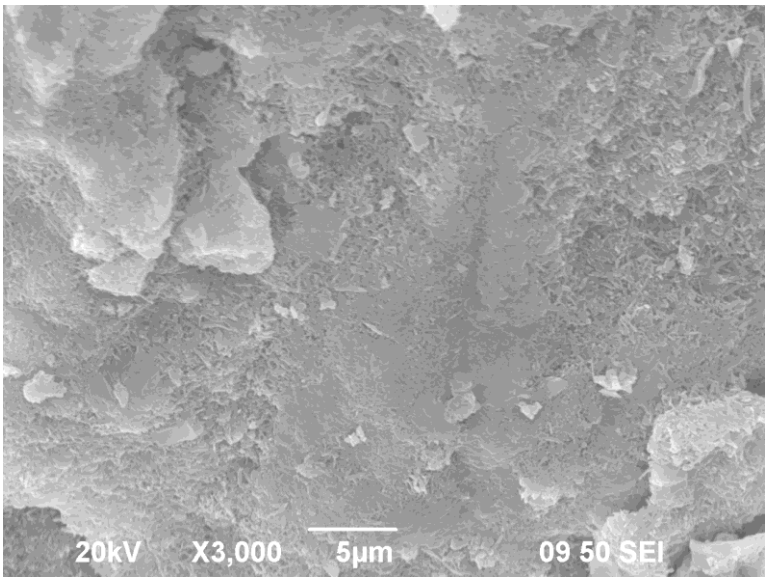

Figure 4-7 SEM analysis of MOC paste after CO_2 curing and 14 days of water soaking

4.4 Summary

This chapter studied the effect of CO_2 curing on the compressive strength and water resistance of MOC paste. The compressive strength of MOC paste decreased slightly after CO_2 curing,

but the strength retention coefficient significantly increased. After 28 days of water immersion, the strength retention coefficient of the control MOC paste was 8.2%, while this value was 40.4% for the sample subjected to CO_2 curing. According to XRD and SEM results, no new crystalline phase was generated during CO_2 curing but the amorphous phase content increased. This amorphous phase was stable in water and interlocked with the hydration products (e.g. Phase 3 and Phase 5), thus protected the hydration products from decomposition.

Reference

Berger, R., J. Young and K. Leung (1972). Acceleration of hydration of calcium silicates by carbon dioxide treatment. Nature **240**(97): 16-18.

Chau, C., J. Chan and Z. Li (2009). Influences of fly ash on magnesium oxychloride mortar. Cement and Concrete Composites **31**(4): 250-254.

Chau, C. and Z. Li (2008). Microstructures of magnesium oxychloride. Materials and structures **41**(5): 853-862.

Cultrone, G., E. Sebastian and M. O. Huertas (2005). Forced and natural carbonation of lime-based mortars with and without additives: Mineralogical and textural changes. Cement and Concrete Research **35**(12): 2278-2289.

De Castellar, M., J. Lorente, A. Traveria and J. Tura (1996). Cracks in Sorel's cement polishing bricks as a result of magnesium oxychloride carbonatation. Cement and Concrete Research **26**(8): 1199-1202.

Deng, D. (2003). The mechanism for soluble phosphates to improve the water resistance of magnesium oxychloride cement. Cement and Concrete Research **33**(9): 1311-1317.

Li, Z. and C. Chau (2007). Influence of molar ratios on properties of magnesium oxychloride cement. Cement and Concrete Research **37**(6): 866-870.

Li, Z. J., F. Qiao and C. K. Chau (2010). Recent Development of Magnesium-Based Cements-Magnesium Phosphate Cement and Magnesium Oxychloride Cement. Advances in Science and Technology, Trans Tech Publ.

Maravelaki-Kalaitzaki, P. and G. Moraitou (1999). Sorel's cement mortars: Decay susceptibility and effect on Pentelic marble. Cement and Concrete Research **29**(12): 1929-1935.

Morandeau, A., M. Thiéry and P. Dangla (2015). Impact of accelerated carbonation on OPC cement paste blended with fly ash. Cement and Concrete Research **67**: 226-236.

Shi, C., F. He and Y. Wu (2012). Effect of pre-conditioning on CO 2 curing of lightweight concrete blocks mixtures. Construction and Building Materials **26**(1): 257-267.

Shi, C., M. Liu, Q. Zou, F. He, C. Leung and K. WAN (2011). A study on factors influencing compressive strength of CO2-cured concrete. International RILEM conference on advances in construction materials through science and engineering, RILEM Publications SARL.

Zhan, B., C. Poon and C. Shi (2013). CO 2 curing for improving the properties of concrete blocks containing recycled aggregates. Cement and Concrete Composites **42**: 1-8.

Zhan, B., C. S. Poon, Q. Liu, S. Kou and C. Shi (2014). Experimental study on CO 2 curing for enhancement of recycled aggregate properties. Construction and Building Materials **67**: 3-7.

Zhan, B. J., C. S. Poon and C. J. Shi (2016). Materials characteristics affecting CO 2 curing of concrete blocks containing recycled aggregates. Cement and Concrete Composites **67**: 50-59.

Chapter 5. Effect of Supplementary Cementitious Materials and CO_2 curing on Water Resistance of Cement Pastes

5.1 Introduction

Many researchers used various additives to overcome the problem of water instability of MOC pastes and found that some additives were very useful, such as sulfate and phosphate (Lu et al. 1994, Li et al. 2016). It was proposed that phosphate could react with MOC to produce insoluble hydration products such as magnesium phosphate that protected the hydration products from decomposing(Li et al. 2008). However, it was argued that the quantity of the insoluble phosphates was not high enough to produce a layer of the insoluble phosphates(Deng 2003). On the other hand, some studies revealed the transformation from the crystalline to gel-like Phase 5, which was believed to be the main reason for the improved water resistance of MOC when adding phosphate(Li et al. 2016).

Although adding additives is an effective way to improve the water resistance of MOC, it increases the cost of producing the material. Another method to improve the water resistance of MOC is adding SCMs.

Fly ash is a promising waste material that can significantly improve the water resistance of MOC. Previous studies found that the residual compressive strength of MOC mortars incorporating 30% fly ash cured in air for 14 days was about 80% of the initial value even after immersion in water for 28 days(Chan and Li 2006, Chau et al. 2009). However, the mechanism of such improvement is still not well understood.

Waste glass beverage bottles consist of non-crystalline silica, sodium oxide, calcium oxide and other components (Shao et al. 2000, Shayan and Xu 2004, Mageswari and Vidivelli 2010). Efforts have been made in the concrete industry to use waste glass as aggregates for the production of concrete or cement mortars (Kou and Poon 2009, Idir et al. 2010, Ling and Poon 2011, Zhan et al. 2013). With high quantities of amorphous silica, crushed glass powder should be an excellent pozzolanic material for the concrete industry(Shi et al. 2005, Chen et al. 2006, Idir et al. 2011). This had been confirmed in previous studies that the glass power-blended cement demonstrated equivalent compressive strength to the control cement when using 30% of glass powder with particle size smaller than 38 μm to replace cement (Shao et al. 2000).

As a consequence of waste water treatment, a large amount of sewage sludge is produced every day in urban municipalities such as Hong Kong. The traditional landfilling method is not acceptable to manage this waste as it adversely impacts human health and the environment(Dean and Suess 1985, Poon and Boost 1996). An alternative for sewage sludge disposal is incineration, which can achieve significant reductions of material volume(Monzo et al. 1999) and leaving only a small residual quantity of ISSA.. The incineration process at T-Park in Hong Kong reduces the volume of the waste. But the residual ISSA still amounts to about 100-200 tonnes/day which is currently disposed of at landfills. Many green approaches have been developed to recycle the ISSA. Test results indicated that the major elements in ISSA are Si, Al, Ca, Fe and P(Cyr et al. 2007, Donatello and Cheeseman 2013). ISSA can be used to manufacture bricks(Alleman and Berman 1984, Okuno and Takahashi 1997, Wiebusch and Seyfried 1997), tiles(Anderson 2002), and lightweight aggregates(Bhatty and Reid 1989, Cheeseman and Virdi 2005), etc. Additionally, a number of investigations have evaluated the potential of ISSA as a supplementary cementitious material due to a presumed moderate pozzolanic activity (Davraz and Gunduz 2005, Chen and Poon 2016). However, it should be noted that factors such as fineness(Pan et al. 2003), acid pre-treatment (Donatello et al.

2010)and test method used (Donatello et al. 2010)will significantly influence any assessment of the pozzolanic activity of ISSA. Considering the moderate pozzolanic nature and its high phosphate content, ISSA may be useful to improve the water resistance of MOC. However, no previous study was conducted before on this.

In this chapter, the effect of three types of SCMs: PFA, GP and ISSA on the water resistance of MOC paste subjected to CO_2 curing was reported in terms of strength retention coefficient and volume stability. The compositions and microstructure of the sample were analyzed by XRD, SEM etc.

5.2 Sample preparation

Table 5-1 and Table 5-2 show the mix proportions of the paste and mortar specimens prepared. The pastes and mortars were mixed in a mechanical mixer and cast in cubic molds (20 mm ×20 mm×20 mm) and cylindrical molds (25 mm ×25 mm×285 mm), respectively. The fresh samples were covered with a polyethylene sheet to avoid evaporation. The samples were then removed from the molds after 24h for air curing. Then, some specimens were further cured in air for 3, 7 and 14 days, respectively. The other specimens were cured in air for 13 days followed by CO_2 curing for 1 day. Then all the specimens were immersed in water for different periods of time.

Table 5-1 Mix proportions of MOC paste

Mixtures	Molar ratios		PFA (%,by	GP (%,by	ISSA (%,by
Notation	$MgO/MgCl_2$	$H_2O/MgCl_2$	weight of MgO)	weight of MgO)	weight of MgO)
P0	9	10	--	--	--

PF1	8.1	10	10	--	--
PF2	7.2	10	20	--	--
PF3	6.3	10	30	--	--
PG1	8.1	10	--	10	--
PG2	7.2	10	--	20	--
PG3	6.3	10	--	30	--
PS1	8.1	10	--	--	10
PS2	7.2	10	--	--	20
PS3	6.3	10	--	--	30

Table 5-2 Mix proportions of MOC mortar

Mixtures	Molar ratios		PFA (%,by	GP (%,by	ISSA (%,by	Sand/powder
Notation	$MgO/MgCl_2$	$H_2O/MgCl_2$	weight of MgO)	weight of MgO)	weight of MgO)	
M0	9	10	--	--	--	
MF1	8.1	10	10	--	--	
MF2	7.2	10	20	--	--	1.5
MF3	6.3	10	30	--	--	
MG1	8.1	10	--	10	--	

MG2	7.2	10	--	20	--
MG3	6.3	10	--	30	--
MS1	8.1	10	--	--	10
MS2	7.2	10	--	--	20
MS3	6.3	10	--	--	30

5.3 Test results and discussion

5.3.1 Effect of PFA on water resistance

5.3.1.1 Compressive strength

Figure 5-1 shows the strength development characteristics of the MOC paste with different amounts of PFA (A_n means air (A) curing for n days; $A_{13}C$ means air curing for 13 days followed by 1 day of CO_2 curing). In general, the compressive strength of all the mixtures increased with the increase in curing age. It can be seen that the compressive strength declined with the increase of PFA dosage at all ages, which were consistent with the results of other research studies(Chau et al. 2009). For instance, the strength values for the paste incorporating 10%, 20%, 30% of PFA were 152.3, 124.3, 118.5 MPa, respectively, at 14 days of air curing. The specimens received CO_2 curing had a slightly lower strength as compared to the one without CO_2 curing. The strength of the paste with 10%, 20% and 30% of PFA were found to be reduced by about 4.4%, 6.7%, and 4.0%, respectively.

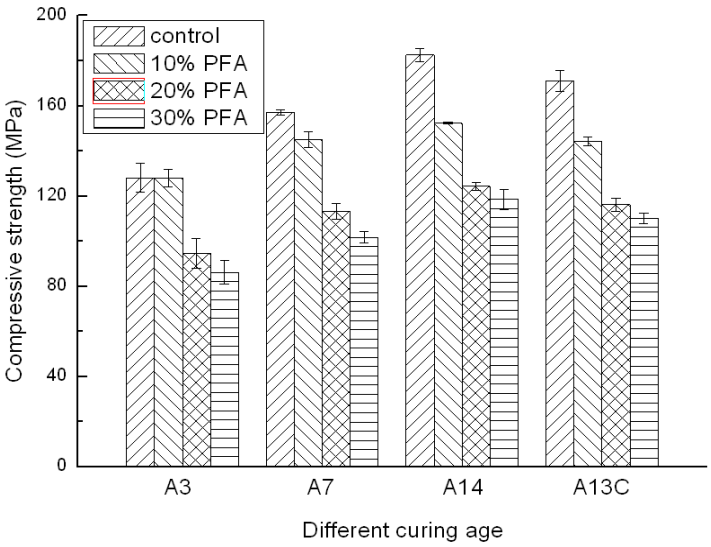

Figure 5-1 Compressive strength of MOC with PFA

Figures 5-2 illustrate the compressive strength of the MOC paste blended with different amounts of PFA before and after water immersion ($A_{14}W_n$ means air curing for 14 days followed by immersion in water for n days). After immersion in water for 28 days, the strength of the MOC paste incorporating with 0%, 10%, 20%, and 30% of PFA decreased by about 170 MPa, 110 MPa, 60 MPa, and 30 MPa, respectively (Figure 5-2). For the specimen subjected to CO_2 curing (Figure 5-3), these values were 100 MPa, 95 MPa, 10 MPa, 20 MPa, which showed that the MOC paste incorporating PFA had much better water resistance after CO_2 curing than the control one.

The effect of PFA incorporation and CO_2 curing on the strength retention coefficient of MOC incorporating PFA is shown in Table 5-3. A higher content of PFA resulted in a higher strength retention coefficient. When adding 30% of PFA, the value reached 72.2%. After CO_2 curing, the mixtures incorporating PFA exhibited even higher retention coefficient, probably because of the formation of new carbonated phases. In this study, the CO_2 curing could improve the water resistance of MOC, which might be due to the reaction of CO_2 and hydration products (Phase 3 or Phase 5) forming stable amorphous products. The MOC incorporating 30% of PFA contained less hydration products compared to that with 20% of PFA. The former composites

might show less effectiveness on the improvement of water resistance compared to the latter one. Therefore, the highest value was obtained when adding 20% of PFA (91%).

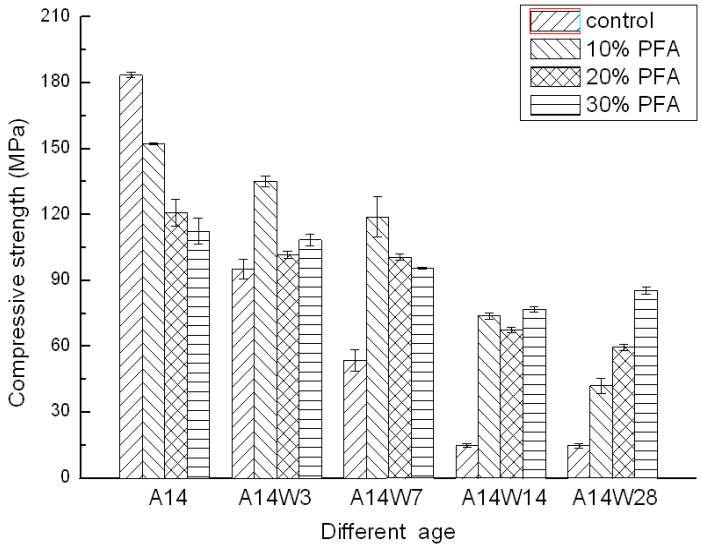

Figure 5-2 Effect of PFA on the water resistance of MOC

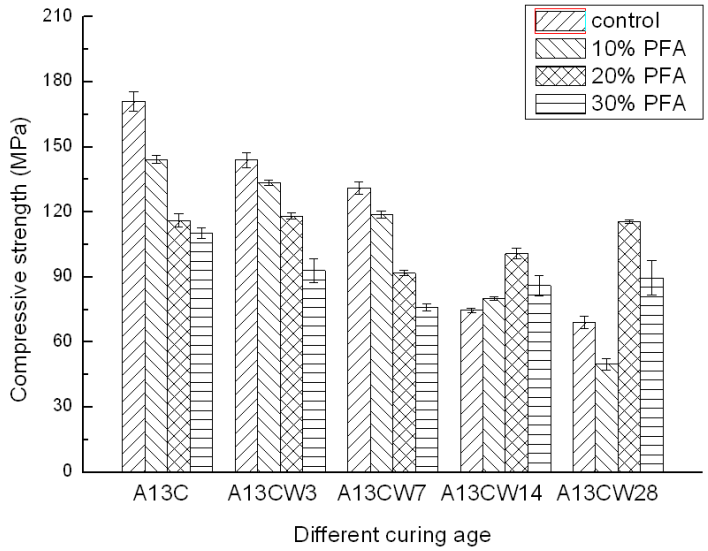

Figure 5-3 Effect of PFA on the water resistance of MOC subjected to CO_2 curing

Table 5-3 Strength retention coefficient (%)

Curing condition	Content of PFA (%)			
	0	10	20	30
Without CO_2 curing	8.2	27.6	47.9	72.2
With CO_2 curing	40.0	34.5	91.0	81.4

5.3.1.2 Volume stability

The volume stability of the MOC mortar incorporating different dosages of PFA is presented in Figure. 5-4. When the mortar specimens were stored in air, expansion occurred at an early age, which was due to the formation of hydration products with larger volumes. This can be calculated using the formulae in (5-1) and (5-2):

$$5MgO + MgCl_2 \bullet 6H_2O + 7H_2O \rightarrow 5Mg(OH)_2 \bullet MgCl_2 \bullet 8H_2O \quad (5\text{-}1)$$

$$3MgO + MgCl_2 \bullet 6H_2O + 5H_2O \rightarrow 3Mg(OH)_2 \bullet MgCl_2 \bullet 8H_2O \quad (5\text{-}2)$$

Table 5-4 Physical properties of raw materials and hydration products (Beaudoin and Ramachandran)

	MgO	$MgCl_2 \bullet 6H_2O$	Phase 5	Phase 3
Density(g/cm^3)	3.58	1.64	1.91	1.86
Molar mass(g/mol)	40	202	528	412
Molar volume(cm^3/mol)	11.17	123.2	276.4	221.5

It can be seen from Table 5-4 that the volume of the solid material was increased by more than 40% during hydration. However, the increase of solid volume does not necessarily result in

bulk expansion. It had been reported that crystal growth processes at non-bonding interfaces were usually responsible for bulk expansion, and the quantity and nature of the bonding interfaces and non-bonding interfaces played a dominant role over the bulk properties of the crystals (Gartner 2009). Therefore, the expansion of MOC mortar was highly likely related to the crystal growth processes at non-bonding interfaces. Further research is needed to explore this hypothesis.

After 7 days of air curing, the expansion reached a plateau. From Figure. 5-4, it is clear that the incorporation of PFA increased the expansion at all ages. For instance, the use of 10%, 20%, and 30% PFA (i.e., MF1, MF2, and MF3) increased the length change by 0.11%, 0.19%, and 0.24%, respectively, after 14 days of air curing. It might be attributed to the formation of a gel-like phase following the addition of PFA that took up a small amount of moisture in air and increased the solid volume (Brew and Glasser 2005). But it is important to note that the early expansion was negligible when compared to the mortar immersed in water as shown in Figure. 5-5.

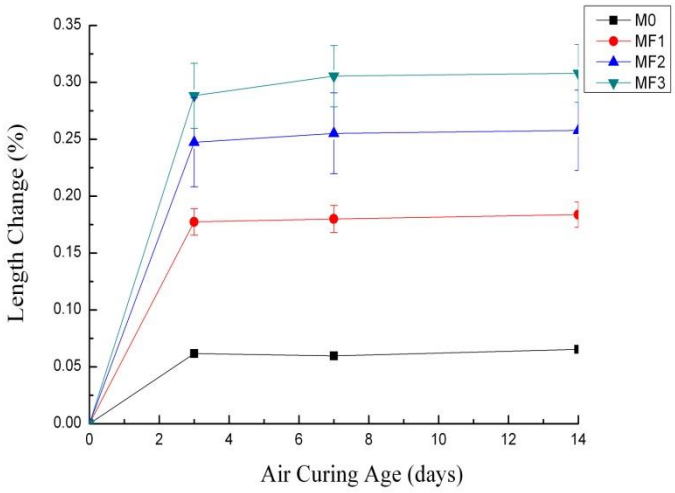

Figure 5-4 Dimensional stability of MOC mortars with PFA under air curing

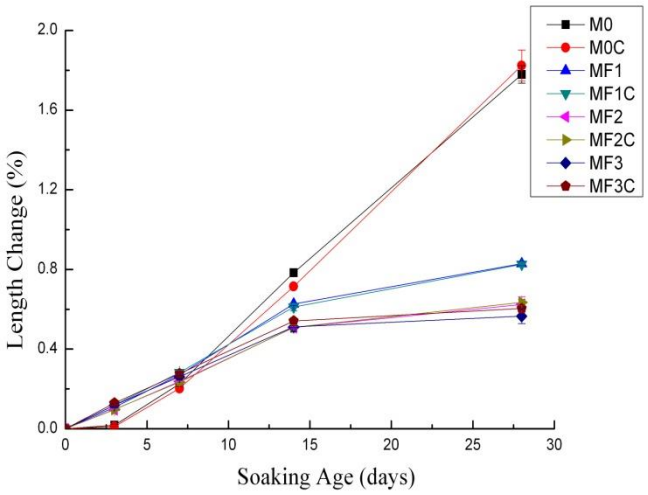

Figure 5-5 Dimensional stability of MOC mortars with PFA under water immersion

Figure 5-5 shows the length change of the mortar specimens incorporating PFA after immersion in water for different periods of time. Even though the adding of PFA increased the expansion in air, it improved the volume stability of the mortar specimens after immersion in water. The expansion of the control mortar increased significantly in water and reached 1.8% after 28 days. Such expansion, which is caused by the hydration of excess MgO and growth of $Mg(OH)_2$ in the control mortar samples, could lead to cracking and damage of the cement structure(Chatterji 1995). The PFA-blended mortar displayed much lower expansion. For instance, the mortar prepared with 10% and 20% of PFA expanded only about 0.8% and 0.6% after 28 days of water immersion. An increase of the PFA content to 30% only induced a slight further decrease in expansion. There are two possible reasons: 1) the lower content of excess MgO due to the replacement of PFA and much less expansion of the amorphous gel than that of the transformation of MgO to brucite; 2) the formation of an inhibiting surface amorphous gel layer surrounding MgO as a result of the reaction between the PFA and MOC. Besides, the mortar subjected to CO_2 curing had similar expansion compared to the ones without CO_2 curing.

Thus, CO_2 curing is needed for enhancing strength retention, while PFA addition is sufficient for improving volume stability.

5.3.1.3 XRD

Figure 5-6 illustrates the XRD spectra of the control specimens before and after immersion in water. The presence of the typical hydration products (Phase 5) and unreacted MgO can be clearly observed after 14 days of air curing. The XRD peaks of Phase 5 were absent but those for $Mg(OH)_2$ increased significantly after the specimens were immersed in water for 14 days. Based on previous research, Phase 5 can be easily decomposed to $Mg(OH)_2$ in water(Deng 2003). On the contrary, the intensity of the Phase 5 in the PFA-blended paste was at about the same level before and after water immersion as shown in Figures. 5-7. This was consistent with the compressive strength result and proved that PFA can improve the water resistance of MOC. However, it is interesting to notice that no new crystalline phase was observed after adding PFA, which meant the products that improved the water resistance of MOC were amorphous in nature. Such amorphous phase could be quantified in QXRD analysis as shown in Table 5-5.

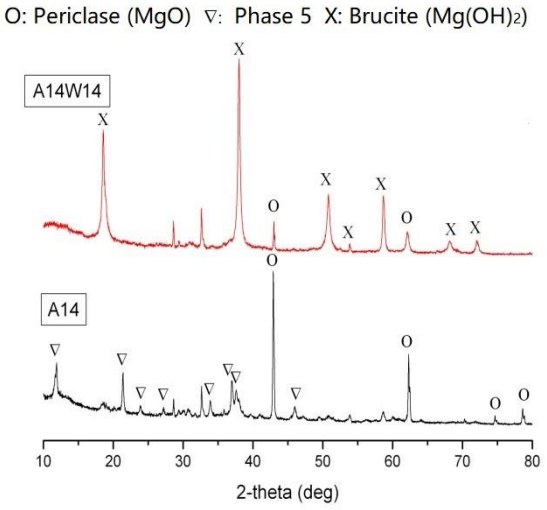

Figure 5-6 XRD spectra of MOC paste

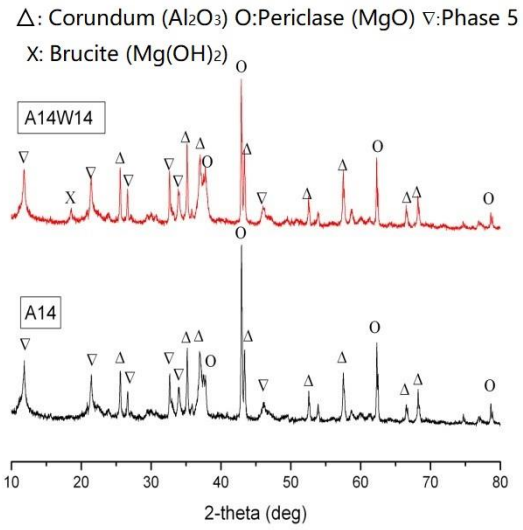

Figure 5-7 XRD spectra of MOC paste with 30% of PFA

The QXRD measurements shown in Table 5-5 (PF3C means PF3 cement paste subjected to CO_2 curing) indicate that the main hydration product in the hardened MOC paste was Phase 5, and the content of which was as high as 69.5% by mass. However, the Phase 5 was easily decomposed in water and produced $Mg(OH)_2$. When adding PFA, no new crystalline phase was found after 14 days of air curing. But more amorphous phase was found and its amount increased after water immersion. The amount of $Mg(OH)_2$ was much lower than the mix prepared without PFA incorporation and after water immersion. This result means that the PFA could react with MOC to generate amorphous products, which were stable in water. Meanwhile, the amount of the crystalline Phase 5 decreased while the formation of Phase 3 was observed after 14 days of water immersion, implying that a certain proportion of the crystalline Phase 5 was transformed to amorphous phases that were insoluble in water(Sorell and Armstrong 1976).The water resistance of this mixture was higher, so an appreciable amount of hydration products were still present even after 14 days of water immersion. The PFA-blended MOC specimens subjected to CO_2 curing showed a slightly higher water resistance than the one without CO_2 curing because more amorphous materials were formed (comparing A_{14} and $A_{13}C$). It was reported that the Phase5 could be carbonated and $Mg(OH)_2 \cdot MgCl_2 \cdot 2MgCO_3 \cdot 6H_2O$ was

generated. So this amorphous material might be Mg-Cl-C-H gel, but this needs to be confirmed by further research.

Table 5-5 Phase compositions of MOC paste incorporating PFA

No.		Phase Contents (by mass %)				
		MgO	Phase 5	Phase 3	$Mg(OH)_2$	Am
P0	A_{14}	27.5	69.5	2.8	--	--
	$A_{14}W_{14}$	5.2	--	--	68.5	25.3
PF3	A_{14}	17.5	53.5	0	--	24.7
	$A_{14}W_7$	15.6	31.1	0	--	50
	$A_{14}W_{14}$	7.3	12.1	13.1	5.8	58.6
PF3C	$A_{13}C$	21.2	40.7	--	0	38.1
	$A_{13}CW_7$	17.5	31.6	--	0	42.3
	$A_{13}CW_{14}$	9.2	11.9	18.1	--	60.8

5.3.1.4 TG

The results of the TG/DTG analysis of MOC with and without PFA are given in Figure. 5-8. In the thermographs of the MOC paste, there are four processes of dehydration and decomposition as follows(Xia et al. 1991):

$$5Mg(OH)_2{\cdot}MgCl_2{\cdot}8H_2O \rightarrow 5\ Mg(OH)_2{\cdot}MgCl_2{\cdot}4H_2O+4H_2O\ (50\text{-}130℃) \quad (5\text{-}3)$$

$$5Mg(OH)_2{\cdot}MgCl_2{\cdot}4H_2O \rightarrow 5\ Mg(OH)_2{\cdot}MgCl_2+4H_2O\ (140\text{-}200℃) \quad (5\text{-}4)$$

$5Mg(OH)_2 \cdot MgCl_2 \rightarrow Mg\ Cl_2 \cdot H_2O + 4H_2O + 5MgO (300\text{-}350℃)$ (5-5)

$MgCl_2 \cdot H_2O \rightarrow MgO + 2HCl\ (350\text{-}500℃)$ (5-6)

The weight loss below 350°C was due to the release of water. The vertical line at around 400-500°C might be due to the rapid release of HCl. Both the mass loss between 350 to 500 ℃ in 0% and 30% PFA incorporation (i.e., P0 and PF3) after 14 days of air curing were about 13%, but the water of crystallization in P0(19.7%) was higher than that of PF3(17.4%) as shown in Table 5-6. This suggested that the amount of water of crystallization associated with PF3 was less than that of P0. This is in agreement with the QXRD result (Table 5-5), which showed that new amorphous phases were produced when adding PFA and the amount of water of crystallization in these amorphous phases was less than that of Phase 5.

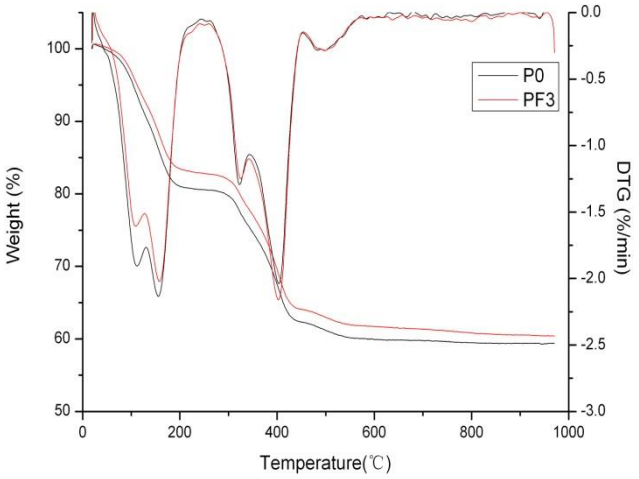

Figure 5-8 TG/DTG curves of MOC paste after 14 days of air curing

Table 5-6 Mass loss in MOC paste (%)

Temperature (℃)		P0	PF3
60-200	H_2O	19.7	17.4
200-350	OH	5.19	4.95

350-450	HCl	13.1	13.9
450-600	CO_2	2.27	2.25

5.3.1.5 FTIR

The FTIR spectra of the original PFA as well as the MOC paste blended with PFA are shown in Figure 5-9(a). The PFA spectrum shows two broad peaks at 1096 cm^{-1} and 460 cm^{-1}, which are the characteristics of the T-O stretching vibrations (T=Si or Al) and Si-O-Si deformation vibrations, respectively(Palomo et al. 1999). These two bands became sharper and shifted towards the higher frequency ranges in the PF3 mixture: 1162 cm^{-1}, 577 cm^{-1}. This was probably resulted from the reaction between PFA and MOC. Figure 5-9(b) and Figure 5-9(c) show the FTIR spectrum of MOC paste with and without the replacement of PFA in the 3600 cm^{-1}- 3800 cm^{-1} range and the 500 cm^{-1} - 1000 cm^{-1} range. The series of bands in the 3600 cm^{-1}- 3800 cm^{-1} range is the characteristics of the stretching modes of water molecules (Figure 5-9(b))(Fernández-Jiménez and Palomo 2005). The band at 3700 cm^{-1} shifted to a lower frequency and almost disappeared after CO_2 curing and blending with PFA, indicating the change of the water molecular structure due to the transformation of crystalline Phase 5 to the amorphous gel in P0C and the formation of an amorphous gel in PF3. The band at 856 cm^{-1} associated to Cl-O asymmetric stretching(Levason et al. 1990) was absent in P0C and PF3 samples because the formation of the amorphous gel changed the Cl-O bond(Figure 5-9(c)).

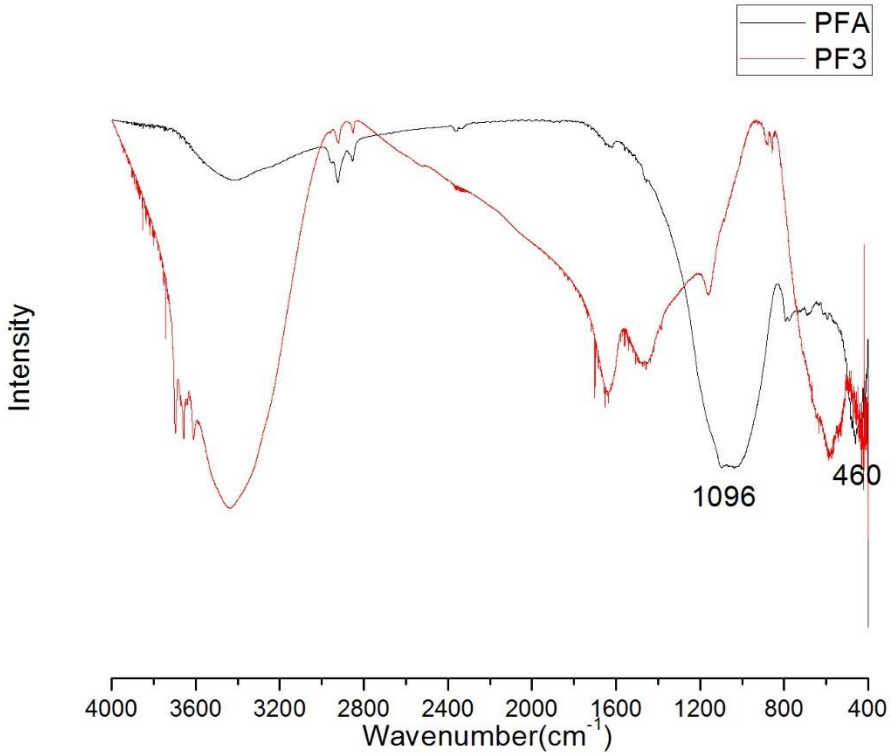
PFA
PF3
Intensity
1096
460
4000
3600
3200
2800
2400
2000
1600
1200
800
400
Wavenumber(cm-1)

(a)

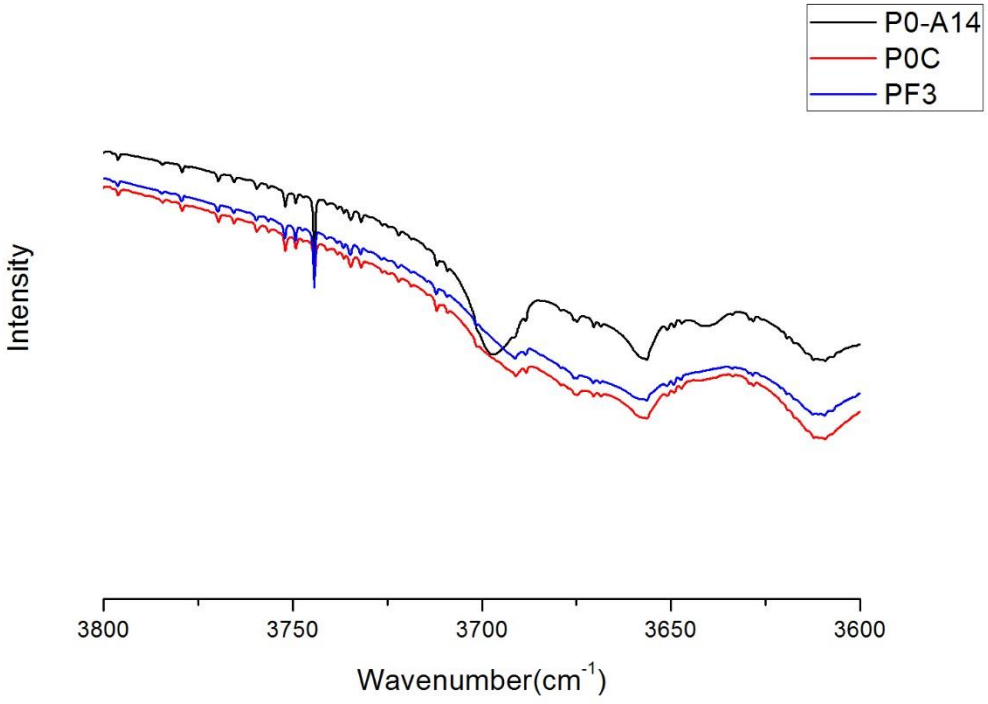
P0-A14
P0C
PF3
Intensity
3800
3750
3700
3650
3600
Wavenumber(cm-1)

(b)

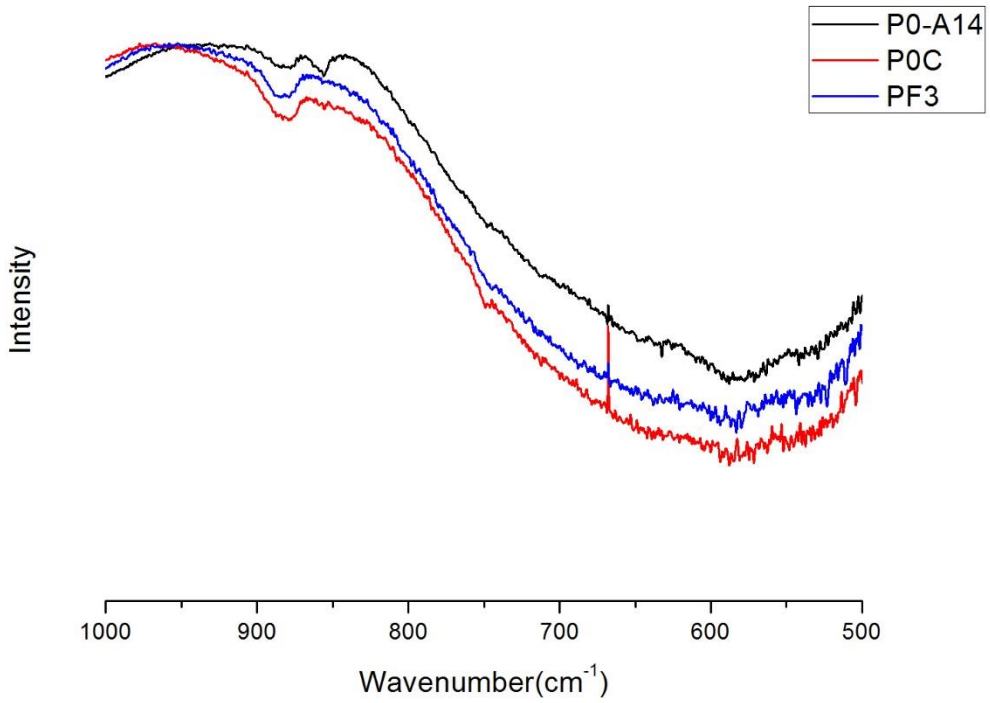

(c)

Figure 5-9 FTIR spectra of samples

5.3.1.6 SEM/EDX

As mentioned above, the main hydration product (i.e., Phase 5) in MOC paste was decomposed to $Mg(OH)_2$ after water immersion. While the MOC paste with 30% PFA (PF3 and PF3C) showed a dense structure after water immersion and no $Mg(OH)_2$ was observed according to EDX analysis (Figure 5-10).

To identify the amorphous gel observed in Figure 5-10, elemental maps were determined by EDX as shown in Figure 5-11. It clearly indicates the presence of irregularly shaped particles with a high concentration of Si, which was originally a PFA particle by EDX analysis. This is

probably the result of the reaction between PFA and MOC and the formation of a magnesium-silicate-hydrate gel (M- S-H gel) (Zhang et al. 2011, Zhang et al. 2014). The neighboring product contained only Mg, Cl, O with a molar ratio of 3.06:1:5. This means that PFA reacted with MOC during air curing and changed the morphology of Phase 5. The M-S-H gel and Phase 5 interlocked with each other and formed a compact and insoluble structure, thus improving the water resistance of MOC.

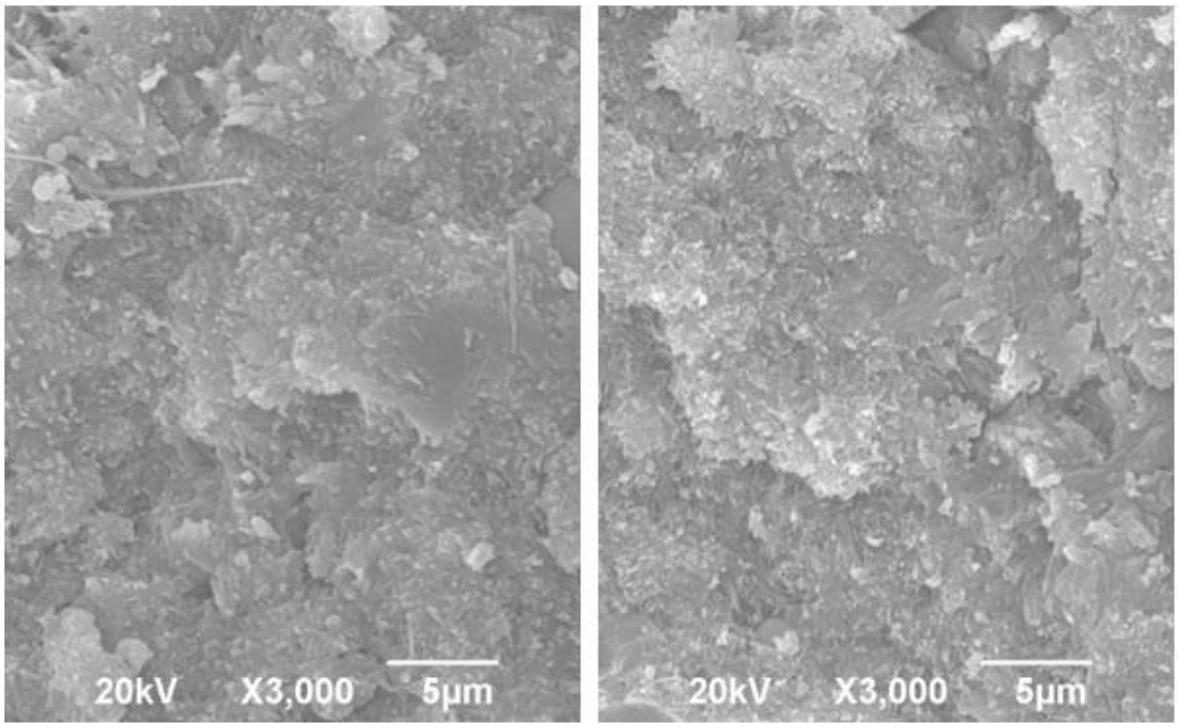

Figure 5-10 SEM analysis of PF3 (left) and PF3C (right) after immersion in water for 14 days

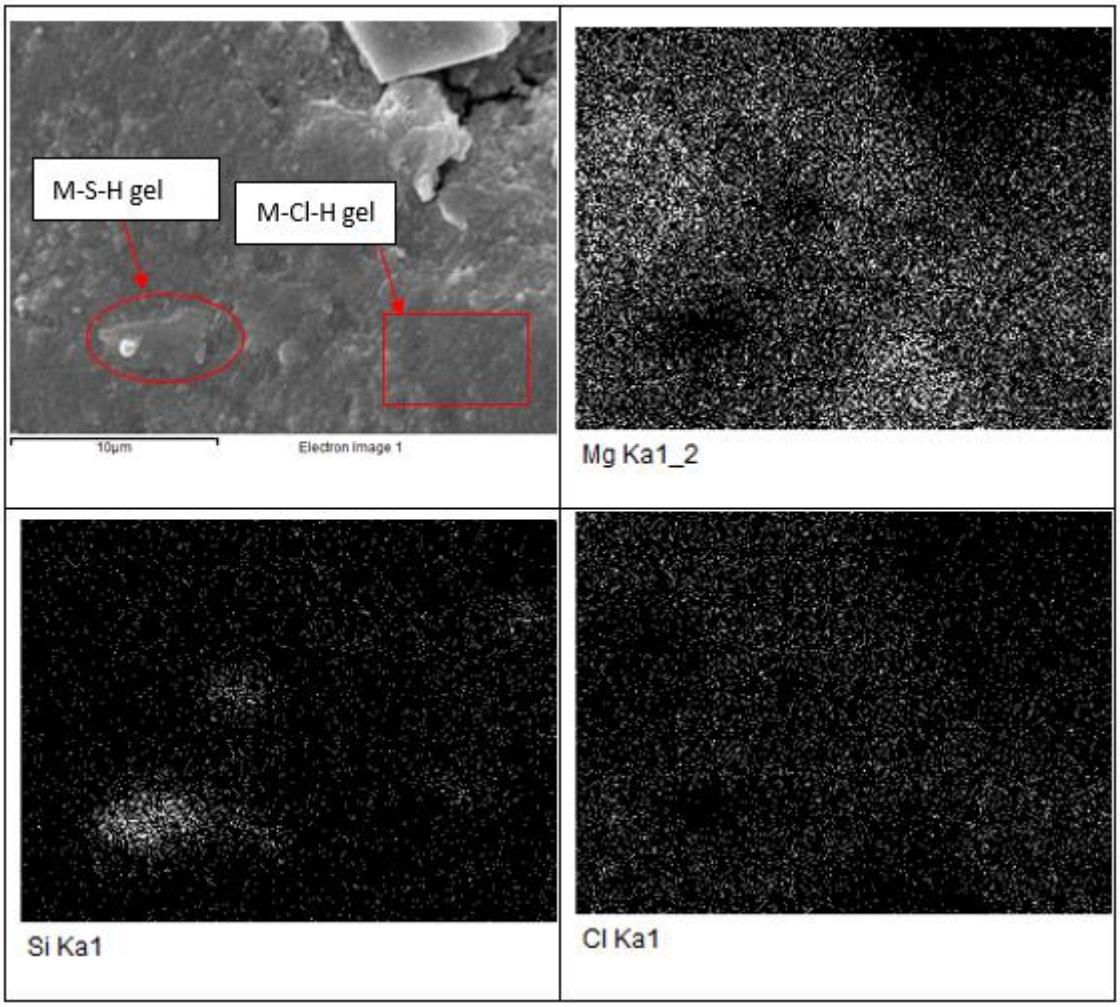

Figure 5-11 SEM-EDX analysis of polished PF3 after air curing for 14 days

5.3.2 Comparison of GP and PFA for improving the water resistance

5.3.2.1 Compressive strength

The characteristics of strength development of MOC paste with different amounts of GP and PFA incorporation are shown in Figure 5-12. The control paste had higher compressive strength than those of the blended pastes at all tested ages. The compressive strength of the blended pastes decreased with the increase in the replacement ratio of GP and PFA, which is consistent with the previous results (Chau et al. 2009). This is because the replacement of MgO decreased the quantity of the main hydration product (i.e., Phase 5) which provides

compressive strength in the MOC system. Besides, the paste prepared with GP showed higher compressive strength than those prepared with the same amount of PFA at all ages. There may be two reasons for that: 1) the lower water absorption of GP allowed more water available for hydration; 2) the pozzolanic reaction of PFA was faster than that of GP(Schwarz and Neithalath 2008, Chen and Poon 2015), thus leading to a lower quantity of Phase 5 in the GP-blended cement.

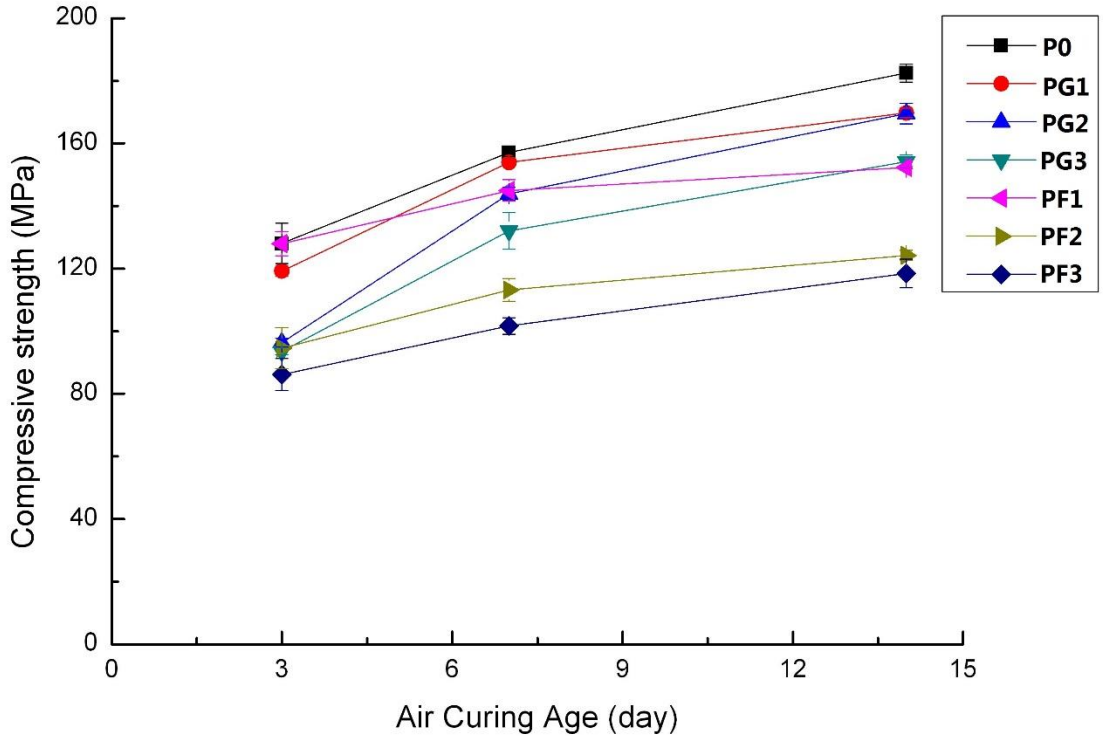

Figure 5-12 Compressive strength of MOC paste

Figure 5-13 shows the effect of GP and PFA on the compressive strength of MOC after water immersion. After water immersion for 28 days, the strength declined for the pure MOC was about 92%. When incorporating different percentages of GP, the residual strength was slightly higher than the control (a decline in the range of 75-80%), implying using GP could improve the water resistance of the paste but the improvement was insufficient. On the other hand, the

strength of F3 (incorporating PFA) was decreased by only 18%, indicating that the water resistance of PFA-blended cement was much higher than that of GP-blended cement.

The CO_2 curing could significantly improve the water resistance of MOC incorporating GP as the strength decreased only by 11%, 34%, and 28% after 28 days of water immersion when the GP amount was 10%, 20%, and 30%, respectively, as shown in Figure 5-14 (C means MOC pastes subjected to CO_2 curing).

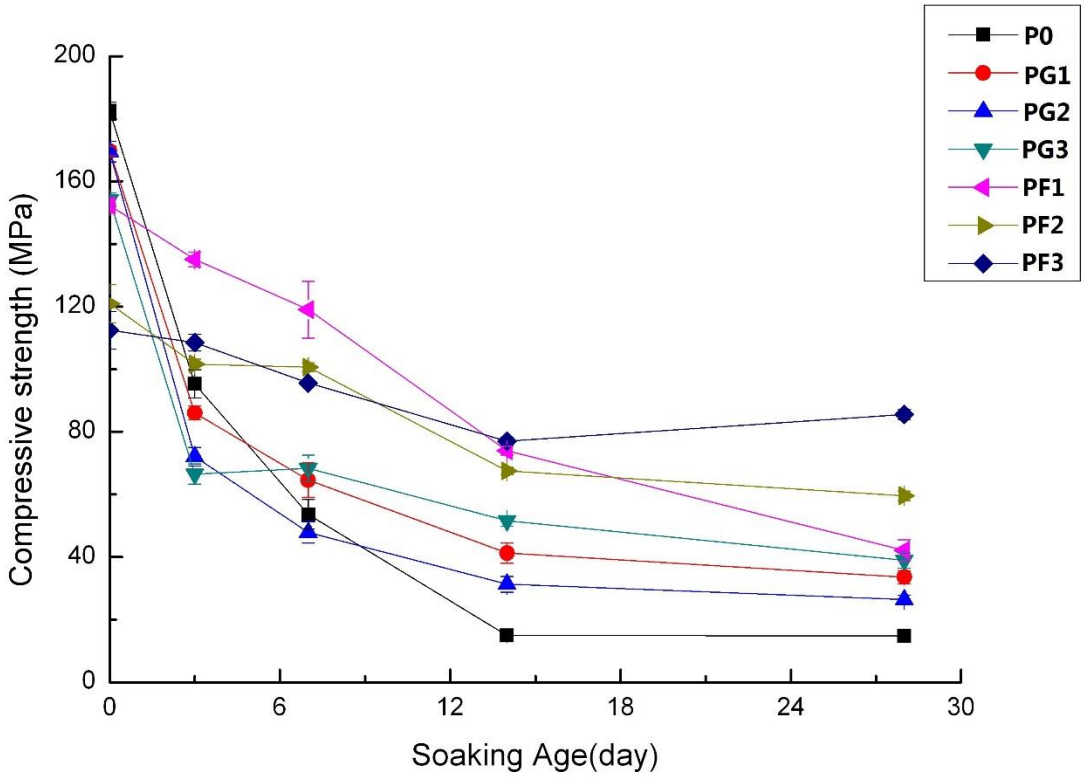

Figure 5-13 Effect of GP and PFA on the water resistance of MOC

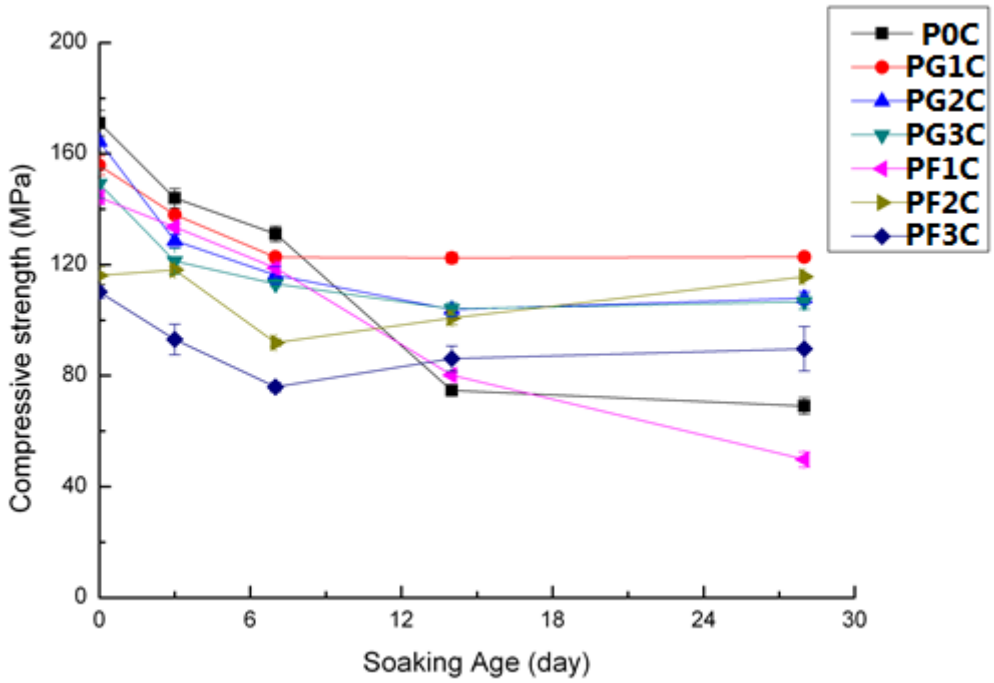

Figure 5-14 Effect of GP and PFA on the water resistance of MOC subjected to CO_2 curing

Table 5-7 summarizes the strength retention coefficient of MOC incorporating GP and PFA. The MOC paste subjected to CO_2 curing exhibited a higher strength retention coefficient than those without CO_2 curing for all the mixtures. For instance, the strength retention coefficient of the control paste was increased by 32.2% after CO_2 curing. The GP-blended paste without CO_2 curing had a slightly higher strength retention coefficient than the control, but it was still much lower than that of the PFA-blended cement. This may be attributed to a lower quantity of insoluble hydration products in the GP mixture. However, when subjected to CO_2 curing, the strength retention coefficient of the GP-blended paste significantly increased, of which the highest value was obtained with 10% GP incorporation. In contrast, the effect of CO_2 curing on the improvement of water resistance of the PFA-blended cement was much lower than that of the GP-blended cement.

Table 5-7 Strength retention coefficient (%)

Curing condition	Amount of GP (%)				Amount of PFA (%)		
	0	10	20	30	10	20	30
Without CO_2 curing	8.2	19.4	15.7	24.6	27.6	47.9	72.2
With CO_2 curing	40.4	78.9	65.7	71.4	34.5	91.0	81.4

5.3.2.2 Volume Stability

Figure 5-15 shows that the MOC mortar expanded during air curing. The expansion of the MOC mortar reached 0.06% at 3 days of air curing and became stable after 1 week. For the mixtures containing GP, an increase of expansion occurred with increasing dosages of GP, because of the negligible water absorption of the glass powder allowed more water for hydration (Schwarz et al. 2008). The same trend can be seen for the PFA-blended mixture, while the expansion of PFA-blended cement was higher than that of GP-blended cement because of the larger extent of pozzolanic reaction (Shayan and Xu 2006)

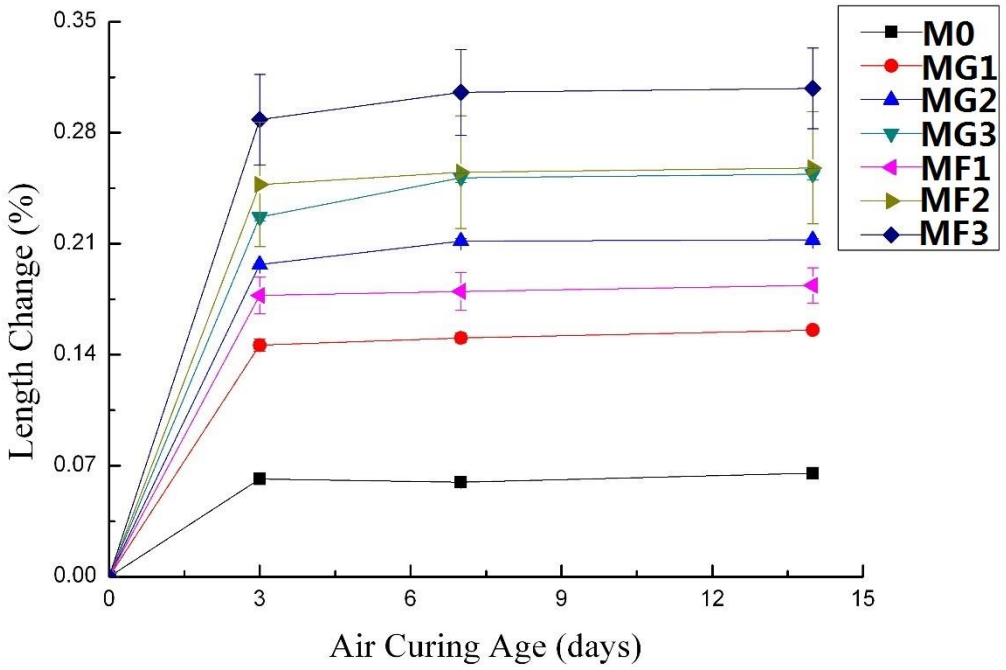

Figure 5-15 Length changes of MOC mortars under air curing

The expansion of the control mortar (as shown in Figure 5-16) increased significantly after immersion in water and reached 1.8% after 28 days, which was the consequence of the decomposition of Phase 5 and the formation of $Mg(OH)_2$. This expansion can induce cracking and damage in the cement structures, and attempts should be made to mitigate or prevent such expansion. On the contrary, the mortars with GP and PFA showed much smaller degrees of expansion. This was related to the lower content of excess MgO and the formation of an inhibiting surface amorphous gel layer surrounding MgO as mentioned above.

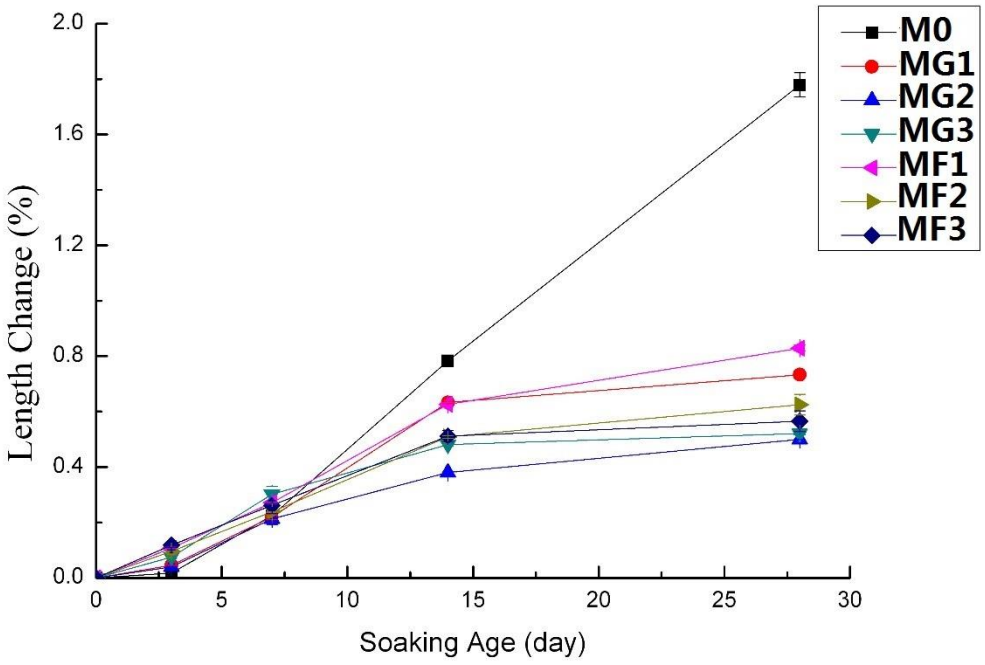

Figure 5-16 Length changes of MOC mortars under water immersion

5.3.2.3 XRD

In the XRD patterns of the MOC cement after 14 days of air curing (Figure 5-17, A_n means air (A) curing for n days; $A_{13}C$ means air curing for 13 days followed by 1 day of CO_2 curing). Wn means water(W) immersion for n days). Compared to the control, no new crystalline phase was observed in the XRD patterns of the GP-blended mixture after 14 days of air curing (Figure 5-19), which was consistent with the above results on the PFA-blended MOC cement. So it can be concluded that the new hydration products that improved the water resistance of the GP-blended cement was amorphous in nature as well, and hence its amount was quantified in QXRD analysis as shown in Table 5-8.

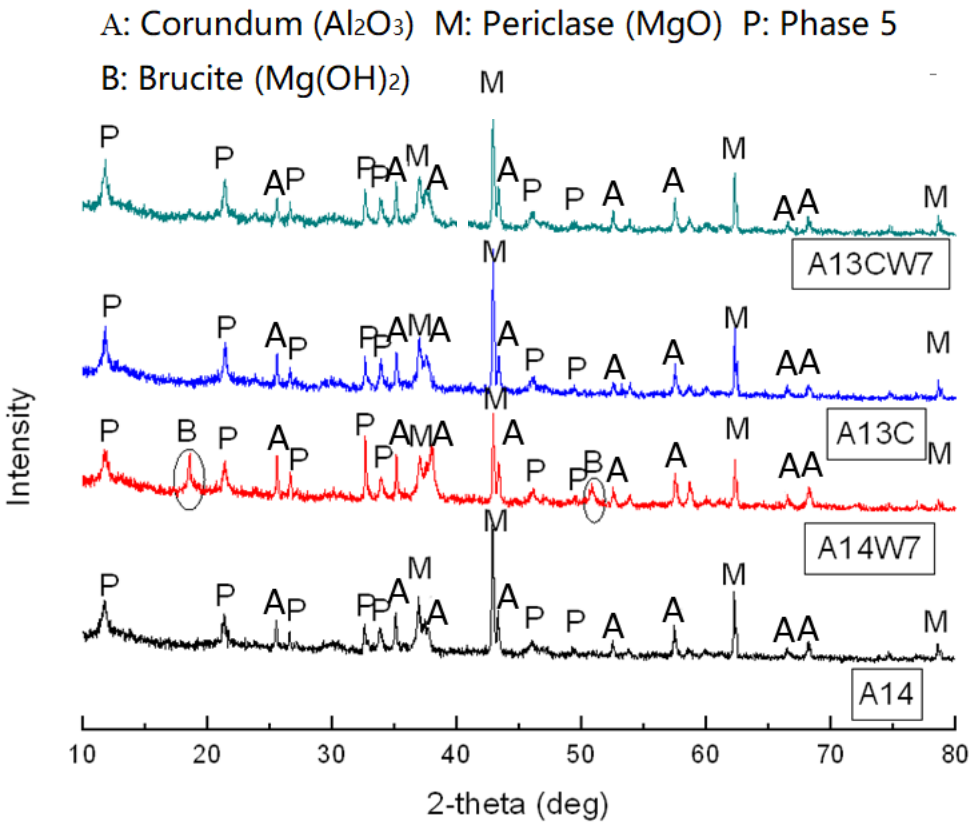

Figure 5-17 QXRD patterns of MOC paste subjected to different curing regimes

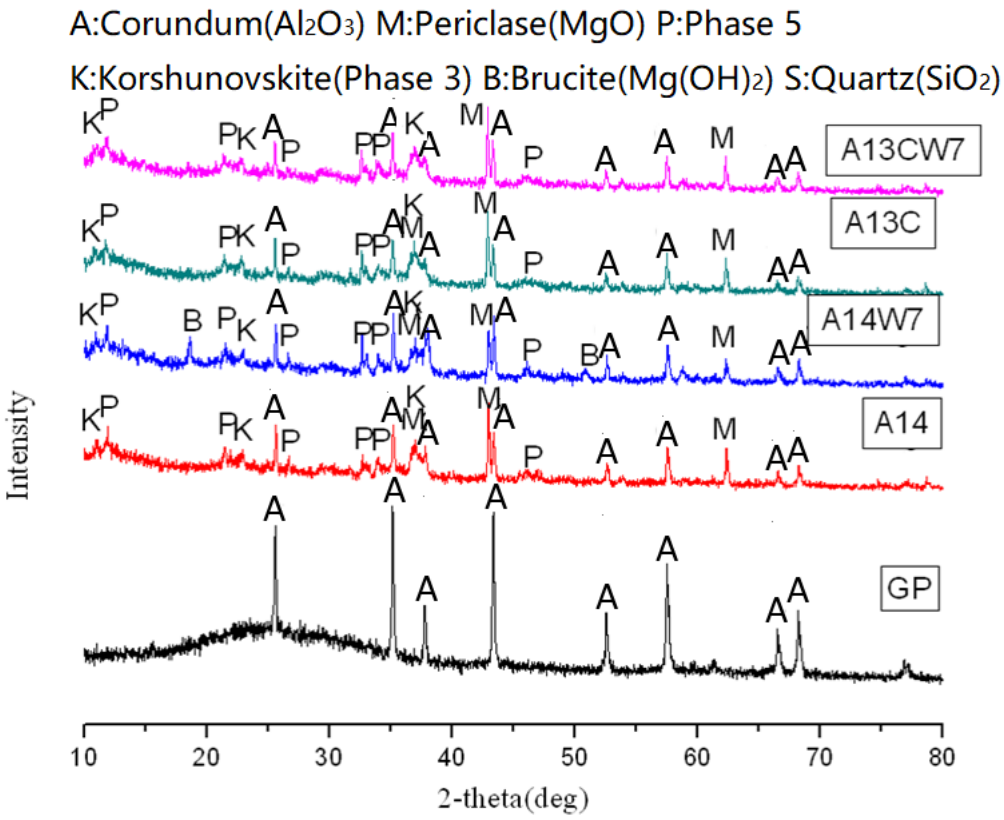

Figure 5-18 QXRD patterns of MOC paste incorporating with 30% GP subjected to different curing regimes

When using GP or PFA to replace MgO (Table 5-8), the quantity of the amorphous phase increased, which can be attributed to the amorphous phase in the respective materials and the M-S-H gel. But the amount of the amorphous phase was larger in the GP-blended than the PFA-blended samples after 14 days of air curing, corresponding to the higher content of amorphous phase in GP (mainly amorphous SiO_2). But after 14 days of water immersion, the amorphous phase content in PFA-blended mixture was higher than that of GP-blended samples due to the greater amount of active pozzolanic activity of PFA that produced more M-S-H gel in the MOC system. For both GP- and PFA-blended MOC, further increases in the amount of the amorphous phase was observed after CO_2 curing. This amorphous phase appears to be not

only stable in water, but also dense enough to provide a network for the protection of Phase 5 and Phase 3, thus the paste exhibited better water resistance.

Table 5-8 Phase compositions of MOC paste

	No.	Phase Contents (by mass %)								
		MgO	Phase 5	Phase 3	$Mg(OH)_2$	$MgCO_3$	SiO_2	$MgSiO_3$	Mg_2SiO_4	Am*
P0	A_{14}	27.5	69.5	2.8	--	--	--	--	--	--
	$A_{14}W_{14}$	5.2	--	--	68.5	--	--	--	--	25.3
P0C	$A_{13}C$	27.4	35.7	--	--	5.4	--	--	--	26.2
	$A_{13}CW_{14}$	12.3	39.1	4.0	18.0	5.2	--	--	--	21.4
PF3	A_{14}	17.5	53.5	--	--	--	4.3	--	--	24.7
	$A_{14}W_7$	15.6	31.1	--	--	--	3.3	--	--	50.0
	$A_{14}W_{14}$	7.3	12.1	13.1	22.58	--5.8	--	--	3.1	58.6
PG3	A_{14}	9.1	21.7	6.8	--	--	9.4	4.3	4.7	43.8
	$A_{14}W_7$	7.7	15.6	10.2	15.7	--	2.0	3.2	4.3	40.5
	$A_{14}W_{14}$	5.4	10.6	20.3	22.5	--	--	3.4	--	37.6
PG3C	$A_{13}C$	10.1	10.3	3.2	--	3.2	3.1	3.2	--	66.9
	$A_{13}CW_7$	10.7	6.78	4.2	--	2.2	4.2	1.3	--	70.5
	$A_{13}CW_{14}$	5.6	12.1	13.2	6.3	1.7	--	--	--	61.0

*amorphous phase

5.3.2.4 SEM/EDX

When adding GP and PFA, the formation of amorphous gel is shown in Figure 5-19. The incorporation of PFA changed the morphology of Phase 5 and the needle-like Phase 5 in F3 was larger and denser than that in G3. The amorphous gel in F3 interlocked and grew with the large cluster of needle-like Phase 5, thus leading to the formation of dense platelets. According to above, M-S-H gel was formed between the reaction products of PFA and MgO, which interlocked with Phase 5 and formed a dense and insoluble network, thus improving the water resistance of MOC. In comparison, the dominant hydration product in G3 was still the individual and thin needle-like Phase 5(Figure 5-20), which is unstable in water, hence this explained the higher water resistance of F3 than G3.

After CO_2 curing, the Phase 5 in G3C (Figure 5-21) was found to be larger in size than the one without CO_2 curing (Figure 5-24). These interlocking products crosslinked with the amorphous gel and formed a dense and insoluble structure after water immersion as shown in Figure 5-22. Such dense structure was present in both G3C and F3C, which could explain their high water resistance after CO_2 curing.

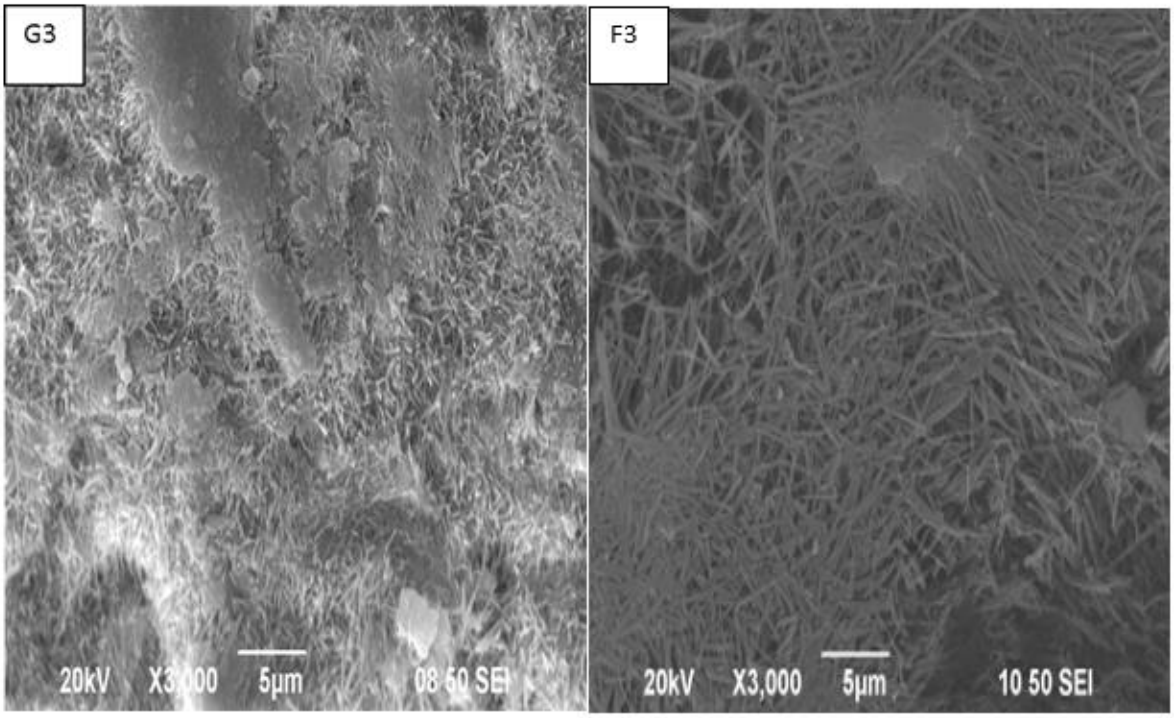

Figure 5-19 SEM images of G3 and F3 after 14 days of air curing

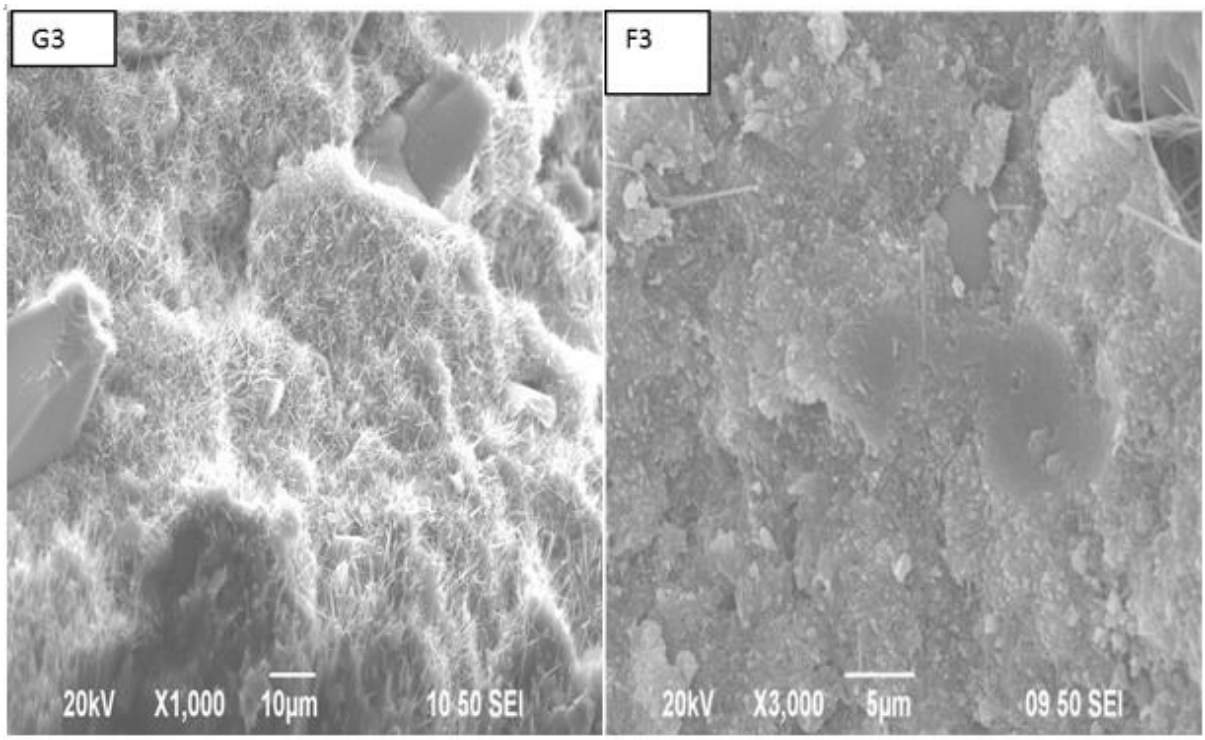

Figure 5-20 SEM images of G3 and F3 after 14 days of water immersion

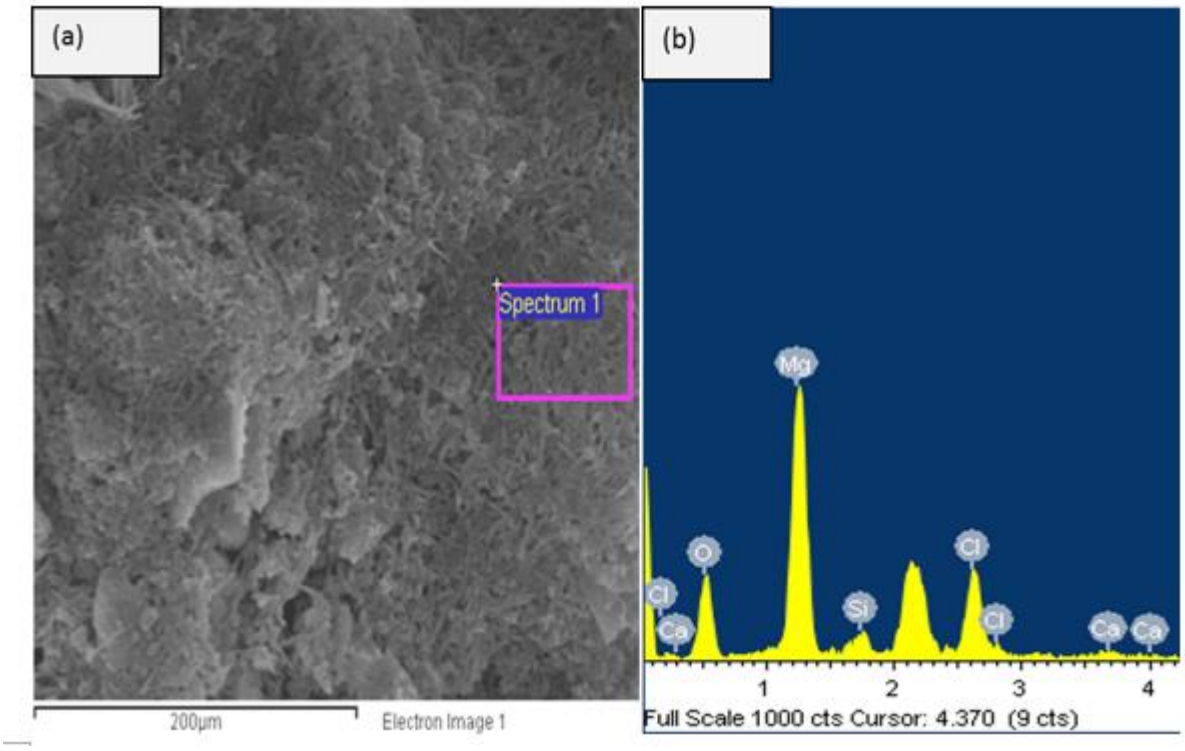

Figure 5-21 SEM-EDX analysis of G3C (a) SEM image (b) EDX pattern

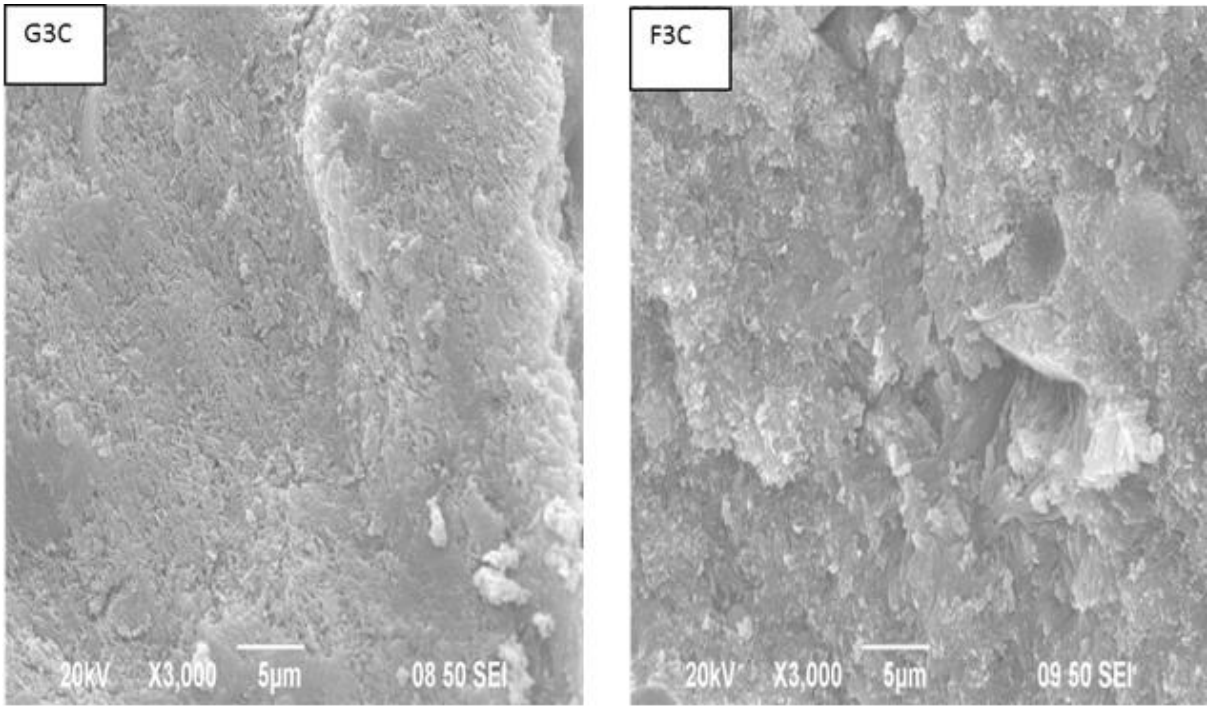

Figure 5-22 SEM images of G3C and F3C after 14 days of water immersion

5.3.3 Effect of ISSA on the water resistance

5.3.3.1 Compressive strength

The effect of ISSA on the compressive strength of the MOC paste before and after water immersion is shown in Figure 5-23（A14 means air curing for 14 days, A14Wn means water immersion for n days）. Each value represents the average of six specimens. The compressive strength of the cement pastes was increased by as much as 10% with the incorporation of 10% of ISSA. In the research using ISSA and Portland cement, ISSA has consistently been shown to absorb water, leading to a reduction in paste consistency and mortar workability for a given water: binder ratio(Monzó et al. 2003). It was reported that the decrease of water/$MgCl_2$ ratio could increase the compressive strength of MOC (Li and Chau 2007). So the increase in strength may have been resulted from the decrease of water to $MgCl_2$ ratio since the ISSA could absorb water (Donatello and Cheeseman 2013).

When adding more ISSA, the strength of the specimens decreased gradually due to the decrease of hydration product content. The compressive strength of MOC paste after immersion in water decreased significantly. After 28 days of water immersion, the reduction of strength for P0 was as much as 90%. When incorporating ISSA, the rate of strength loss was much lower, which can also be observed from the result listed in Table 5-9.

When soaked in water for 28 days, the strength retention left was at about 7% for P0. It is clear that the strength retention of PS1 was much higher than that of P0. Even though the strength of PS1 decreased slightly with a longer immersion time, the strength retention was still much higher than P0 after 28 days of water immersion. The similar trend can be found for PS2. And the strength retention increased with the increase of ISSA content. It is interesting to notice that the strength retention of PS3 increased gradually when immersed in water, which might be because more hydration products were produced during water immersion. The strength retention of MOC incorporating ISSA was higher than that blending with fly ash. This result may be contributed by the presence of phosphate as phosphate could significantly improve the water resistance of MOC (Deng 2003, Li et al. 2016).

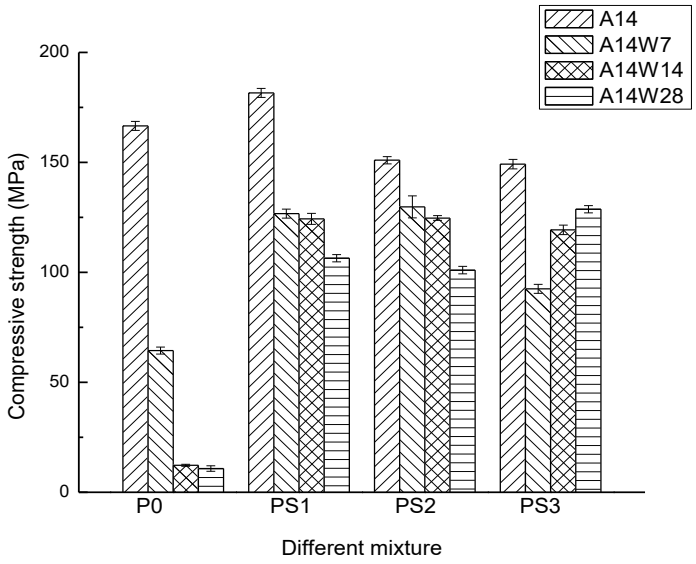

Figure 5-23 Compressive strength of cement pastes

Table 5-9 Strength retention (%)

No.	W7	W14	W28
P0	30.7	11.7	8.2
PS1	69.5	68.3	58.2
PS2	86.2	82.7	67.1
PS3	61.0	77.6	84.6

5.3.3.2 Volume stability

The results of volume changes of the mortar bars during air curing are shown in Figure 5-24. The expansion of MS1 was very close to that of M0. While adding 20% and 30% of ISSA, the expansion increased by about 30%. This result may be attributed to the gel phases in the mortar bars absorbed moisture in air and hence increased the solid volume, which need further research. The expansion behavior of the mortar specimens during water immersion are shown in Figure 5-25. When the M0 was immersed in water, a strong and continual expansion took place and reached 2% after 28 days of water immersion. This expansion was related to the hydration of the excess MgO to $Mg(OH)_2$, thus increasing the volume of the mortar bars (Chatterji 1995).

Adding ISSA could largely reduce the expansion due to two reasons: 1) the incorporation of ISSA decreased the content of excess MgO; 2) the formation of an insoluble layer due to the reaction of MOC and ISSA could protect the MgO from hydration. The rate of expansion decreased with the increase of the content of ISSA.

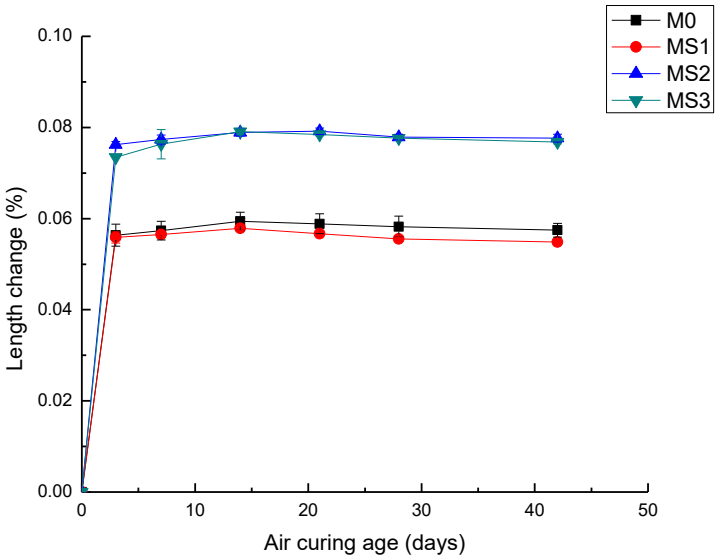

Figure 5-24 Length change of MOC mortar during air curing

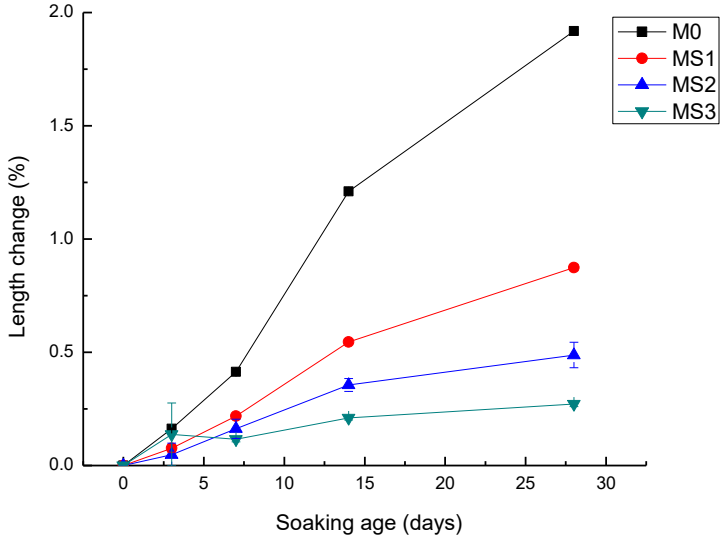

Figure 5-25 Length change of MOC mortar during water immersion

5.3.3.3 XRD

The XRD analyses of MOC paste are shown in Figure 5-26. The XRD pattern of PS3-A14 is similar to that of P0-A14, except that a certain content of Phase 3 ($3Mg(OH)_2 \cdot MgCl_2 \cdot 8H_2O$) was generated. The stability of Phase 3 was higher in water than that of Phase 5, which improved the water resistance of MOC (Ba and Guan 2009). Apparently, the formation of Phase 3 was not the only reason for the improvement, as the Phase 3 could also be transformed to brucite with a longer period of water immersion. So there must be some other new phase(s) that could protect the Phase 3 and Phase 5 from decomposition, which could be found in the Q-XRD analysis result as summarized in Figure 5-27.

Figure 5-27 shows that PS1, PS2, PS3 contained large amounts of amorphous phases compared to P0 after 14 days of air curing. Even PS1, PS2, PS3 contained a certain amount of amorphous phase (3.56%, 7.11%, 10.68%) before hydration due to the inherent amorphous phase in ISSA, and this value is negligible compared to that in the cement paste after 14 days of air curing (60%,70%,76.1%) indicating that new amorphous phase(s) was formed when adding ISSA. The amorphous phase was stable in water so that its content was still very high even after 28

days of water immersion. While the amount of amorphous phase in PS1 and PS2 was not high enough to protect the Phase 3 and Phase 5, so the content of Phase 3 and Phase 5 decreased with age. On the contrary, the content of Phase 3 and Phase 5 increased with the protection of amorphous phase in PS3, thus it slightly increased the compressive strength in water. It is interesting to notice that the sample with a lower content of brucite showed higher compressive strength when immersed in water. That is because less Phase 3 and Phase 5 were decomposed in these samples, and these hydration products showed higher strength than brucite.

No new phosphate phase was detected from the spectrum and it shows that the presence of phosphate in ISSA could improve the water resistance of MOC as it could improve the water stability of Phase 3 and Phase 5 instead of producing new crystalline phosphate phases.

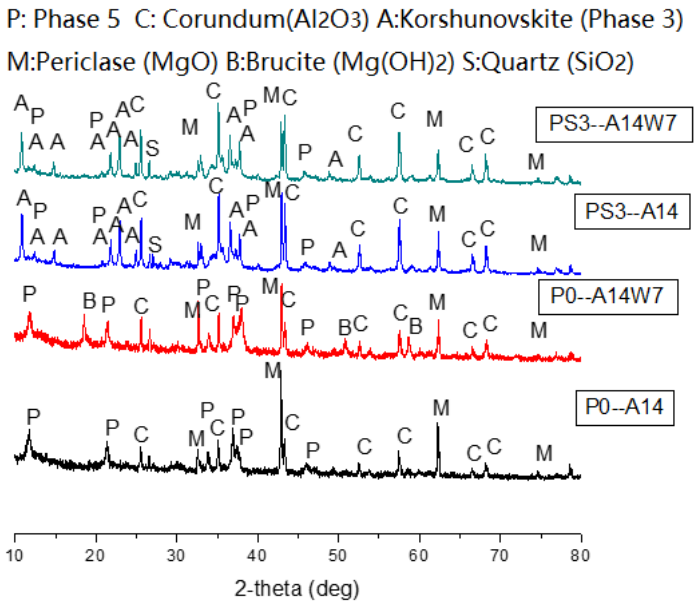

Figure 5-26 X-ray diffractogram of MOC paste

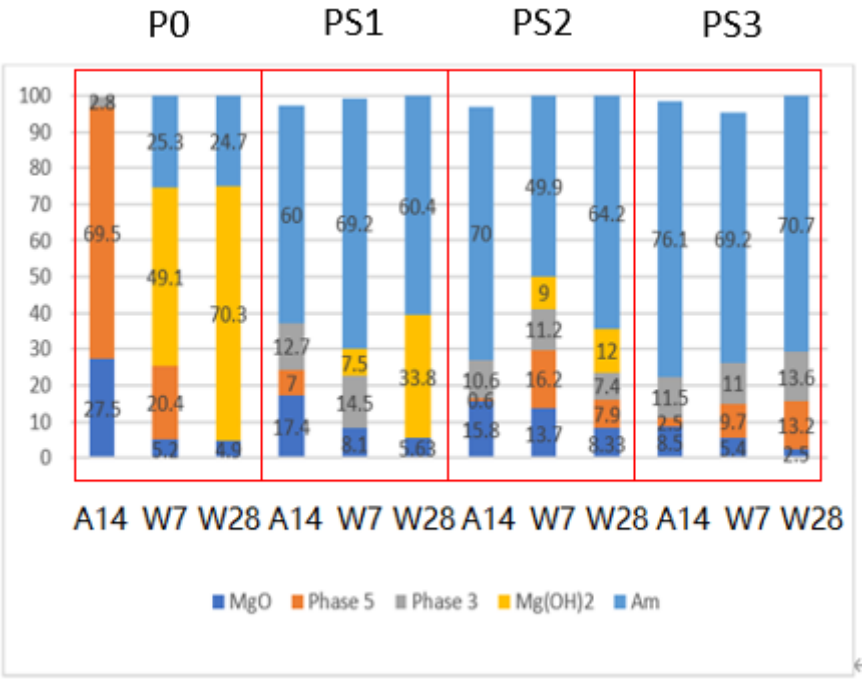

Note: Am = amorphous phase

Figure 5-27 Phase composition in MOC paste (by mass %)

5.3.3.4 SEM

SEM micrographs of PS3 before and after water immersion are shown in Figure 5-28. ,The main hydration product of MOC paste was the needle-like Phase 5. When adding ISSA, the hydration products were consisted of needle-like Phase 5 and Phase 3 and the particle size of Phase 3 was smaller than that of Phase 5 as shown in Figure 5-28 (a). The particles in Figure 5-28 (a) were identified as ISSA by EDX analysis (Figure 5-28 (b)). Elemental Mg was absent in the spectrum. That is because the low content of Mg in ISSA. The edge of the ISSA particle is diffused , which indicates the possible chemical reaction between ISSA and MOC. As mentioned before, a large amount of amorphous phase was present in PS3, while the presence of the amorphous phase was not evident during air curing. As a comparison, when the sample was soaked in water for 28 days, the delineation of Phase 3 and Phase 5 were not clear and they

had intermixed with the amorphous gel and formed an insoluble dense structure in Figure 5-28(c), thus improving the water resistance of PS3. The main elements contained in this gel are Mg, Cl, Si, Al as shown in Figure 5-28(d).

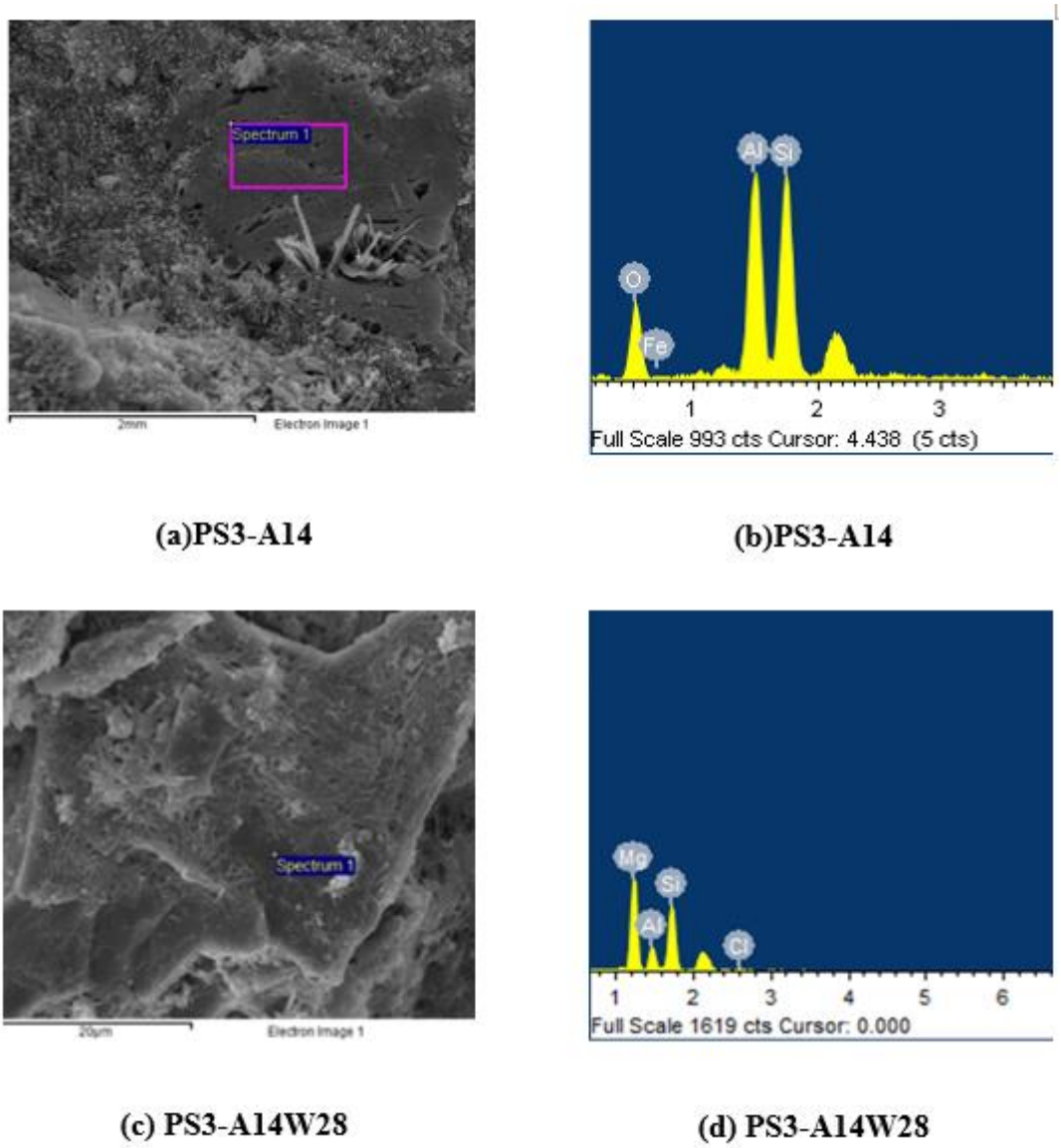

Figure 5-28 SEM pictures and EDX spectrum of MOC incorporating ISSA

5.4 Summary

This chapter investigated the effect of SCMs on the water resistance and volume stability of MOC. For the PFA-blended paste, the water resistance was improved significantly, and the strength retention coefficient increased with the increase of PFA content. The compressive

strength of MOC paste incorporating 30% of PFA was decreased only 30% after immersion in water for 28 days. This is because a considerable content of insoluble amorphous gel was generated during air curing and water immersion. This gel contained M-S-H gel and phase 5, indicating that PFA could not only react with MOC to produce M-S-H gel, but also changed the morphology of Phase 5 crystalline. Adding PFA could increase the expansion of MOC mortars during air curing because the reaction between PFA and MOC produced an amorphous gel which took up a small amount of moisture in air. The control MOC mortar exhibited a large expansion after immersion in water as a result of the hydration of excess MgO. Incorporating up to 20% PFA in MOC could significantly reduce the expansion due to the lower content of excess MgO and the formation of an inhibiting surface layer around MgO.

The PFA-blended cement demonstrated a much higher water resistance than GP-blended cement due to the higher pozzolanic reactivity of PFA.

The CO_2 curing could further improve the water resistance of the MOC paste incorporating PFA and GP, because more amorphous materials were formed. However, CO_2 curing could not decrease the expansion of the mortar specimens after immersion in water.

Adding ISSA could dramatically improve the compressive strength and volume stability of MOC in water. There are three reasons. Firstly, More Phase 3 was produced when adding ISSA, which had a higher stability in water than Phase 5. Secondly, when there were excess MgO, they could be hydrated, and increase the volume instability of MOC, thus leading to the expansion and cracking. Adding ISSA could decrease the content of MgO and improve the volume stability in water. Last but not the least, the silica and alumina in ISSA could react with MgO, $MgCl_2$ and generated a gel containing Mg, Cl, Si, Al. This insoluble dense gel interlocked with Phase 3 and Phase 5 and protected them from decomposing. The content of\Phase 3 and Phase 5 even increased slightly in the MOC paste prepared with 30% of ISSA during water immersion, which indicates the stable structure of ISSA blended cement.

Reference

Alleman, J. E. and N. A. Berman (1984). Constructive sludge management: biobrick. Journal of Environmental Engineering **110**(2): 301-311.

Anderson, M. (2002). Encouraging prospects for recycling incinerated sewage sludge ash (ISSA) into clay - based building products. Journal of Chemical Technology and Biotechnology **77**(3): 352-360.

Ba, H. and H. Guan (2009). Influence of MgO/MgCl2 molar ratio on phase stability of magnesium oxychloride cement. Journal of Wuhan University of Technology-Mater. Sci. Ed. **24**(3): 476-481.

Beaudoin, J. J. and V. S. Ramachandran (1975). Strength development in magnesium oxychloride and other cements. Cement and Concrete Research **5**(6): 617-630.

Bhatty, J. I. and K. J. Reid (1989). Compressive strength of municipal sludge ash mortars. Materials Journal **86**(4): 394-400.

Brew, D. and F. Glasser (2005). Synthesis and characterisation of magnesium silicate hydrate gels. Cement and Concrete Research **35**(1): 85-98.

Chan, J. and Z. Li (2006). Influence of fly ash on the properties of magnesium oxychloride cement. Measuring, Monitoring and Modeling Concrete Properties, Springer**:** 347-352.

Chatterji, S. (1995). Mechanism of expansion of concrete due to the presence of dead-burnt CaO and MgO. Cement and Concrete Research **25**(1): 51-56.

Chau, C., J. Chan and Z. Li (2009). Influences of fly ash on magnesium oxychloride mortar. Cement and Concrete Composites **31**(4): 250-254.

Cheeseman, C. and G. Virdi (2005). Properties and microstructure of lightweight aggregate produced from sintered sewage sludge ash. Resources, Conservation and Recycling **45**(1): 18-30.

Chen, C., R. Huang, J. Wu and C. Yang (2006). Waste E-glass particles used in cementitious mixtures. cement and concrete research **36**(3): 449-456.

Chen, Z. and C. Poon (2015). Maximizing the recycling of waste glass as construction materials.

Chen, Z. and C. S. Poon (2016). Comparing the use of sewage sludge ash and glass powder in cement mortars. Environmental Technology: 1-9.

Cyr, M., M. Coutand and P. Clastres (2007). Technological and environmental behavior of sewage sludge ash (SSA) in cement-based materials. Cement and Concrete Research **37**(8): 1278-1289.

Davraz, M. and L. Gunduz (2005). Engineering properties of amorphous silica as a new natural pozzolan for use in concrete. Cement and Concrete Research **35**(7): 1251-1261.

Dean, R. B. and M. J. Suess (1985). The risk to health of chemicals in sewage sludge applied to land. Waste management & research **3**(3): 251-278.

Deng, D. (2003). The mechanism for soluble phosphates to improve the water resistance of magnesium oxychloride cement. Cement and Concrete Research **33**(9): 1311-1317.

Donatello, S. and C. R. Cheeseman (2013). Recycling and recovery routes for incinerated sewage sludge ash (ISSA): A review. Waste Management **33**(11): 2328-2340.

Donatello, S., A. Freeman-Pask, M. Tyrer and C. Cheeseman (2010). Effect of milling and acid washing on the pozzolanic activity of incinerator sewage sludge ash. Cement and Concrete Composites **32**(1): 54-61.

Donatello, S., M. Tyrer and C. Cheeseman (2010). Comparison of test methods to assess pozzolanic activity. Cement and Concrete Composites **32**(2): 121-127.

Fernández-Jiménez, A. and A. Palomo (2005). Composition and microstructure of alkali activated fly ash binder: effect of the activator. Cement and concrete research **35**(10): 1984-1992.

Gartner, E. M. (2009). Cohesion and expansion in polycrystalline solids formed by hydration reactions—The case of gypsum plasters. Cement and Concrete Research **39**(4): 289-295.

Idir, R., M. Cyr and A. Tagnit-Hamou (2010). Use of fine glass as ASR inhibitor in glass aggregate mortars. Construction and Building Materials **24**(7): 1309-1312.

Idir, R., M. Cyr and A. Tagnit-Hamou (2011). Pozzolanic properties of fine and coarse color-mixed glass cullet. Cement and Concrete Composites **33**(1): 19-29.

Kou, S. and C. Poon (2009). Properties of self-compacting concrete prepared with recycled glass aggregate. Cement and Concrete Composites **31**(2): 107-113.

Levason, W., J. S. Ogden, M. D. Spicer and N. A. Young (1990). Characterization of dibromine monoxide (Br2O) by bromine K-edge EXAFS and IR spectroscopy. Journal of the American Chemical Society **112**(3): 1019-1022.

Li, J., G. Li and Y. Yu (2008). The influence of compound additive on magnesium oxychloride cement/urban refuse floor tile. Construction and building materials **22**(4): 521-525.

Li, Y., Z. Li, H. Pei and H. Yu (2016). The influence of FeSO 4 and KH 2 PO 4 on the performance of magnesium oxychloride cement. Construction and Building Materials **102**: 233-238.

Li, Z. and C. Chau (2007). Influence of molar ratios on properties of magnesium oxychloride cement. Cement and Concrete Research **37**(6): 866-870.

Ling, T.-C. and C.-S. Poon (2011). Utilization of recycled glass derived from cathode ray tube glass as fine aggregate in cement mortar. Journal of hazardous materials **192**(2): 451-456.

Lu, H., P. Wang and N. Jiang (1994). Design of additives for water-resistant magnesium oxychloride cement using pattern recognition. Materials Letters **20**(3): 217-223.

Mageswari, M. and B. Vidivelli (2010). The use of sheet glass powder as fine aggregate replacement in concrete. Open Civil Engineering Journal **4**: 65-71.

Monzó, J., J. Payá, M. Borrachero and I. Girbés (2003). Reuse of sewage sludge ashes (SSA) in cement mixtures: the effect of SSA on the workability of cement mortars. Waste Management **23**(4): 373-381.

Monzo, J., J. Paya, M. Borrachero and E. Peris-Mora (1999). Mechanical behavior of mortars containing sewage sludge ash (SSA) and Portland cements with different tricalcium aluminate content. Cement and Concrete Research **29**(1): 87-94.

Okuno, N. and S. Takahashi (1997). Full scale application of manufacturing bricks from sewage. Water science and technology **36**(11): 243-250.

Palomo, A., M. Grutzeck and M. Blanco (1999). Alkali-activated fly ashes: a cement for the future. Cement and Concrete Research **29**(8): 1323-1329.

Pan, S.-C., D.-H. Tseng, C.-C. Lee and C. Lee (2003). Influence of the fineness of sewage sludge ash on the mortar properties. Cement and Concrete Research **33**(11): 1749-1754.

Poon, C. and M. Boost (1996). The stabilization of sewage sludge by pulverized fuel ash and related materials. Environment international **22**(6): 705-710.

Schwarz, N., H. Cam and N. Neithalath (2008). Influence of a fine glass powder on the durability characteristics of concrete and its comparison to fly ash. Cement and Concrete Composites **30**(6): 486-496.

Schwarz, N. and N. Neithalath (2008). Influence of a fine glass powder on cement hydration: Comparison to fly ash and modeling the degree of hydration. Cement and Concrete Research **38**(4): 429-436.

Shao, Y., T. Lefort, S. Moras and D. Rodriguez (2000). Studies on concrete containing ground waste glass. Cement and Concrete Research **30**(1): 91-100.

Shayan, A. and A. Xu (2004). Value-added utilisation of waste glass in concrete. cement and concrete research **34**(1): 81-89.

Shayan, A. and A. Xu (2006). Performance of glass powder as a pozzolanic material in concrete: a field trial on concrete slabs. Cement and Concrete Research **36**(3): 457-468.

Shi, C., Y. Wu, C. Riefler and H. Wang (2005). Characteristics and pozzolanic reactivity of glass powders. Cement and Concrete Research **35**(5): 987-993.

Sorell, C. and C. Armstrong (1976). Reactions and equilibria in magnesium oxychloride cements [J]. J Am Ceram Sa **59**: 51-59.

Wiebusch, B. and C. F. Seyfried (1997). Utilization of sewage sludge ashes in the brick and tile industry. Water Science and Technology **36**(11): 251-258.

Xia, S., P. Xing and S. Gao (1991). Studies on the basic compounds of magnesia cement: the thermal behaviour of magnesium oxychlorides. Thermochimica acta **183**: 349-363.

Zhan, B., C. Poon and C. Shi (2013). CO 2 curing for improving the properties of concrete blocks containing recycled aggregates. Cement and Concrete Composites **42**: 1-8.

Zhang, T., C. Cheeseman and L. Vandeperre (2011). Development of low pH cement systems forming magnesium silicate hydrate (MSH). Cement and concrete research **41**(4): 439-442.

Zhang, T., L. J. Vandeperre and C. R. Cheeseman (2014). Formation of magnesium silicate hydrate (MSH) cement pastes using sodium hexametaphosphate. Cement and Concrete Research **65**: 8-14.

Chapter 6. Mechanism of Improvement of Water Resistance

6.1 Introduction

According to the above study, the use of SCMs- PFA, GP, and ISSA could improve the water resistance of MOC. The compressive strength of MOC incorporating 20% PFA and 30% ISSA decreased by only 30% and 25% respectively when immersed in water for 28 days. The Q-XRD result showed that the amorphous content increased when adding PFA and ISSA. The amorphous phase was very stable in water and interlocked with the hydration products to protect them from decomposition. The length change of the MOC mortar incorporating PFA and ISSA was around 0.5%, which was much lower than that prepared without PFA and ISSA. This is because the SCMs replaced a certain amount of MgO. It also indicated the stability of the amorphous phase. It is difficult to distinguish the amorphous phase with Phase 5 or Phase 3 using SEM as they intermixed with each other and the chemical compositions and the structures of SCMs are complex. The TEM-EDX is an effective technique for investigating the microstructure of intermixed phases(Richardson 2000, Richardson et al. 2010). However, few researchers have used this method to observe the morphology and elemental compositions of the product of MOC. This study compared the results observed by using SEM and TEM-EDX and to further understand the mechanism of how PFA and ISSA improved the water resistance of MOC.

6.2 Sample preparation

The bischofite was mixed with water and poured into the mixing bowl before adding the MgO.

The molar ratio of MgO/ $MgCl_2$ and water/ $MgCl_2$ were 9 and 10 respectively. The PFA and ISSA were used to replace MgO at a dosage level of 30% by mass of MgO. The slurries were cast into a plastic tube which was placed in an air curing chamber for 14 days. Sections 2 mm long were cut from the cylinder, polished down to 30 thickness μm, glued between 3mm diameter nickel grids. Then they were argon ion-beam milled and carbon coated. The bright field images and chemical analyses were collected using a field emission gun transmission electron microscope.

6.3 Test results and discussions

6.3.1 Results

6.3.1.1 Control MOC

The morphology of the MOC paste after 14 days of air curing is displayed in Figure 6-1. The SEM micrograph (Figure6-1a) shows that the surface of the cement paste was covered with a large quantity of needle-like crystals, which is typical of Phase 5 ($MgO\cdot MgCl_2\cdot H_2O$) and this was confirmed by EDX analysis result. TEM was used to further examine the particle size, crystallinity and morphology of the samples with a higher magnification as shown in Figure6-1b, which was a bright field image of the MOC paste. It can be estimated that the width of this needle-like phase was about 30nm. A gauzelike homogeneous morphology can be observed (Figure6-2 a) after when further increasing the magnification (Figure 6-1b). The corresponding selected area electron diffraction (SAED) pattern of the needle-like phase is shown in Figure 2b. A small tip ("beam stopper") above the observation screen was inserted to cover the bright spot in the center to avoid the damage of camera(Thomas and Gemming 2014). It shows the (0 1 2), (4 0 -1), (0 1 3), and (5 1 0) lattice spacing value of 2.42 Å, 2.39 Å, 1.97 Å, and 1.54 Å respectively. This diffraction pattern indicated the needle-like phase in Figure 6-1b is Phase 5.

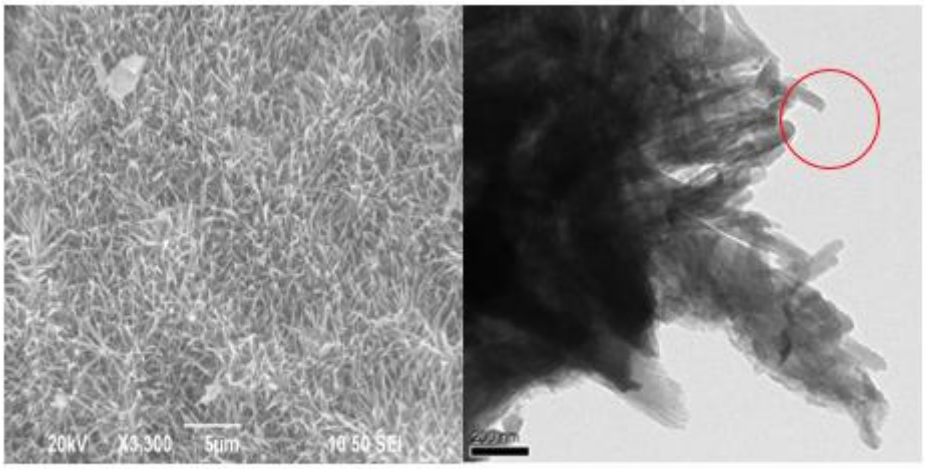

(a) (b)

Figure 6-1 SEM image (a) and TEM image (b) of MOC

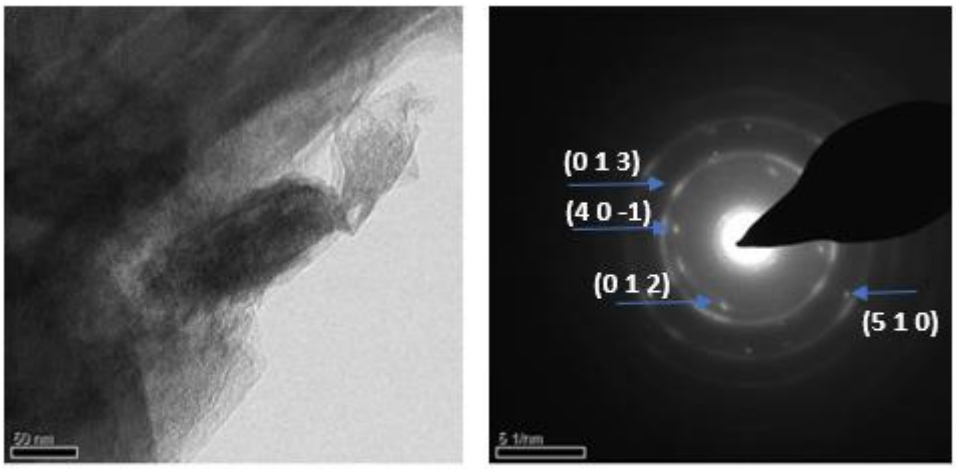

(a) (b)

Figure 6-2 TEM (higher magnification) image (a) and selected area electron diffraction pattern (b) from the circled zone in Figure 6-1

6.3.1.2 MOC incorporating PFA

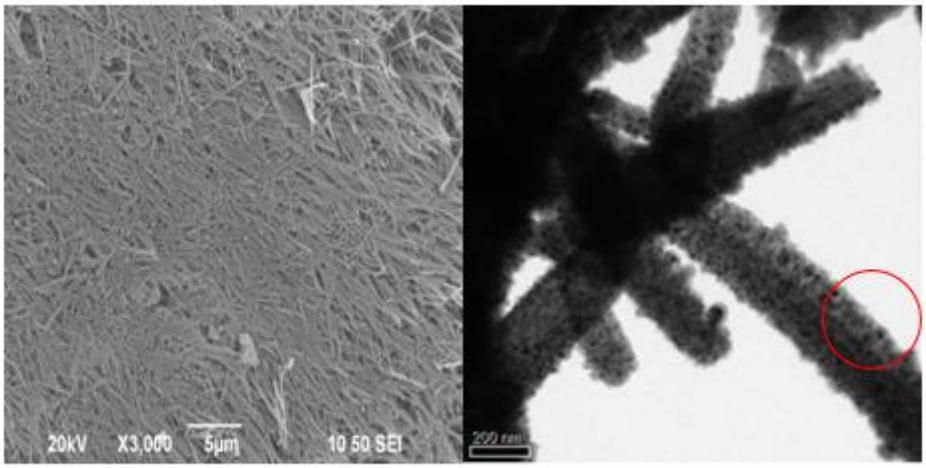

(a) (b)

Figure 6-3 SEM image (a) and TEM image (b) of MOC incorporating PFA

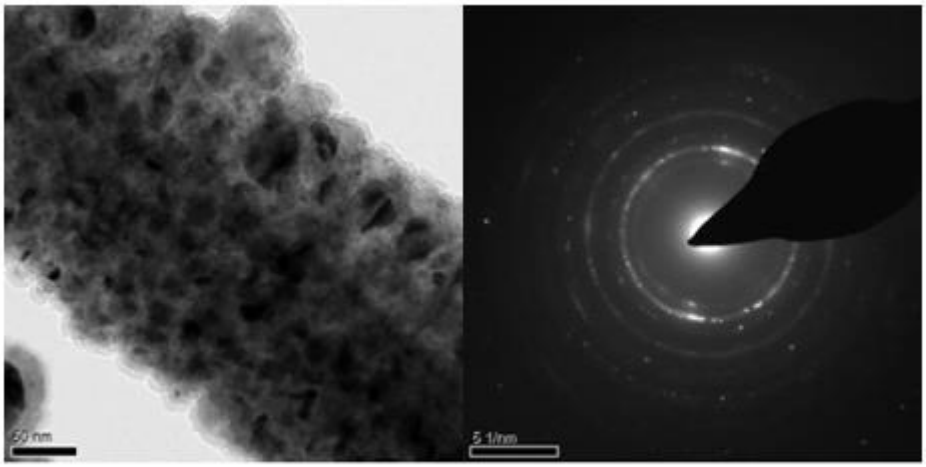

(a) (b)

Figure 6-4 TEM image (a) selected area electron diffraction pattern (b) from the circle zone in Figure 6-3

The incorporation of PFA in the MOC mix was found to influence the hydration behavior and led to differences in the microstructure of the hydration products. It seems that the main hydration product was a lath-like phase as shown in Figure 6-3a. In order to avoid intermixing,

TEM was used as shown in Figure 6-3b to reveal the detailed microstructure. The width of this lath-like phase was approximately 200nm. With further increasing in magnification (Figure 6-4a), dark-grain structures could be observed. Electron diffraction analysis of this lath-like phase showed spotty ring patterns, which can be interpreted as semi-crystalline particles. The EDX detected Si and Al in addition to Mg and Cl, among which the Mg/Al /Si/Cl atomic ratios was 13.8:2.3:0.77:1. This indicates an amorphous magnesium aluminosilicate was formed which interspersed with the crystalline particles-Phase 5.

Apart from the lath-like phase, a foil-like phase could also be observed in the MOC paste incorporating PFA as shown in Figure 6-5. Electron diffraction analysis of this foil-like phase showed a faint, diffused ring, which was produced by amorphous particles. The EDX detected Mg, Al, Si in a molar ratio of 14.2:2.8: 1. As reported in a previous study, the PFA could improve the water resistance of MOC paste due to the formation of an amorphous phase according to the Q-XRD analysis. But the microstructure of this amorphous phase was not clear in the SEM picture as it was presented as an intermixed morphology. TEM technique can analyze the individual particles, which avoids interferences from other phases. From Figs. 6-3 to 6-5, it can be seen that the silicate and aluminum in PFA could react with the MOC and the product formed not only in the matrix individually but also interspersed with the crystalline particle-Phase 5 and then changed the morphology of Phase 5.

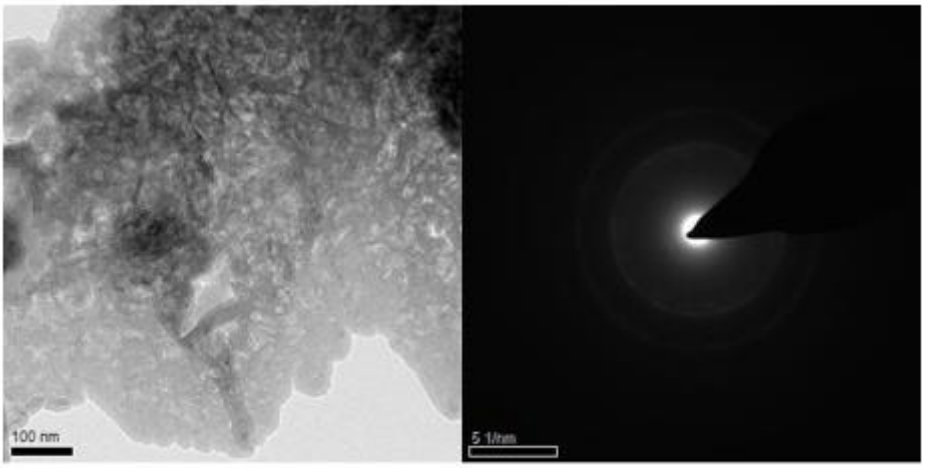

(a) (b)

Figure 6-5 TEM image (a) and selected area electron diffraction pattern (b) of MOC incorporating PFA

6.3.1.3 MOC incorporating ISSA

When incorporating ISSA in the MOC, the main hydration product in the MOC paste was with a short needle like morphology, forming a compact matrix as shown in Figure 6-6a. The width of this fibroid phase was around 100nm according to the TEM picture in Figure 6-6b. With increased magnification, a dark-grain structure similar to that in Figure 4a can be observed (Figure 6-7). But it was much thinner than that in the PFA-incorporated MOC paste. The EDX detected a molar ratio of Mg, Si, and Cl of 10.6:0.7:1, which indicated that the silicate in ISSA could react with MgO and the product was dispersed on the needle-like Phase 5. In addition to the fibroid phase, granular particles could be observed as well, which was an amorphous phase as shown in Figure 6-8. The EDX detected a molar ratio of Mg, Si, and Cl of 20:2.1:1.

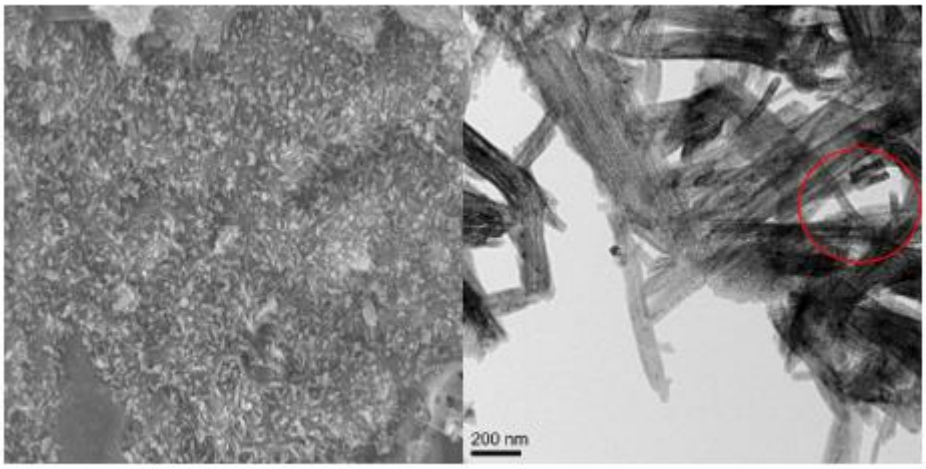

(a) (b)

Figure 6-6 SEM image (a) and TEM image (b) of MOC incorporating ISSA

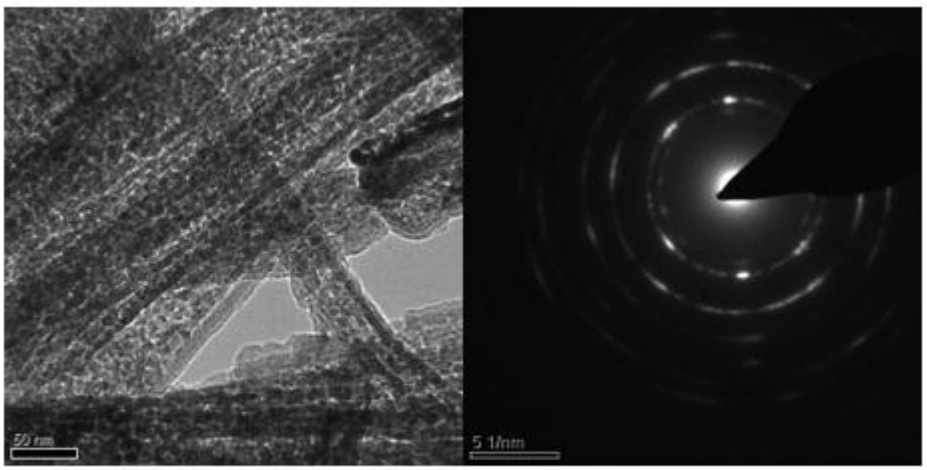

(a) (b)

Figure 6-7 TEM image (a) and selected area electron diffraction pattern (b) from the circled zone in Figure 6-6

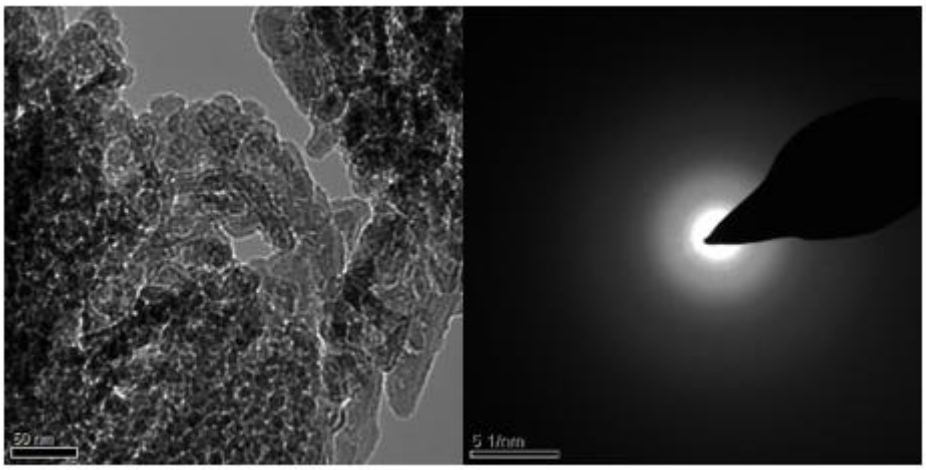

Figure 6-8 TEM image (a) and selected area electron diffraction pattern (b) of MOC incorporating ISSA

6.3.2 Discussion

Table 6-1 Summary of results of hydration products formed and water resistance of different MOC mixtures

	Control MOC	PFA-blended MOC	ISSA-blended MOC
Compressive strength (14 days of air curing)	165±7.5MPa	112±4.3MPa	150±2.2MPa
Strength retention coefficient (water immersion for 28 days)	10%	73%	87%
Expansion (water immersion for 28 days)	1.80±0.08%	0.60±0.02%	0.25±0.01%

SEM micrographs of hydration products	needle-like phase	flat and wide plates	lath-like structure
TEM micrographs of hydration products	thin needle	a) lath-like phase and b) foil-like phase	a) fibroid-like structure and b) granular-like structure
EDX (TEM) results of hydration products (atomic ratio)	Mg:Cl=3	a) Mg:Al:Si:Cl=13.8:2.3:0.77:1 b) Mg:Al:Si=14.2:2.8: 1	a) Mg:Si:Cl=10.6:0.7:1 b) Mg:Si:Cl=20:2.1:1

Note: Strength retention coefficient was estimated using the compressive strength of specimens before water immersion to divide residual compressive strength of the specimens after water immersion for a period of time. When calculating expansion, the length of specimens before water immersion was recorded as the initial length.

As can be seen from Table 6-1, the MOC paste had high compressive strength and the strength was 165MPa after 14 days of air curing. However, the compressive strength decreased significantly when immersed in water due to the decomposition of hydration products (Phase 3 and Phase 5) and the strength retention coefficient was only 10% after 28 days of water immersion. When adding PFA or ISSA, the compressive strength decreased slightly during air curing (112MPa and 150 MPa respectively). However, the strength retention coefficient after immersion in water significantly increased and reached more than 70%. Based on our past test results, the expansion of pure MOC mortar was 1.8% after 28 days of water immersion which was due to the hydration of excess MgO. This value was 0.6% and 0.25% for the MOC mortars incorporating PFA and ISSA respectively, which was due to the reduction of excess MgO and the increased stability of the hydration

products adding PFA or ISSA. The compressive strength results and length change results showed that PFA and ISSA could significantly improve the water resistance of MOC mixture and ISSA induced better improvement of the water resistance.

According to our previous study, the hydration product of pure MOC paste was Phase 5 and no new crystalline phase was found after adding PFA and ISSA. However, the content of amorphous phases in the PFA/ISSA incorporated MOC pastes was much higher after air curing for 14 days than that in the raw materials. Therefore, the amorphous phases generated after adding PFA and ISSA maybe the reason for the improvement of water resistance of MOC.

The ISSA-blended MOC paste had higher water resistance compared to the PFA-blended MOC paste, which might be due to three reasons. Firstly, ISSA-blended mixture had a higher content of amorphous phases. According to our previous study, the Phase 3 and Phase 5 in pure MOC paste decomposed completely after 28 days of water immersion. However, a certain amount of Phase 3, Phase 5 and amorphous phases were detected after water immersion in the MOC paste incorporating PFA or ISSA, indicating that the amorphous phases were stable in water, interlocked with Phase 3 and Phase 5 and protected them from decomposition. The initial amorphous phase contents in the raw materials preparing the MOC pastes with ISSA or PFA incorporation were similar (around 10% of the total raw materials), but the ISSA-blended MOC paste had much higher amorphous content (76%) compared to PFA-blended MOC (24.7%) after 14 days of air curing. Therefore, the higher amorphous phase content produced might be one of the reasons that the ISSA-blended MOC had better water resistance.

The second reason may be due to the different chemical compositions of the hydration products. It can be seen from Table 6-1 that both of the hydration products in the PFA-

blended MOC and the ISSA-blended MOC were wider and bigger than that in pure MOC paste according to SEM micrographs. TEM micrographs showed that the amorphous phases interspersed with Phase 5 and changed the morphology of Phase 5 from a needle-like structure to a lath-like structure. Besides, the amorphous phase could be observed separately in the matrix. The amorphous phase in the PFA-blended MOC contained Mg, Al and Si in an atomic ratio of 14.2:2.8:1. While the amorphous phase in the ISSA-blended MOC contained Mg, Si and Cl in an atomic ratio of 20:2.1:1. The different chemical compositions of the amorphous phase may result in the different morphologies of the hydration products and water resistance.

The third reason may be the phosphorus (P) content in ISSA-blended MOC mixture. The pH of the pore solution in MOC paste was about 10-11(Li and Chau 2007), and the dissolution of P was 5-10 mmol/L when using $Na(OH)_2$ to extract ISSA under this pH range(Fang et al. 2018). It was reported that a small amount of phosphate (0.74-1% of MOC paste) could significantly improve the water resistance of MOC(Deng 2003). Therefore, the P extracted from ISSA might also had positive effects on improving the water resistance of MOC. However, P was not detected in the ISSA-blended MOC paste, which might be due to the small concentration of P (around 3% in the raw materials).

The MOC deteriorates significantly under moist climate due to the decomposition of hydration products- Phase 3 and Phase 5, which might lead to the leaching of free chloride and the corrosion of steel when it is used in reinforced concrete. When adding PFA and ISSA, the amorphous alumino-silicate gel was generated by the reaction of the reactive SiO_2 and Al_2O_3 contents in PFA/ISSA and MOC. The production with large surface interlocked with Phase 3 and Phase 5, changed the morphology of the hydration products, formed a network and protected them from decomposition. That is why a certain amount

of Phase 5 could be observed after water immersion for 28 days in MOC incorporating PFA and ISSA and the strength retention coefficient was much higher than pure MOC. Even though the chloride bonding type in amorphous gel was not clear, it can be suggested that the leaching of free chloride was significantly prohibited. Therefore, the chance of steel corrosion might be decreased. The leaching of free chloride still needs further research.

6.4 Summary

MOC demonstrated poor water resistance due to the instability of the hydration products in water. Using PFA or ISSA could significantly improve the water resistance. New amorphous phases were observed in PFA or ISSA blended MOC, which may be the reason why they improved the water resistance.

The morphology of magnesium oxychloride cement incorporating PFA and ISSA was examined using SEM and TEM/EDX. The SEM result showed that the main hydration product in MOC paste was needle-like crystalline- Phase 5. When adding PFA and ISSA, the main hydration product presented a lath -like structure. This change in structure was the reason for the improvement of water resistance of MOC. But it was difficult to clearly observe the microstructure and elemental compositions of this structure due to the intermixing of different phases. The TEM result showed that two phases were formed when adding PFA and ISSA, including a lath-like or fibroid-like phase and an amorphous phase. The former phase was much bigger than the needle-like Phase 5 and contained Mg, Si(Al) and Cl, indicating that the product generated due the reaction between PFA /ISSA and MgO interspersed with Phase 5 and changed the morphology of Phase 5. The latter amorphous phase was magnesium aluminosilicate. These two phases interlocked with each other and formed a stable structure which was resistance to the dissolution of water.

Reference

Deng, D. (2003). The mechanism for soluble phosphates to improve the water resistance of magnesium oxychloride cement. Cement and Concrete Research **33**(9): 1311-1317.

Fang, L., J.-s. Li, S. Donatello, C. Cheeseman, Q. Wang, C. S. Poon and D. C. Tsang (2018). Recovery of phosphorus from incinerated sewage sludge ash by combined two-step extraction and selective precipitation. Chemical Engineering Journal **348**: 74-83.

Li, Z. and C. Chau (2007). Influence of molar ratios on properties of magnesium oxychloride cement. Cement and Concrete Research **37**(6): 866-870.

Richardson, I. (2000). The nature of the hydration products in hardened cement pastes. Cement and Concrete Composites **22**(2): 97-113.

Richardson, I., J. Skibsted, L. Black and R. J. Kirkpatrick (2010). Characterisation of cement hydrate phases by TEM, NMR and Raman spectroscopy. Advances in Cement Research **22**(4): 233-248.

Thomas, J. and T. Gemming (2014). Analytical transmission electron microscopy: an introduction for operators, Springer Science & Business.

Chapter 7. Water Resistance Behavior of MOC with the Incorporation of Wood Fibres

7.1 Introduction

It was reported that timber formwork can be used to produce wood-cement board which performed better than neat cement based products with higher flexural strengths (Soroushian et al. 1994), and when compared to wood products only, the wood-cement board had a high resistance to harmful effects of sunlight, rain and insects(Lee 1986). However, the incompatibility between wood and Portland cement, which is caused by the inhibitory effect of extractable contents in wood on cement hydration, need to be addressed (Fan et al. 2012, Quiroga et al. 2016).

Compared with wood Portland cement composites, wood-MOC composites showed less incompatibility(Simatupang and Geimer 1990). It was found that the extractives in wood retard the hydration of Portland cement and the typical cement-hardening inhibitory components can be classified into two groups. One group is comprised of carbohydrates of sucrose in beech and arabinogalactan in larch, and the other are phenolic compounds with a catechol unit of plicatic acid in western red cedar, teracacidin in acacia mangium, and sequirin C in sugi (Na et al. 2014). Simatupang and Geimer compared the relative hydration time of magnesia cement and Portland cement and found the value of wood-Portland cement was much longer than that of wood-magnesia cement for most wood species(Simatupang and Geimer 1990). So MOC could significantly reduce this problem and be used to produce building components such as door panels and partition walls (Zhou and Li 2012). Besides, MOC has high fire resistance and

flexural strength and its hardening is achieved without the need of steam curing, which can reduce production costs (Simatupang and Geimer 1990). Nevertheless, the poor water resistance of MOC paste has limited the application of wood-MOC boards(Deng 2003). Above studies showed that the incorporation SCMs such as PFA and ISSA could significantly improve the water resistance of MOC as the amorphous phase generated due to the reaction between PFA/ISSA with MOC was stable in water and protected the MOC hydration products from decomposing. Adding wood may decrease water resistance of MOC as it absorbs water. Therefore, the water resistance and microstructure of wood-MOC board incorporating SCMs were investigated in this chapter. The wood was crushed in fibre and incorporated in MOC paste. The effect of wood fibre length on the water resistance of wood-MOC pastes was studied.

7.2 Sample preparation

The timber formworks were crushed by a wood crusher and the resulted fibres were categorized by sieving as Fine (0-0.6mm), Medium (0.6-2.36mm), Coarse (2.36-5mm), and Mixed (without sieving). The mixed wood contained 20% fine wood, 40% medium wood and 40% coarse wood. Figure7-1 shows the particle sizes of the different fibres used in the wood fibre cement composites. The production of longer, bulky fibres is more difficult and expansive. Therefore, the aspect ratio of wood fibre are normally low. The microstructure of the porous fibre is shown in Figure 7-2.

Figure 7-1 Wood fibres with different lengths (a) Fine (b) Medium (c) Coarse

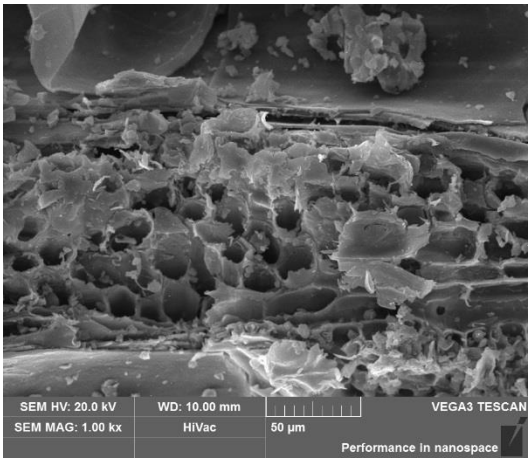

Figure 7-2 SEM image of wood fibre

The mix proportions of the wood-MOC cement paste and wood-MOC cement mortar are shown in Table 7-1 and Table 7-2. The wood cement paste and mortar were used to test the flexural strength and volume stability respectively. SCMs was used in the mix design according to our previous study, which concluded that MOC pastes incorporating 20% of PFA, 10% of GP or 30% ISSA as a replacement of MgO demonstrated high strength retention after water immersion. Using the mix proportions, wood cement paste specimens with the size of 5×100×200 mm and wood MOC cement mortars with the size of 25×25×285 mm were cast in steel molds which were covered with polyethylene sheets for 24 h before demolding. The length of the wood cement mortar was recorded immediately after demolding as the initial length. After air curing for 14 days (25 °C, RH=50%) or 13 days air curing plus 1day CO_2 curing (as shown in Table 7-1), all the specimens were immersed in water as the strength had reached a steady state. As the previous study showed that the cement paste blended with 30% ISSA showed high strength retention even without CO_2 curing, they were immersed in water after 14 days of air curing without using the CO_2 curing procedure.

Table 7-1 . Mix proportions of wood MOC pastes

Mixtures Notation	Molar ratios		PFA (%, by weight of powder)	GP (%, by weight of powder)	ISSA (%, by weight of powder)	Wood (%, by weight of powder)	Wood fibre length	Curing condition
	MgO/ $MgCl_2$	H_2O/ $MgCl_2$						
MOC paste	9	10	--	--	--	--	--	14 days of Air curing
C0	9	20	--	--	--	15	Mixed	14 days of Air curing
C(F)	9	20	--	--	--	15	Fine	13 days of air curing + 1 day of CO_2 curing
C(M)	9	20	--	--	--	15	Medium	
C(C)	9	20	--	--	--	15	Coarse	
C(MI)	9	20	--	--	--	15	Mixed	
F(F)	7.2	20	20	--	--	15	Fine	13 days of air curing + 1 day of CO_2 curing
F(M)	7.2	20	20	--	--	15	Medium	
F(C)	7.2	20	20	--	--	15	Coarse	
F(MI)	7.2	20	20	--	--	15	Mixed	
G(F)	8.1	20	--	10	--	15	Fine	13 days of air curing + 1 day of CO_2 curing
G(M)	8.1	20	--	10	--	15	Medium	
G(C)	8.1	20	--	10	--	15	Coarse	
G(MI)	8.1	20	--	10	--	15	Mixed	
S(F)	6.3	20	--	--	30	15	Fine	

S(M)	6.3	20	--	--	30	15	Medium	14 days of Air curing
S(C)	6.3	20	--	--	30	15	Coarse	
S(MI)	6.3	20	--	--	30	15	Mixed	

Table 7-2 Mix proportions of wood MOC mortars

Mixtures	Molar ratios		PFA	GP	ISSA	Wood	Wood fibre	Curing	Sand/
Notation	MgO/ $MgCl_2$	H_2O/ $MgCl_2$	(%, by weight of powder)	(%, by weight of powder)	(%, by weight of powder)	(%, by weight of powder)	length	condition	powder (mass ratio)
MC(F)	9	20	--	--	--	15	Fine	14 days of Air curing	1.5
MC(M)	9	20	--	--	--	15	Medium		
MC(C)	9	20	--	--	--	15	Coarse		
MC(MI)	9	20	--	--	--	15	Mixed		
MF(F)	7.2	20	20	--	--	15	Fine		
MF(M)	7.2	20	20	--	--	15	Medium		

MF(C)	7.2	20	20	--	--	15	Coarse
MF(MI)	7.2	20	20	--	--	15	Mixed
MG(F)	8.1	20	--	10	--	15	Fine
MG(M)	8.1	20	--	10	--	15	Medium
MG(C)	8.1	20	--	10	--	15	Coarse
MG(MI)	8.1	20	--	10	--	15	Mixed
MS(F)	6.3	20	--	--	30	15	Fine
MS(M)	6.3	20	--	--	30	15	Medium
MS(C)	6.3	20	--	--	30	15	Coarse
MS(MI)	6.3	20	--	--	30	15	Mixed

7.3 Test results and discussion

7.3.1 Flexural strength

Figure 7-3 (a) shows the variation of flexural strength of the wood cement paste prepared without the addition of SCMs and prepared with four types of wood fibres after air curing and water soaking (A14 means the flexural strength before water soaking, A14W14 means the flexural strength after water soaking for 14 days, A14W28 means the flexural strength after water soaking for 28 days). The results show that the strength increased with the increase of wood fibre length when they were cured in air despite there was a reduction in workability (spread for C(F), C(M), C(C), C(MI): 180mm, 160mm, 125mm, 150mm) with the incorporation of the wood fibres due to the increase of nonuniformity of wood

distribution with the increase of fiber length. After 14 days of air curing, the strength of C(F), C(M), C(C) was 12, 13.5, 17.5 MPa, respectively. And the flexural strength of C(MI) was slightly lower than that of C(C). When immersed in water for 14 days, the strength of the wood cement paste decreased dramatically. But the strength reached a steady state when prolonging the water immersion time. After 28 days of water immersion, C(MI) had the highest flexural strength (8MPa). This trend can be found in the wood cement paste incorporating PFA, GP and ISSA as shown in Figs. 3(b), (c) and (d) as well, except that the wood cement pastes incorporating coarse wood fibres had the highest flexural strength. Moreover, the strengths of F(C), G(C) and S(C) were higher than 12MPa even after 28 days of water immersion.

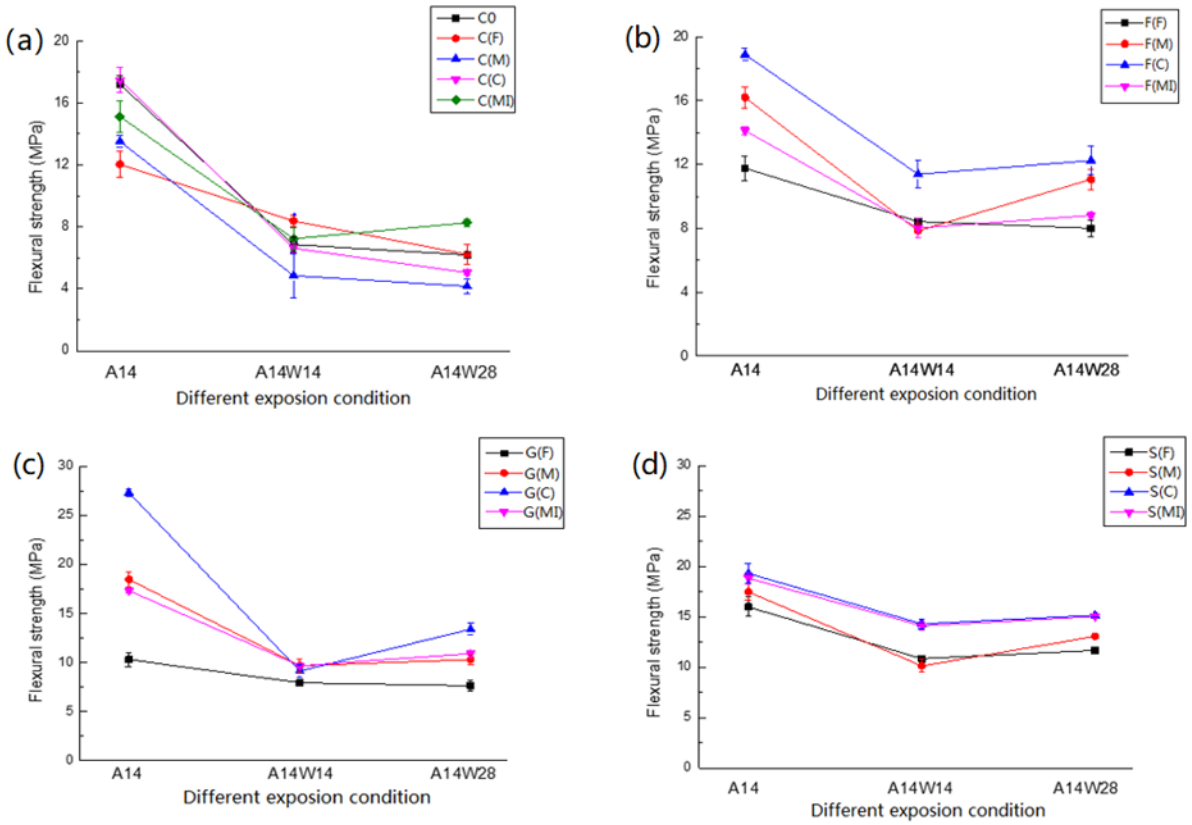

Figure 7-3 Flexural strength development of wood MOC pastes before and after water immersion (a)control wood MOC paste (b) wood MOC paste incorporating PFA (c) wood MOC paste incorporating GP (d) wood MOC paste incorporating ISSA

Figure 7-4 shows the strength retention of the wood cement paste incorporated with different supplementary cementitious materials. It can be seen that the strength retention increased when using SCMs to replace MgO. This result was in agreement with the previous studies that PFA, GP and ISSA could increase the water resistance of MOC due to the pozzolanic reaction. Besides, the composite blended with ISSA demonstrated the highest strength retention as phosphate in ISSA could significantly increase the water resistance of MOC. There was no clear trend about the effect of fibre length on the water resistance of wood MOC paste. The mixture prepared with the Mixed wood fibre (C(MI), S(MI)) showed the highest strength retention for the control wood cement paste and the cement paste incorporating ISSA. While for the cement paste incorporating FA and GP, the

mixture prepared with the fine wood fibre (F(F), G(F)) had the highest strength retention.

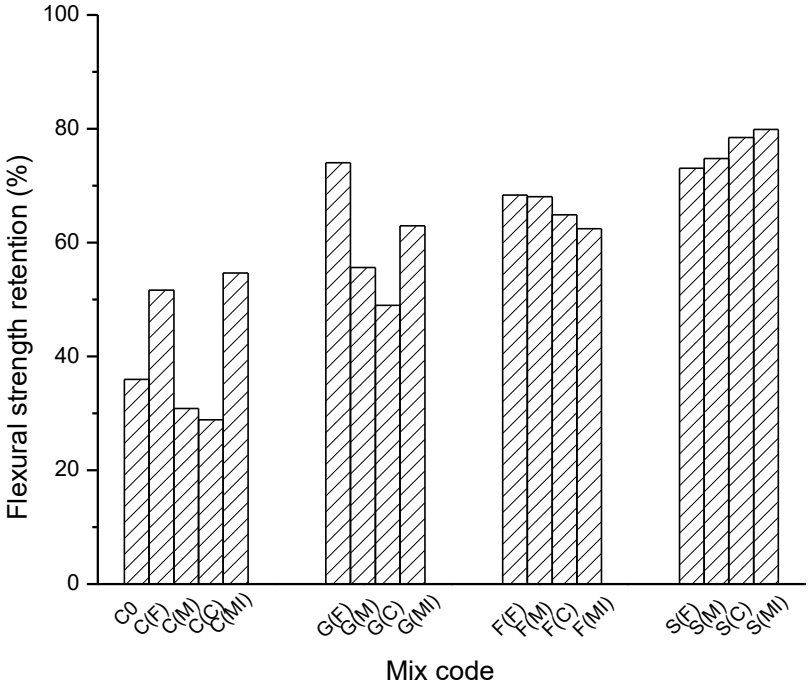

Figure 7-4 Strength retention of wood MOC pastes

7.3.2 Volume stability

The volume stability test results of the wood-cement composites without SCMs is shown in Figure 7-5(a). It is clear that the mortars expanded significantly at the beginning and became stable after 7 days of air curing. That is because of the expansion of the MOC matrix during hydration. Besides, it can be found that the expansion decreased with the increase of fibre length. The length change of C(F) was 0.465% after 7 days of air curing, while this value was only 0.189% for C(M). The same trend could be found in the composites incorporating SCMs as shown in Figs. 7-5(b)-(d)

The wood-cement composites for all the mixtures showed smaller expansion in water than that in air as shown in Figs. 7-6(The initial length was recorded right before water immersion). It was known that excess MgO would be transformed to brucite and led to an

increase in solid volume, which resulted in expansion in water. Above study showed that the expansion of MOC mortars after immersion in water for 28 days was 1.8%. While this value was reduced to around 0.15% for all the mixtures prepared in this study. This might be because the higher porosity of the wood cement pastes provided additional space (in terms of porosity) to accommodate the volume expansion of the wood-cement mortar in water (see section 7.3.3).

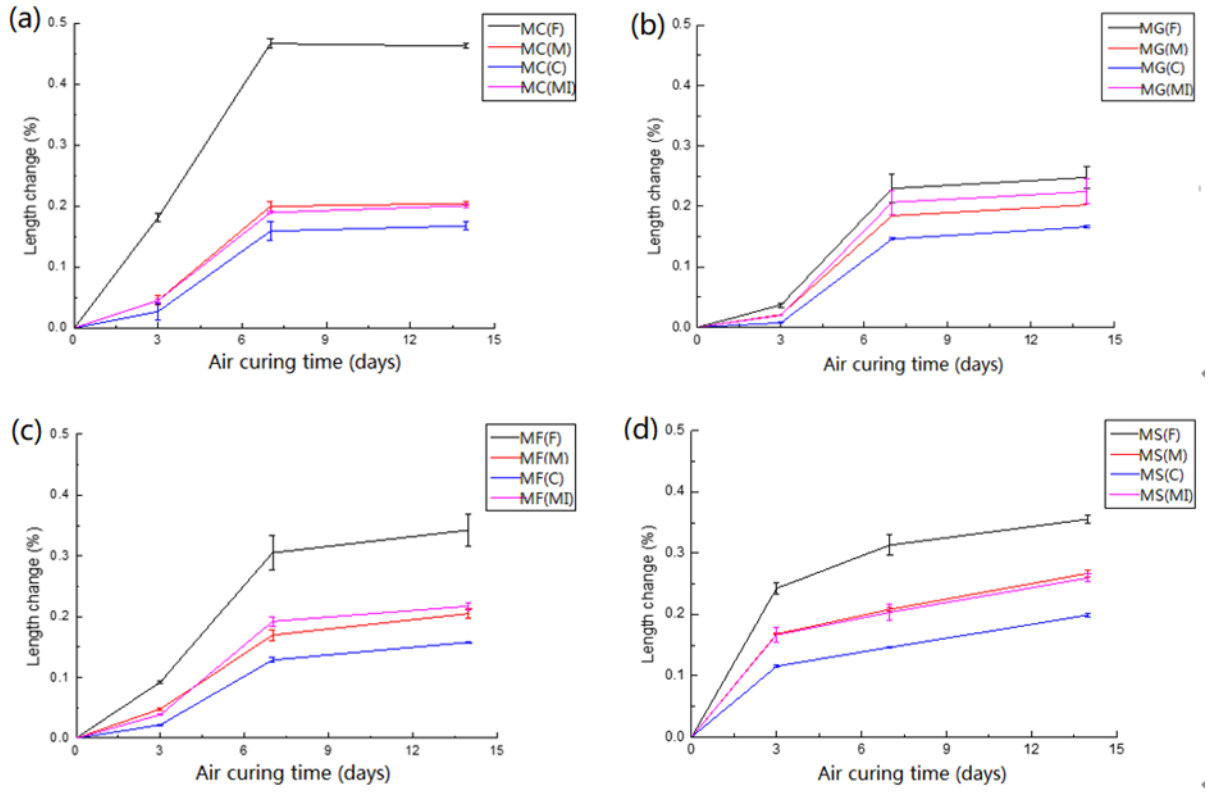

Figure 7-5 Length changes of wood-MOC mortars during air curing (a)control wood MOC paste (b) wood MOC paste incorporating PFA (c) wood MOC paste incorporating GP (d) wood MOC paste incorporating ISSA

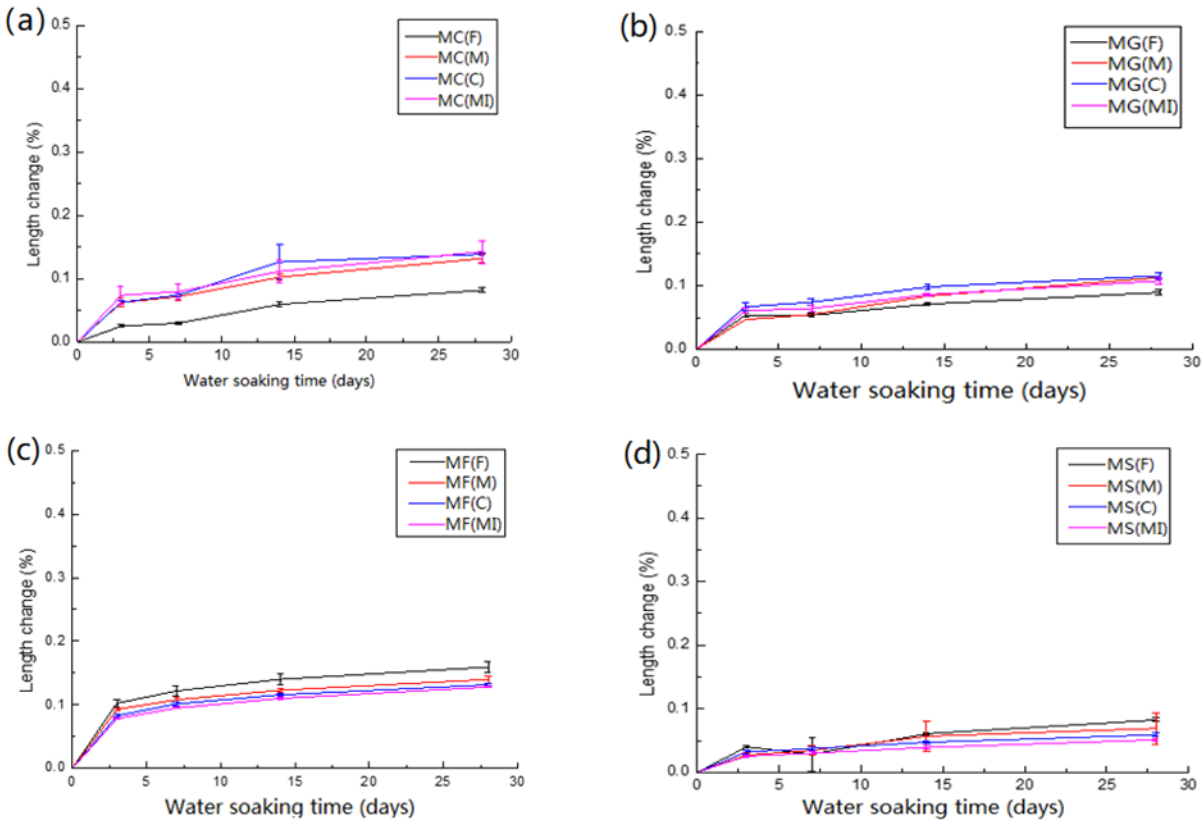

Figure 7-6 Length changes of wood-MOC mortars after water immersion (a)control wood MOC paste (b) wood MOC paste incorporating PFA (c) wood MOC paste incorporating GP (d) wood MOC paste incorporating ISSA

7.3.3 MIP

The effect of fibre length on the pore structure is presented in Figure 7-7. The total porosity can be calculated by dividing the total intruded volume by the bulk volume of the sample. From Fig.7-7(a), it can be seen that the porosity of MOC paste (3.173%) was much lower than that of wood MOC pastes (More than 20%). And the cumulative porosity of the wood-MOC composites incorporating fibres with different lengths shows the porosity increased with the increase of fibre length. The porosity of C(F) C(M), C(C), C(MI) was 20.34%, 25.83%, 27.72%, 24.13% respectively and this should be related to the workability as mentioned above that the C(C) had the lowest slump spread value. The density of C0, C(F) C(M), C(C), C(MI) was 1790kg/m^3,1370 kg/m^3,1340 kg/m^3,1310 kg/m^3,1360 kg/m^3 respectively, which was in agreement with the porosity results. Even though it was difficult to accurately test the

porosity of the wood fibre, the effect of the wood fibre on the volume stability of wood-MOC composites was related to the total porosity rather than the porosity of wood or cement matrix alone. The higher porosities in the MOC wood composites incorporating longer wood fibre provided more voids for the expansion of the cement matrix. Therefore, C(C) had the lowest volume change during air curing as shown in Fig. 7-5. Figure 7-7(b) provides more details of the pore structure distribution. The pore size distribution can be separated into two regions. Pores with sizes larger than 50 nm are associated to macro pores, while the pores less than 50 nm are associated to meso pores(Rockne et al. 2000, Nochaiya and Chaipanich 2011, Clarkson et al. 2013). The pores in MOC paste were mainly meso pores, while wood MOC paste contained both meso pores and macro pores. Besides, the composites incorporating longer wood fibres had a higher amount of meso pores and macro pores, which might be due to the lower workability resulting in more voids. The critical pore size, corresponding to the steepest slope of the differential of the cumulative pore size distribution curve, shifted from 38.6nm to 48.03nm when the longer fibre was used. The other peaks shifted to larger pore sizes as well.

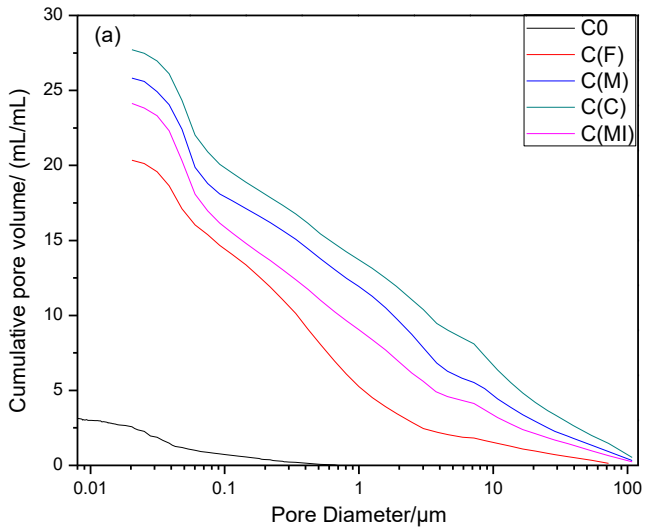

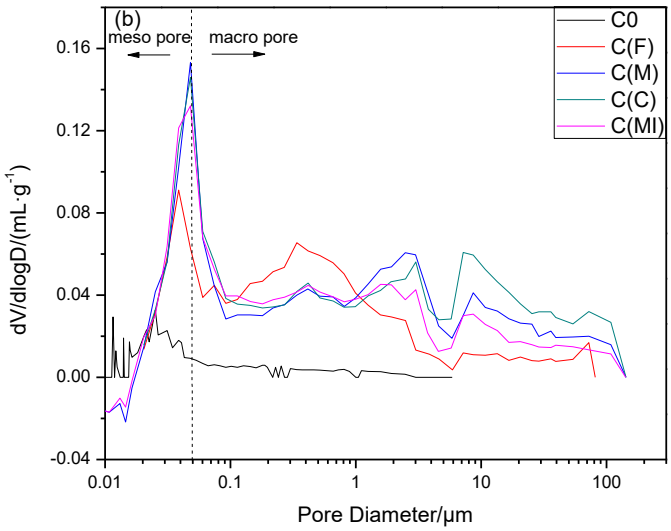

Figure 7-7 Effect of wood fibre length on MIP results (a) cumulative porosity; (b) first derivatives of the cumulative pore size distribution curves

7.3.4 ATR-FTIR

Figure 7-8 shows the ATR-FTIR spectra of wood, MOC paste and wood-MOC paste. The broad peak around 3300cm^{-1} corresponds to the OH stretching, appears in all the three spectra (Figure 7- 8(a)). The spectra in Figure 7-8(b) corresponding to the fingerprint region is more important to identify the unknown phases. The new bends detected in the wood-MOC paste are summarized in Table 7-3. These new bends were produced during the hydration of MOC with the incorporation of wood fibres, indicating the possible chemical reaction between the wood fibres and the MOC pastes.

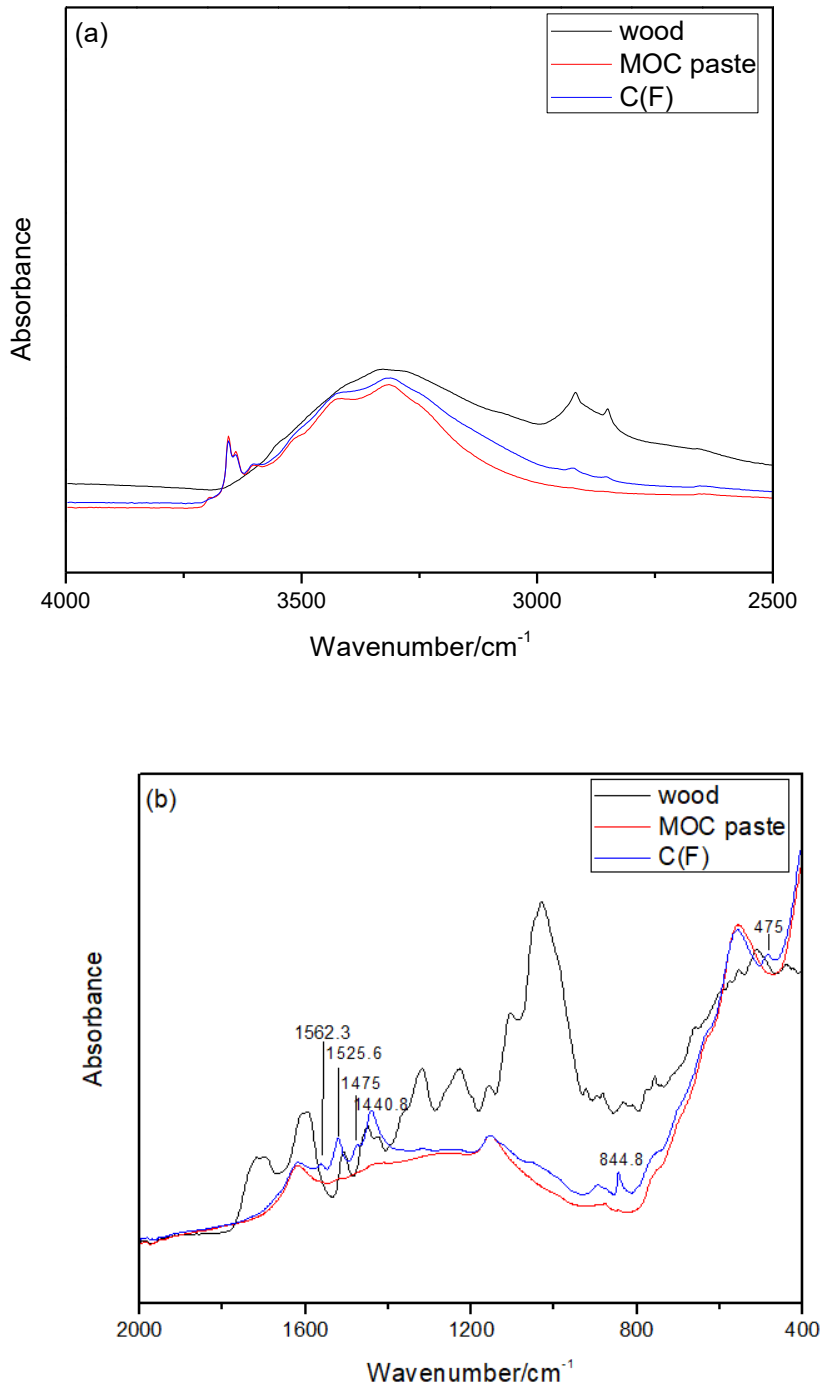

Figure 7-8 FTIR spectra of wood, MOC pastes and wood MOC paste (C(F)) (a) in the region 4000cm^{-1}-2500cm^{-1} (b) in the region 2000 cm^{-1}-400cm^{-1}

Table 7-3 Band characteristics of new phases in wood MOC paste C(F) compared with MOC paste by ATR-FTIR spectra

Wavenumber (cm-1)	Assignment	Sources
1562	COO- asymmetric stretching	(S.F.Weng 2010)
1526	carboxylate	(Odani and Matsumoto 2002)
1475	-CH_2 bending	(Datka and Tużnik 1985)
1441	-CH_3 bending	(Katsyuba et al. 2008)
845	Epoxide function group	(Xin et al. 2014)

7.3.5 XRD

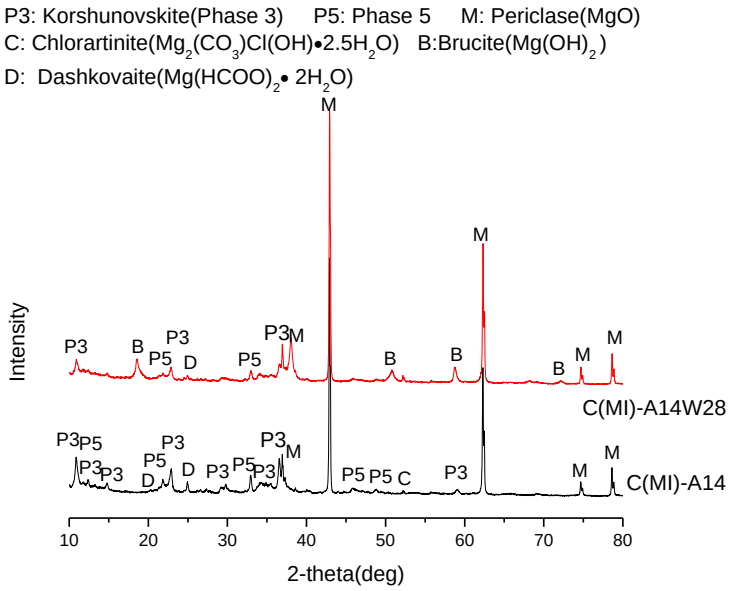

Figure 7-9 XRD patterns of wood-MOC pastes (C(MI)) before and after water immersion

Figure 7-9 shows the XRD patterns of C(MI) before and after 28 days of water immersion. According to the previous study, the main crystalline phases observed in MOC paste were Phase 5, Phase 3 and unreacted MgO after 14 days of air curing. In this study, the new

phase produced in the wood-MOC paste (C(MI)-A14) was dashkovaite ($Mg(HCOO)_2 \cdot 2H_2O$), which was in agreement with FTIR results that a small amount of carboxylate was formed due to the reaction between the wood fibre and the MOC paste matrix. Chlorartinite was observed in the C(MI)-A14 due to the carbonation of MOC. The band for CO_3^{2-} was not observed in the FTIR result, which might be due to the low content of Chlorartinite. After C(MI) was immersed in water for 28 days, the content of Phase 3 and Phase 5 decreased, which was in agreement with the flexural strength result that the strength decreased due to the decomposition of Phase 3 and Phase 5 in water. Moreover, the generation of $Mg(OH)_2$ provided the proof of the expansion of the wood-MOC paste after immersion in water.

7.3.6 SEM

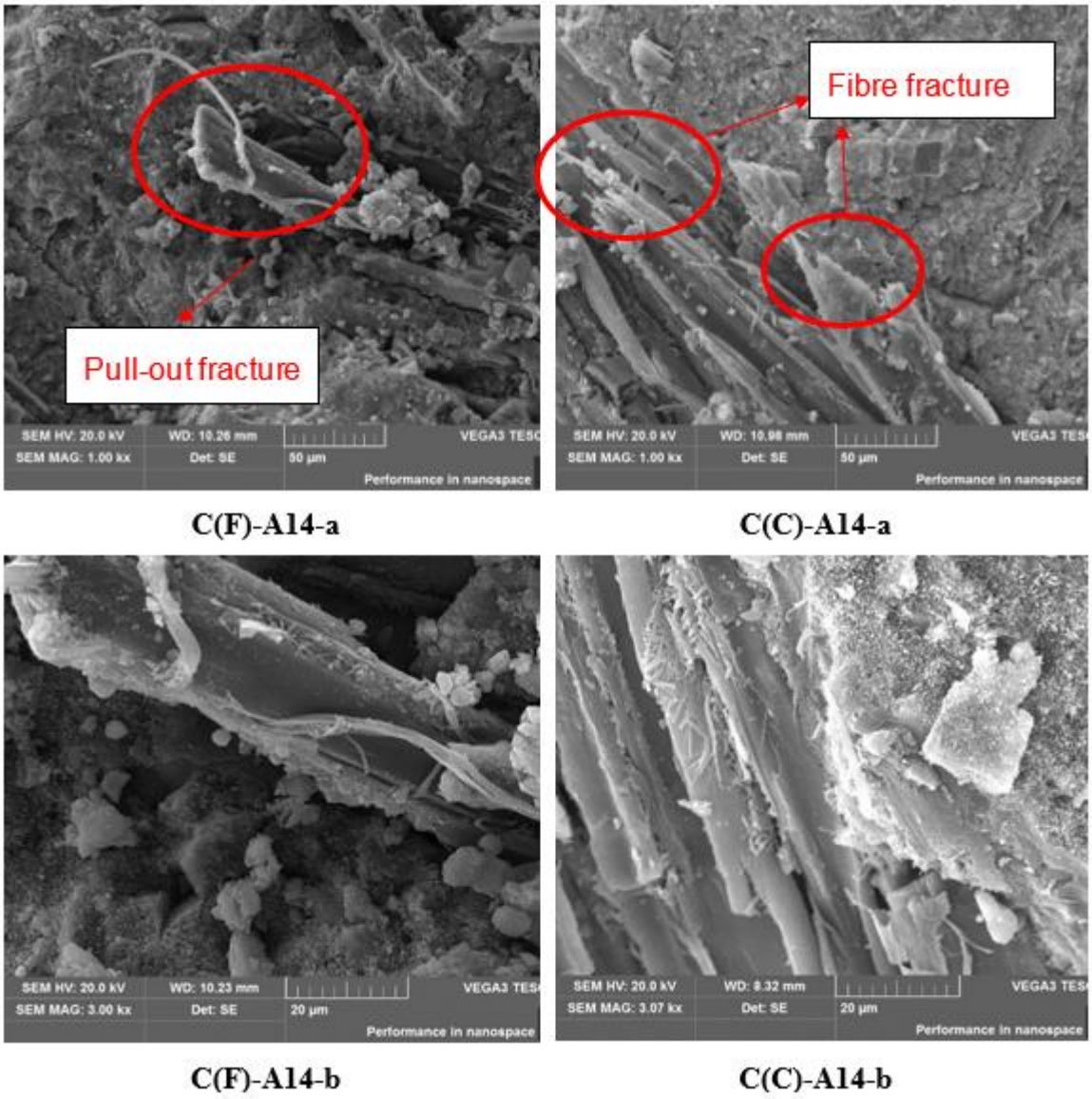

Figure 7-10 Scanning electron micrographs of fractured surfaces of C(F) and C(C) after 14 days of air curing

SEM micrographs of the fracture surface of the wood cement paste with the shorter wood fibre (C(F)-A14) and the longer wood fibre (C(C)-A14) are displayed in Figure 7-10. It can be seen that the short fibre was pulled-out from the matrix (C(F)-A14-a) while the long fibre was fractured in the matrix (C(C)-A14-a). Besides, it is clear that the needle-like hydration products

(i.e. Phase 5 and Phase 3 according to the EDX result) were interlocked with the wood fibres (refer to C(F)-A14-b and C(C)-A14-b). The particle size of the hydration products in C(C) (C(C)-A14-b) was larger than that in C(F) (C(F)-A14-b).

During water immersion, the hydration products grew bigger continuously around the wood fibre. The hydration products were very fine long needles in C(C) (C(C)-A14W14). While that in the dense structure of C(MI) (C(MI)-A14W14) were interlocked shorter needles and showed no clear edges (Figure 7-11). These products in C(C)-A14W14 and C(MI)-A14W14 were a mixture of Phase 5 and Phase 3 according to the EDX results. This was in agreement with the XRD result that a certain amount of P5 and P3 remained in the wood-fibre composites after water immersion.

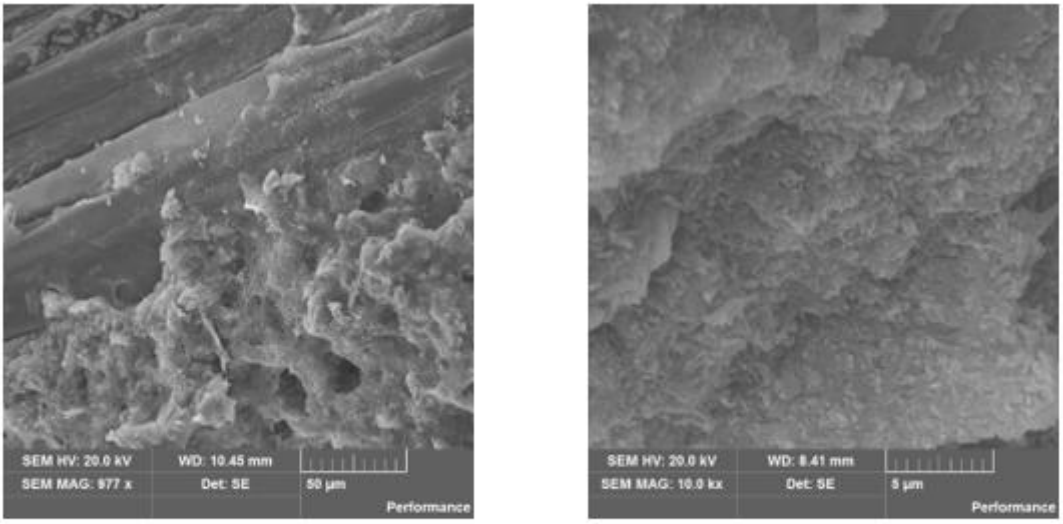

Figure 7-11 Scanning electron micrographs of fractured surfaces of C(C) and C(MI) after 14 days of water immersion

7.4 Discussion

The bonding between the wood fibre and the matrix includes physical bonds and chemical bonds. Physical bonds are formed during the hydration process when the hydration products formed and interlocked with each other. As shown in the SEM micrographs , the Phase 5 and Phase 3 grew into the fibre and enhanced the physical bonding between the fibre and the matrix. Chemically, the metal hydroxyl groups in the matrix could react with the carboxylic groups in the wood fibre and new chemical bondings such as carboxylate were identified in the wood-MOC composites as shown in Figure 7-8. And the new phase (dashkovaite) was observed from XRD could further prove the chemical reaction between the wood fibre and the MOC paste matrix. The flexural strength of the wood-MOC paste decreased dramatically after immersion in water, but it reached a steady state and a certain amount of hydration products was observed after 14 days of water immersion. Therefore, the flexural strength of the wood-MOC paste could still be higher than 8 MPa after 28 days of water immersion. The water resistance was further improved when adding SCMs, which was because the SCMs could react with MOC and formed stable hydration products. The wood cement paste incorporating ISSA presented the highest strength retention due to the high water resistance of the SCM modified matrix.

The MOC paste expanded during air curing and water immersion, which was due to the hydration of MOC and the excess MgO respectively. The incorporation of the wood fibres could improve the volume stability of the MOC. This might be attributed to the fibre provided hollow space and voids for the expansion of the MOC matrix which is consistent with the data presented in Fig 7-2 and Fig. 7-7. Adding SCMs could further improve the volume stability of the wood fibre-cement mortar due to the lower content of MgO in these mixtures.

In terms of fibre length, the wood fibre-cement composite prepared with the longer fibre showed higher flexural strength. It was reported that fibre pull-out dominated the flexural strength of the wood-cement composites. The larger frictional force of the longer fibre due to its larger surface area compared with the short ones might increase the bond between the fibre and the matrix (Lindhagen and Berglund 2000). Therefore, the flexural strength of the wood-MOC composites incorporating longer fibres was higher than that prepared with the shorter fibres. The short fibres limited the width of crack that can be bridged and would slip from the paste matrix(Campbell and Coutts 1980, Lindhagen and Berglund 2000), which can be observed from the SEM pictures that the wood-cement composites prepared with the shorter fibres and the longer fibres failed by fibre pull-out and fibre fracture respectively. Besides, the particle size of the hydration products was larger (as large thin needles) in the wood-MOC paste incorporating the longer fibres , which was consistent with a previous study stating similar observations for MOC pastes containing larger voids (Matkovic and Young 1973). Moreover, the longer fibre could enhance the volume stability of the wood-cement composites subject to air curing, which was related to its higher porosity.

7.5 Summary

The flexural strength of wood MOC paste was similar to that of MOC paste during water immersion but adding SCMs could improve the water resistance of the wood cement paste as SCMs could enhance the water resistance of cement matrix. The flexural strength of the wood MOC cement paste for all the mixtures increased with the increase of wood fibre length when cured in air. That is because the longer fibre enabled a substantial amount of fibre fractures whereas the short fibre composites failed mainly by fibre pull-out. Besides, the wood cement pastes prepared with the longer fibres had higher volume stability in air curing due to the higher porosity providing more space for the expansion of MOC matrix.

Compared to wood fibre and pure MOC paste, new chemical bondings such as carboxylate were detected and a new phase (dashkovaite) was observed in the wood-cement paste indicating the formation of chemical bonds between wood fibre and the MOC matrix.

The hydration of excess MgO in MOC was the principal cause of expansion of the MOC mortar when it is immersed in water. The wood fibre cement mortar showed lower expansion in water due to the inclusion of a certain amount of voids during fibre incorporation to reduce the expansion.

Reference

Campbell, M. and R. Coutts (1980). Wood fibre-reinforced cement composites. Journal of Materials Science **15**(8): 1962-1970.

Clarkson, C. R., N. Solano, R. Bustin, A. Bustin, G. Chalmers, L. He, Y. B. Melnichenko, A. Radliński and T. P. Blach (2013). Pore structure characterization of North American shale gas reservoirs using USANS/SANS, gas adsorption, and mercury intrusion. Fuel **103**: 606-616.

Datka, J. and E. Tużnik (1985). Hydroxyl groups and acid sites in Na ZSM-5 zeolites studied by ir spectroscopy. Zeolites **5**(4): 230-232.

Deng, D. (2003). The mechanism for soluble phosphates to improve the water resistance of magnesium oxychloride cement. Cement and Concrete Research **33**(9): 1311-1317.

Fan, M., M. K. Ndikontar, X. Zhou and J. N. Ngamveng (2012). Cement-bonded composites made from tropical woods: Compatibility of wood and cement. Construction and Building Materials **36**: 135-140.

Gokak, I. B. and T. Taranath (2014). Phytosynthesis of silver nanoparticles using leaf extract of Wattakaka volublis (LF) Stapf., and their antibacterial activity. Int J Sci Env Tech **3**: 93-99.

Katsyuba, S. A., E. E. Zvereva, A. V. Chernova, A. R. Shagidullin, S. E. Solovieva, I. S. Antipin and A. I. Konovalov (2008). IR and NMR spectra, intramolecular hydrogen bonding and conformations of mercaptothiacalix [4] arene molecules and their para-tert-butyl-derivative. Journal of Inclusion Phenomena and Macrocyclic Chemistry **60**(3-4): 281-291.

Lee, A. W. (1986). Compressive strength of cylindrical samples as an indicator of wood-cement compatibility. Forest Products Journal **36**(11): 87-90.

Lindhagen, J. E. and L. A. Berglund (2000). Application of bridging-law concepts to short-fibre compositesPart 1: DCB test procedures for bridging law and fracture energy. Composites Science and Technology **60**(6): 871-883.

Matkovic, B. and J. Young (1973). Microstructure of magnesium oxychloride cements. Nature physical science **246**(153): 79.

Na, B., Z. Wang, H. Wang and X. Lu (2014). Wood-cement compatibility review. Wood Research **59**(5): 813-826.

Nochaiya, T. and A. Chaipanich (2011). Behavior of multi-walled carbon nanotubes on the porosity and microstructure of cement-based materials. Applied Surface Science **257**(6): 1941-1945.

Odani, T. and A. Matsumoto (2002). Solvent-free synthesis of layered polymer crystals. Polymer journal **34**(11): 841-846.

Quiroga, A., V. Marzocchi and I. Rintoul (2016). Influence of wood treatments on mechanical properties of wood–cement composites and of Populus Euroamericana wood fibers. Composites Part B: Engineering **84**: 25-32.

Rockne, K. J., G. L. Taghon and D. S. Kosson (2000). Pore structure of soot deposits from several combustion sources. Chemosphere **41**(8): 1125-1135.

S.F.Weng (2010). Fourier transform and spectrum analysis (in Chinese). , Beijing: Chemical Industry Press.

Simatupang, M. H. and R. L. Geimer (1990). Inorganic binder for wood composites: feasibility and limitations. Proceedings of Wood Adhesive Symposium, Forest Product Resources Society.

Soroushian, P., S. Marikunte and J.-P. Won (1994). Wood fiber reinforced cement composites under wetting-drying and freezing-thawing cycles. Journal of Materials in Civil Engineering **6**(4): 595-611.

Xin, Z., B. Du, S. Yan, S. Du, J. Ding, Z. Yang and W. Ren (2014). Surface modification of poly (styrene-b-(ethylene-co-butylene)-b-styrene)(SEBS) elastomer via covalent immobilization of nonionic sugar-based Gemini surfactants. Journal of Biomaterials Science, Polymer Edition **25**(10): 1045-1061.

Zhou, X. and Z. Li (2012). Light-weight wood–magnesium oxychloride cement composite building products made by extrusion. Construction and Building Materials **27**(1): 382-389.

Chapter 8. Effect of Fiber Content on properties of Wood-MOC Board

8.1 Introduction

The utilization of waste wood in making cement-bonded construction materials offers many advantages including lower density, lower thermal conductivity, high flexural strength compared to cement. Furthermore, they have much higher flexural strength, higher fire resistance and lower water absorption compared to wood production. Based on the above result, it was found that wood could enhance the water resistance of MOC paste. However, litter research has been focused on the properties of wood-MOC composites.

In this chapter, waste timber formwork from construction sites was used as fibre to prepare wood- MOC board. The effect of wood fibre content, PFA and ISSA on the mechanical and durability properties of wood-MOC board was investigated. Greenhouse gases (GHGs) emission, one of the representative and most globally concerned environmental impacts, for the production of different types of composite boards was assessed and compared by using LCA technique. The ‘cradle-to-gate’ system boundary with 1 kg of board production was considered as the functional unit in this assessment. This study focused on using alternate methods to “produce” the durable MOC. So a cradle to gate approach was used for LCA. If the cradle to grave method is used, much more detailed information regarding the application and eventual disposal of the products are needed which are beyond the scope of this study.

8.2 Sample preparation

The wood-MOC board was prepared with the proportion shown in Table 8-1. The crushed wood without sieving (refers to the "MIX" wood in Chapter 7) was used to reduce cost. The incorporation of PFA and ISSA and CO_2 curing condition were adopted to obtain high water resistance according to our previous studies. The prepared composites after mixing thoroughly using a mechanical mixer were transferred into steel molds (160×160×20mm) and covered with polyethylene sheets.

After 24h of hardening, the wood-MOC board was demolded and placed into a curing chamber at 25±1℃ with a controlled humidity of 50%±5% for air curing. After 13 days of air curing, some samples were placed into a steel chamber for CO_2 curing. The chamber was vacuumed to -0.5 bar before the CO_2 injection. CO_2 used for CO_2 curing was at >99% purity and the pressure was 0.1bar.

Table 8-1 Mix proportions of wood MOC board

Mixtures Notation	Molar ratios		PFA (%, by weight of powder)	ISSA (%, by weight of powder)	Wood (%, by weight of powder)	Wood (%by weight of sample)	Curing condition
	$MgO/MgCl_2$	$H_2O/MgCl_2$					
C0	9	10	--	--	--	--	14 days of air curing
C15	9	20	--	--	15	5.53	13 days of air curing +
C20	9	20	--	--	20	7.24	
C25	9	20	--	--	25	8.89	

F15	7.2	20	20	--	15	5.53	1 day of CO_2 curing
F20	7.2	20	20	--	20	7.24	
F25	7.2	20	20	--	25	8.89	
S0	6.3	10	--	30	--	--	
S15	6.3	20	--	30	15	5.53	14 days of air curing
S20	6.3	20	--	30	20	7.24	
S25	6.3	20	--	30	25	8.89	

8.3 Test results and discussions

8.3.1 Flexual strength

The flexural strength of the wood-MOC boards incorporating different types and percentages of SCMs after 14 days of air curing are summarized in Figure 8-1(a). It can be seen that the flexural strength of the wood-cement board prepared with 15%, 20% and 25% wood fibre was 11.4 MPa, 16.3MPa, and 18.9MPa, respectively. This indicates that the increase of wood fibre content would lead to an increase of flexural strength. Similar observations were found for the wood-MOC board prepared with the incorporation of PFA and ISSA as well. The flexural strength of wood-MOC board incorporating 20% PFA and 15% wood fibre (F15) was slightly higher than C15, which might be due to the filler effect of PFA (Chindaprasirt and Rukzon 2008) and the products generated from the reaction between PFA and MOC enhancing the bonding between the wood fibre and the cement matrix. However, F20 and F25 had lower strength than C20 and C25. That was probably because F20 and F25 had higher porosity than F15(Chindaprasirt et al. 2005), which reduced the filler effect. In spite of this, the F20 and F25

met the minimum requirements of International Standard, ISO 8335-1987 (ISO 1987) (i.e. 9MPa).

The wood-MOC board incorporating ISSA had higher flexural strength than the one without ISSA incorporation, which was consistent with our previous study. This is probably because the ISSA particles are porous with irregular shape that enhanced the bonding between the cement matrix and the wood fiber (Lin et al. 2008). Besides, the higher content of hydration products in the ISSA-blended composites compared to the PFA-blended composites improved the flexural strength as well.

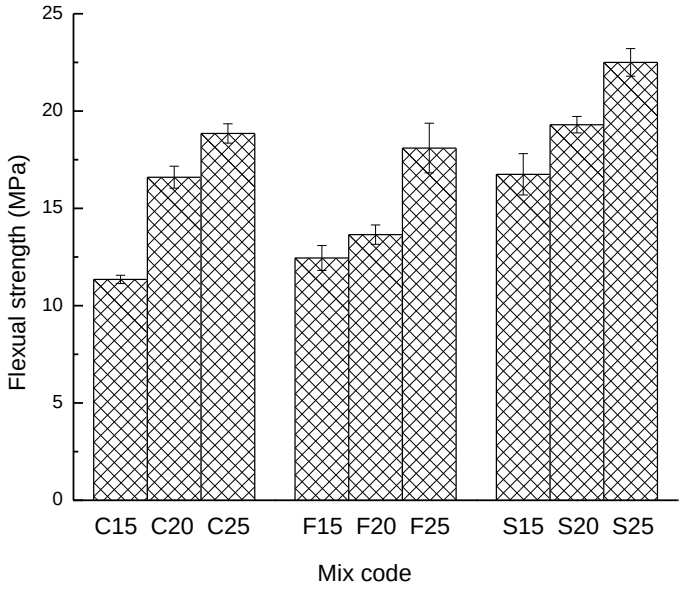

(a)

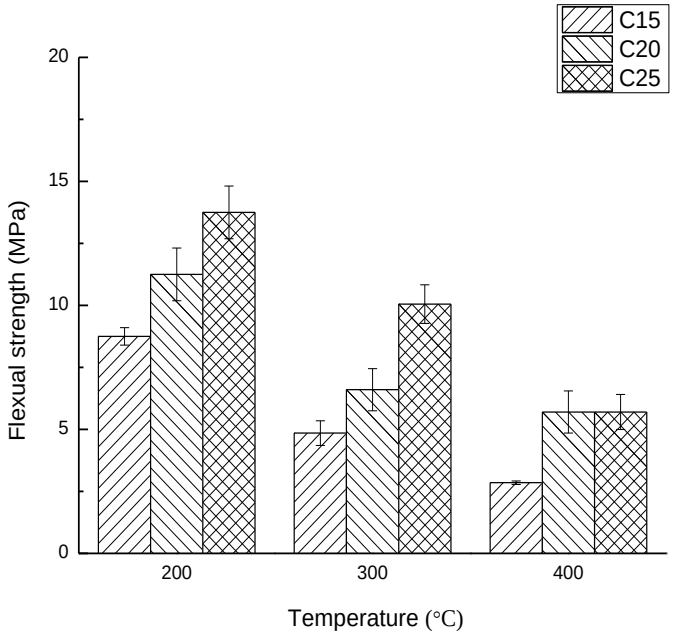
C15
C20
C25
Flexual strength (MPa)
0
5
10
15
20
200
300
400
Temperature (°C)

(b)

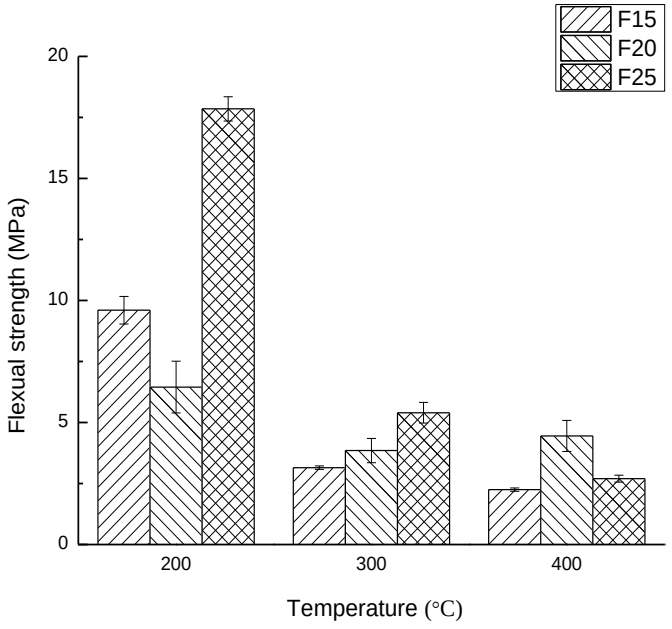
F15
F20
F25
Flexual strength (MPa)
0
5
10
15
20
200
300
400
Temperature (°C)

(c)

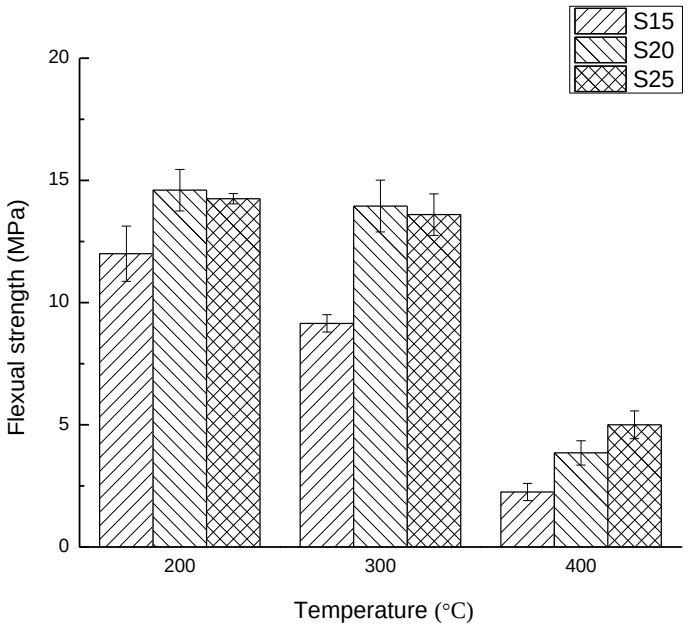

(d)

Figure 8-1 Flexural strength of wood-MOC boards before and after exposed to elevated temperatures; (a) control wood-MOC boards after 14 days of air curing;(b) wood-MOC boards after elevated temperature exposure;(c) wood-MOC boards incorporating PFA after elevated temperature exposure;(d) wood-MOC boards incorporating ISSA after elevated temperature exposure

8.3.2 High temperature resistance

Even though the MOC is known to have high fire resistance and has been used as a fire retardant material (Montle and Mayhan 1974, Montle and Mayhan 1974), the charring temperature of wood is normally between 120 ºC -150 ºC (Babrauskas 2002). So it is necessary to test the properties of wood-MOC board after exposure to elevated temperatures. The flexural strength of wood-MOC boards are shown in Figure 8-1(b)-(d). It can be seen that the strength decreased with the increase in exposure temperature, due to two reasons. The first is the decomposition of hydration products. According to a previous study, free water was evaporated from MOC when it was exposed to 200 ºC and crystalline water would be lost when the temperature was

above 200 ºC. When exposed to the higher temperature, the hydration products of MOC, phase 3 and phase 5 were decomposed to MgO and HCl. The second reason is the charring of wood fibres. The increase of porosity due to the loss of hydration products and the wood fibre led to the decrease in strength.

For the control board (Figure 8-1(b)), C25 had the highest strength when compared to C15 and C20 after the exposure temperature was up to 300 ºC, which was related to the higher wood fibre content of C25 because there were still some wood fibres remained in the composite (pls see Fig 8-2). Notwithstanding the loss of strength, C25 still had appreciable strength value after exposure to 300 ºC. The flexural strength of the wood-MOC board incorporating PFA was lower than the control board, while the wood-MOC board incorporating ISSA retained a higher strength when the exposure temperature was up to 300 ºC, indicating the higher thermal stability of the hydration products in the latter. All the mixtures lost most of the original strength when the temperature reached 400 ºC. Although the wood-MOC board may not withstand temperatures higher than 400 ºC, it performed much better than pure wood board as the ignition point of wood is approximately 190 ºC -260 ºC (Babrauskas 2002).

The mass losses of the wood-cement boards were recorded after the specimens were exposed to the elevated temperatures (Table 8-2). It can be seen the mass loss increased with the increase of temperature. Besides, the composites incorporating higher contents of wood fibre showed higher mass losses. As shown in Fig. 8-2, the colour of MOC matrix and wood fibre changed gradually after the different elevated temperature exposures. Before heating, both the MOC matrix and wood were yellowish in colour. When the exposure temperature reached 400 ºC, the MOC matrix turned white due to the formation of MgO. Meanwhile, the wood fibre charred and turned black.

Table 8-2 Mass loss of wood-MOC boards after exposure to elevated temperatures

Mixtures			Mass (g)			Mass loss (%)	
Notation	20 ºC	200 ºC	300 ºC	400 ºC	200 ºC	300 ºC	400 ºC
C15	911.4	879.2	852.6	828.8	3.53	6.45	9.06
C20	900.6	837.8	813.6	789.9	6.97	9.66	12.29
C25	863.2	793.8	749.3	704.5	8.04	13.2	18.39
F15	870.4	834.5	822.7	774.7	4.13	5.48	10.99
F20	858.1	807.9	794.0	742.7	5.85	7.47	13.45
F25	844.8	772.6	732.4	691.8	8.55	13.3	18.11
S15	912.9	893.5	881.7	836.8	2.12	3.42	8.34
S20	903.7	842.3	817.1	782.2	6.79	9.58	13.44
S25	897.0	799.9	752.0	734.1	10.83	16.17	18.16

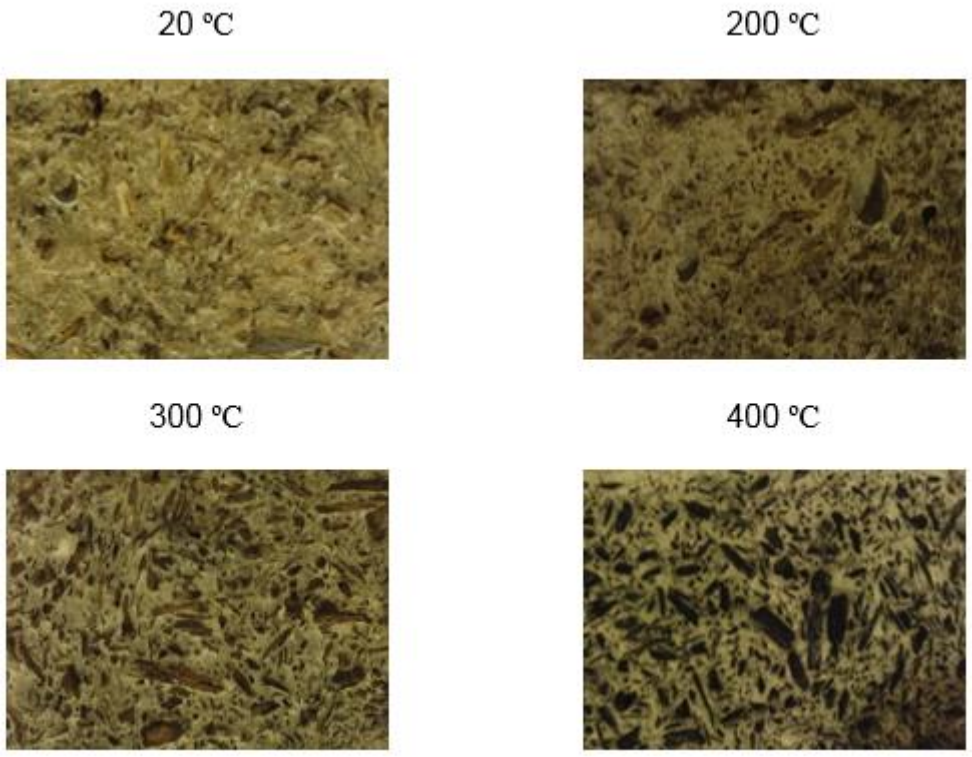

Figure 8-2 Colour changes of the internal cross-section of C20 subjected to different elevated temperatures

8.3.3 Water absorption and thickness swelling

Figure 8-3 shows the effect of wood fibre content and the incorporation of PFA and ISSA on the water absorption (WA) of the wood-MOC boards. It can be seen that increase of wood fibre content increased WA of the boards, which could be related to two reasons. First, the higher

content of wood induced more voids which absorbed more water. Second, the hydrophilic nature of wood (Bledzki et al. 1998) as the free OH groups of the wood cellulose contacted with water and formed hydrogen bonding. It can also be observed that the WA of the wood-MOC board slightly increased with the use of PFA and ISSA, which is consistent with our previous study. Even though F25 showed the highest WA (4.22%), it can still be considered as a low value. The thickness swelling (TS) values of the wood-MOC board are summarized in Table 8-3. It can be seen that the TS values of all the boards were lower than 2% which is stipulated by the standard (ISO 8335, 1987) (Aggarwal et al. 2008), indicating the wood-MOC boards had good dimensional stability respect to water absorption. As the wood-MOC board has a lower water resistance than wood-Portland cement boards, its application as a flooring material should be limited to indoor use. But it is generally suitable for partition applications as the water absorption and thickness swelling could meet the requirement of wood-cement particle board.

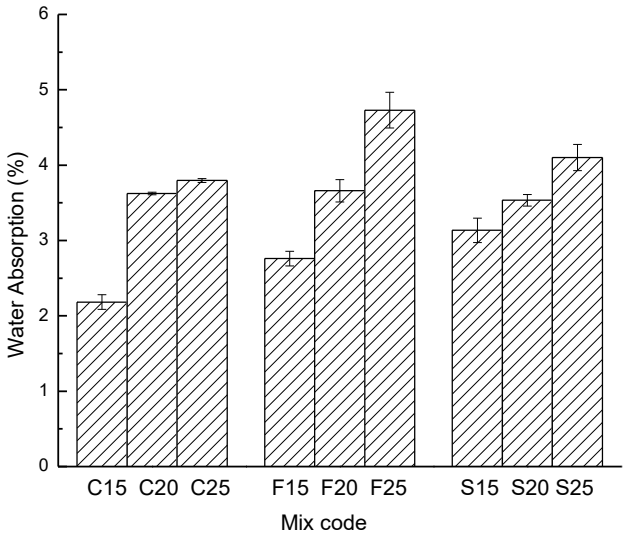

Figure 8-3 WA of wood-MOC boards

Table 8-3 TS of wood-MOC boards

Specimen code	TS (%)	Specimen code	TS (%)	Specimen code	TS (%)
C25	0.24	F25	0.25	S25	0.44
C20	0.12	F20	0.15	S20	0.4
C25	0.11	F25	0.23	S25	0.21

8.3.4 Water resistance

Figure 8-4 shows the change of flexural strength of the wood-MOC boards after water immersion. The flexural strength decreased after water immersion in all the mixes, which was due to the decomposition of the MOC hydration products. This figure also shows that the higher the wood fibre content in the wood-MOC board, the higher was their residual flexural strength. Table 8-4 summarizes the flexural strength retention (FSR) of the boards. The FSR decreased with increasing wood content, which might be due to the softening of the wood fibres with water immersion. The boards prepared with PFA and ISSA had higher FSR values than the control as the MOC hydration products in these composites had higher water resistance.

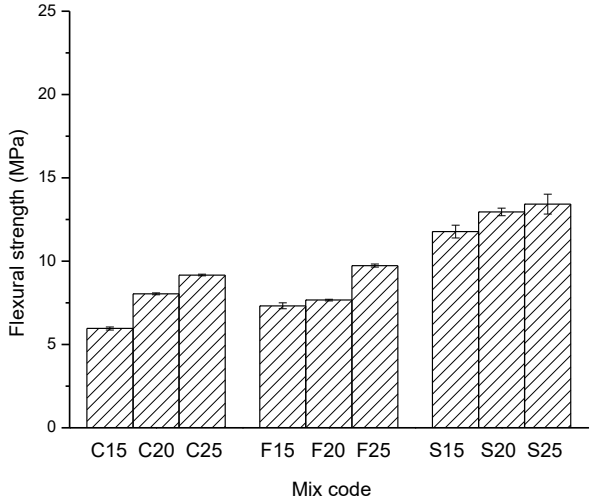

Figure 8-4 Flexural strength of wood-MOC boards after water immersion for 28 days

Table 8-4 Flexural strength retention (FSR) of wood-MOC boards

Specimen code	FSR (%)	Specimen code	FSR (%)	Specimen code	FSR (%)
C15	52.9	F15	60.0	S15	71.7
C20	49.5	F20	56.5	S20	68.3
C25	48.3	F25	53.7	S25	61.3

8.3.5 Noise reduction

The impact noise reduction results are shown in Figure 8-5 and Figure 8-6. Figure 8-5 shows the noise reduction effect at individual frequencies range from 630 Hz to 3150 Hz. It can be seen that even though the wood-cement board exhibited lower noise reduction effect than that of plywood, it has much better noise reduction effect compared to the pure MOC paste (C0). C25 showed excellent sound insulation at frequencies range from 630Hz to 2000Hz and attained 21 dB noise level reduction at 1600Hz. All the composites showed better sound insulation at the frequencies higher than 1600 Hz. Figure 8-6 shows the overall noise reduction effect of all the prepared boards. It illustrates that the wood-MOC boards incorporating higher contents of wood fibre exhibited better sound insulation properties. When adding 0%(C0), 15%(C15), 20%(C20), 25%(C25) of wood fibre, the noise reduction was 2.5 dB, 4.1 dB, 8.2 dB and 13.1 dB respectively. This may also be due to the higher air void content in the composites prepared with higher contents of wood. Adding PFA and ISSA could slightly decrease the noise reduction effect, which may due to the overall denser structure.

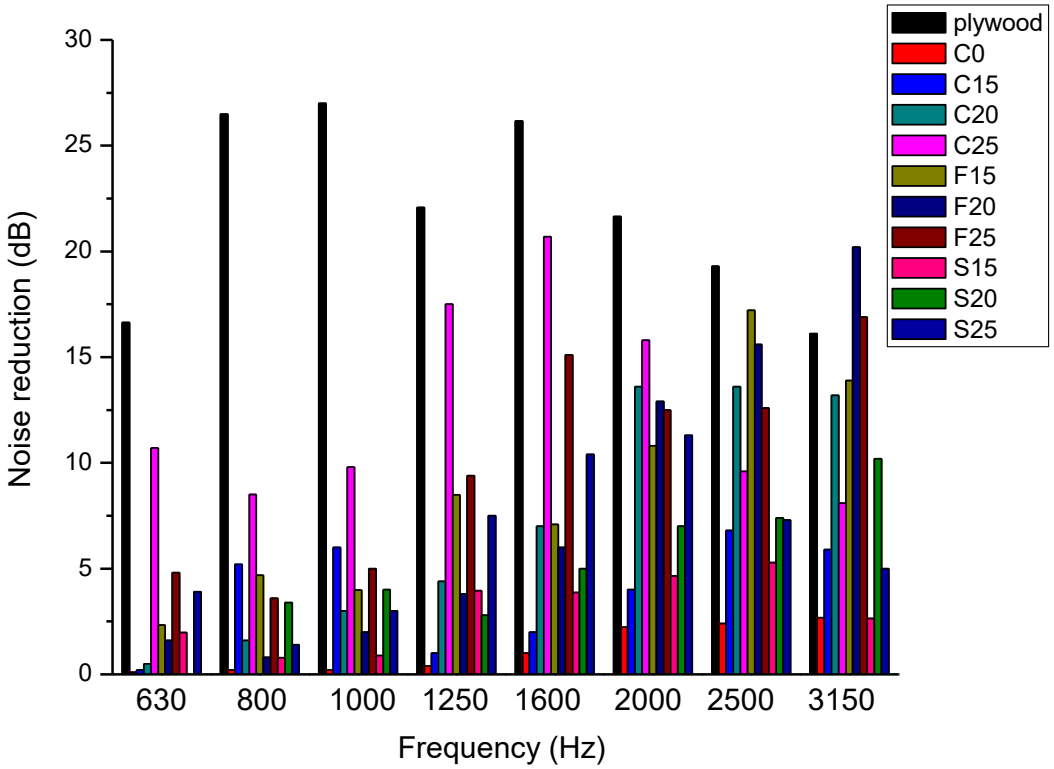

Figure 8-5 Impact sound reduction for plywood, MOC paste and different wood-MOC boards at 630Hz-3150Hz

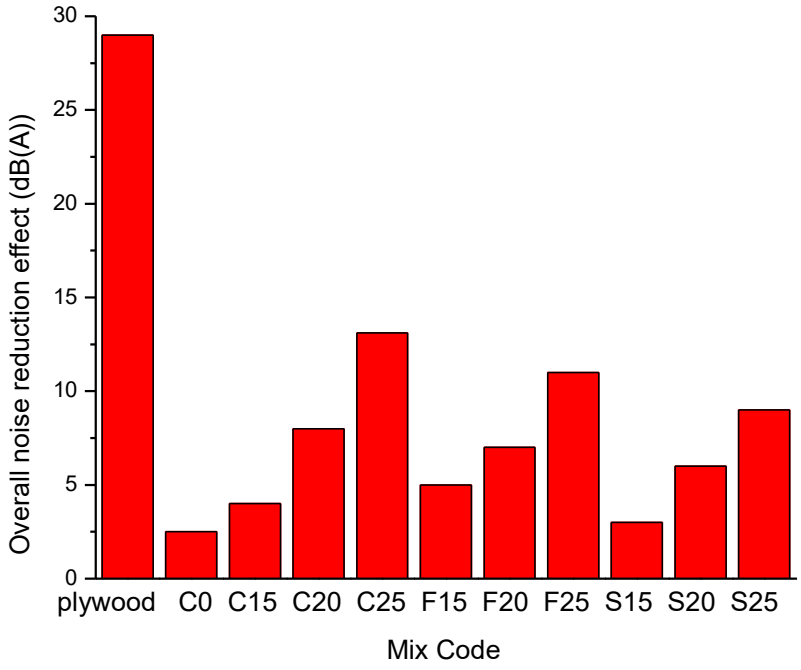

Figure 8-6 Overall noise reduction for plywood, MOC paste and different wood-MOC boards

8.3.6 Thermal conductivity

The thermal conductivity values of plywood, MOC paste and the wood-cement board are presented in Figure 8-7. Plywood showed excellent thermal insulation properties. The thermal conductivity of wood-cement board decreased with the increase of wood fibre content. Similar trends were observed for the boards prepared with the incorporation of PFA and ISSA. The reduction of thermal conductivity of C15, C20 and C25 was 13.5%, 26.5%, and 41.5%, respectively compared to C0. The thermal conductivity of wood-cement board decreased with the increase of wood fibre content due to two reasons. Firstly, it was related to the lower thermal conductivity of wood fibre (less than 0.2 W/(m•k)) compared to that of MOC paste (2.0 W/(m•k)) (Xu et al. 2016). Secondly, the increase of wood fibre content led to the decrease of density, thus the thermal conductivity decreased due to its opposite relationship with density(Al Rim et al. 1999). The use of fly ash and ISSA decreased the thermal conductivity of wood-MOC boards. And S25 had the lowest thermal conductivity (0.97W/(mk)). The effect

of PFA and ISSA on the thermal conductivity of wood-MOC boards may be due to the addition of PFA and ISSA induced more air voids during mixing when preparing the samples (Fu and Chung 1997, Demirboğa and Gül 2003)

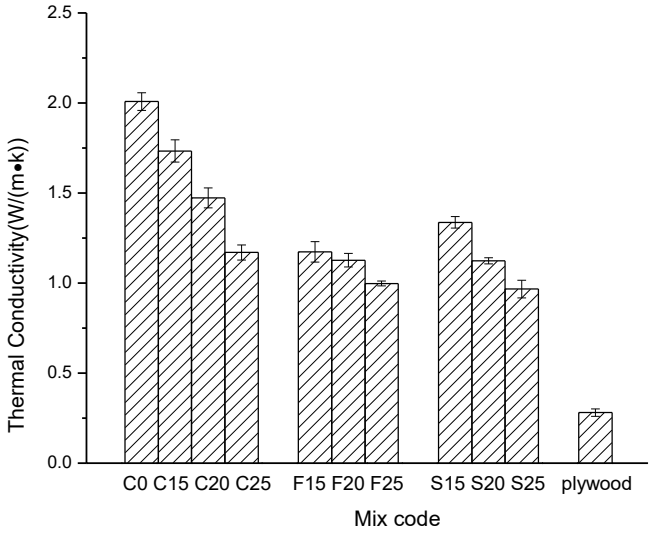

Figure 8-7 Thermal conductivity of plywood, MOC paste and wood-cement boar

8.3.7 Environmental impact assessment

A comparison of the GHGs emissions of the wood-MOC board production with their conventional counterparts (plywood and resin-based particleboards) are shown in Figure 8-8. The results show that GHGs emission of C0, S0 and S25 was 0.82 kg, 0.55 kg and 0.51 CO_2 eq/kg board, which was 54%, 69% and 71%, respectively, lower when compared to that of plywood production (1.78 CO_2 eq/kg plywood). However, the emission was 40%, 11% and 4% higher for C0, S0 and S25, respectively, when compared to the traditional particleboard production. For the conventional resin based particleboards, the use of wood chips, UF resin and wax contributed 72% of the total GHGs emission (and the rest was from the production process), and in which half (about 36%) of the emission was contributed by UF resin (Hossain and Poon 2018). For the MOC boards (C0, S0 and S25) production, higher GHGs emission was associated mainly for MgO production along with its long transport distance (contributed

over 80% of the total GHG emission). However, lower GHGs emission was associated with S25 board production due to the use of ISSA and wood chips (with lesser amount of MgO) compared to C0 and S0, and the value was also comparable to the resin-based particleboard. Furthermore, the GHG emission could be reduced when a shorter transport distance associated with the supply of MgO and $MgCl_2$ are available.

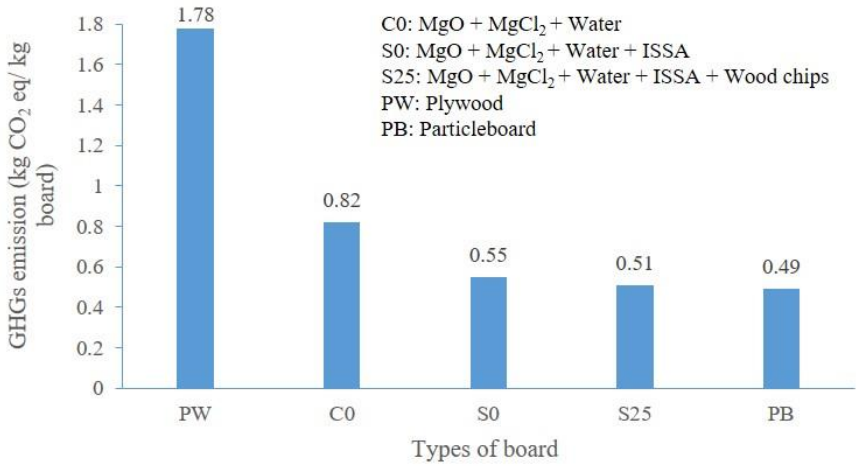

Figure 8-8 Comparative GHGs emissions of different types of board

But compared with the conventional resin-based particleboards, the new wood-MOC has the following advantages: higher flexural strength, lower water absorption, lower thickness swelling, and better elevated temperature resistance (as shown in Table 8-5). In addition, the human toxicity (assessed by LCA) associated with S25 board production was significantly lower compared to the conventional resin-based particleboard production (shown in Table 8-5), as the resin used in the conventional particleboard production leads to significantly higher toxic impacts to human (Kouchaki-Penchah et al. 2016). Based on the LCI data, the human toxicity of S25 was assessed using CML method, and compared with that of the particleboard production (Kouchaki-Penchah et al. 2016). For S25 board, the human toxicity value was 0.101 kg 1,4-DB eq / kg board which was 58% lower when compared to conventional particleboard

(0.239 1,4-DB eq / kg board) (Table 8-5).

Therefore, the MOC board produced with ISSA had the highest environmental benefits in terms of GHGs emission. In addition, about 36% waste materials (wood waste and ISSA) were used. Due to the reduction of substantial amounts of GHGs emission, human toxicity and saving of virgin resources, wood-MOC board can be considered as an eco-product and used as an alternate material to plywood or conventional resin-based particleboards.

Table 8-5 Comparison between conventional resin based and MOC based particleboards

Properties	Types of board	
	MOC (with ISSA) based	Resin based (Melo et al. 2014, Lee et al. 2017)
Flexural strength (MPa)	22	<15
Manufacturing technique	Casting molding	Compression molding
Residual flexural strength after heated to 300 ºC (MPa)	14	0
Water absorption (%)	4	>60
Thickness swelling (%)	0.2	>16
Human toxicity (kg 1,4-DB eq / kg board)	0.101	0.239

8.4 Summary

In this chapter, the properties of wood-MOC boards prepared with or without PFA/ISSA were evaluated and compared with traditional plywood and resin-based particleboards.

As the wood fibre content increased, the flexural strength of wood-MOC board increased. The wood-MOC board incorporating ISSA had the highest flexural strength among all the MOC mixes. The flexural strength of wood-MOC board was reduced and mass loss increased when exposed to high temperatures. ISSA blended board showed higher elevated temperature resistance than other composites up to 300 ºC. All the mixture lost most of the original flexural strength when the temperature was raised up to 400 ºC.

The increase of wood fibre contents and the addition of PFA/ISSA slightly increased the water absorption values. Nevertheless, the water absorption values of all the composites was considered to be low. Besides, the thickness swelling of all the wood-MOC boards could meet the requirement of the standard. The test results on impact sound noise reduction showed that all the composites showed better sound insulation at the frequencies of higher than 1600 Hz. The wood fibre could enhance the sound insulation of the MOC board. Increasing of wood fibre content and incorporating of PFA or ISSA increased the thermal insulation properties of the boards.

GHGs emission associated with wood-MOC board incorporating ISSA was 71% lower compared to plywood production, and comparable to the resin-based particleboard. Moreover, the human toxicity of the wood-MOC board was 58% lower compared to the conventional resin-based particleboard production due to the latter uses a large high amount of highly toxic UF resin.

Reference

Aggarwal, L., S. Agrawal, P. Thapliyal and S. Karade (2008). Cement-bonded composite boards with arhar stalks. Cement and Concrete Composites **30**(1): 44-51.

Al Rim, K., A. Ledhem, O. Douzane, R. Dheilly and M. Queneudec (1999). Influence of the proportion of wood on the thermal and mechanical performances of clay-cement-wood composites. Cement and Concrete Composites **21**(4): 269-276.

Babrauskas, V. (2002). Ignition of wood: a review of the state of the art. Journal of Fire Protection Engineering **12**(3): 163-189.

Bledzki, A., S. Reihmane and J. Gassan (1998). Thermoplastics reinforced with wood fillers: a literature review. Polymer Plastics Technology and Engineering **37**(4): 451-468.

Chindaprasirt, P., C. Jaturapitakkul and T. Sinsiri (2005). Effect of fly ash fineness on compressive strength and pore size of blended cement paste. Cement and Concrete Composites **27**(4): 425-428.

Chindaprasirt, P. and S. Rukzon (2008). Strength, porosity and corrosion resistance of ternary blend Portland cement, rice husk ash and fly ash mortar. Construction and Building Materials **22**(8): 1601-1606.

Demirboğa, R. and R. Gül (2003). The effects of expanded perlite aggregate, silica fume and fly ash on the thermal conductivity of lightweight concrete. Cement and Concrete Research **33**(5): 723-727.

Fu, X. and D. Chung (1997). Effects of silica fume, latex, methylcellulose, and carbon fibers on the thermal conductivity and specific heat of cement paste. Cement and Concrete Research **27**(12): 1799-1804.

Hossain, M. U. and C. S. Poon (2018). Comparative LCA of wood waste management strategies generated from building construction activities. Journal of Cleaner Production **177**: 387-397.

ISO (1987). Cement-bonded particleboards -- Boards of Portland or equivalent cement reinforced with fibrous wood particles.

Kouchaki-Penchah, H., M. Sharifi, H. Mousazadeh, H. Zarea-Hosseinabadi and A. Nabavi-Pelesaraei (2016). Gate to gate life cycle assessment of flat pressed particleboard production in Islamic Republic of Iran. Journal of Cleaner Production **112**: 343-350.

Lee, S. H., Z. Ashaari, F. R. Jamaludin, C. N. Yee and W. N. Ahamad (2017). Physico-mechanical properties of particleboard made from heat-treated rubberwood particles. European Journal of Wood and Wood Products **75**(4): 655-658.

Lin, D., K. Lin, W. Chang, H. Luo and M. Cai (2008). Improvements of nano-SiO2 on sludge/fly ash mortar. Waste Management **28**(6): 1081-1087.

Melo, R. R., D. M. Stangerlin, R. R. C. Santana and T. D. Pedrosa (2014). Physical and mechanical properties of particleboard manufactured from wood, bamboo and rice husk. Materials Research **17**(3): 682-686.

Montle, J. and K. Mayhan (1974). Magnesium oxychloride as a fire retardant material. Journal of Fire Flam/Fire Retard Chemistry **1**: 243-254.

Montle, J. and K. Mayhan (1974). The role of magnesium oxychloride as a fire-resistive material. Fire Technology **10**(3): 201-210.

Xu, B., H. Ma, C. Hu and Z. Li (2016). Influence of cenospheres on properties of magnesium oxychloride cement-based composites. Materials and Structures **49**(4): 1319-1326.

Chapter 9. Conclusions and Recommendation

9.1 Conclusions

This study has proposed a value-added approach to transform end-of-life formwork into high-performance, eco-friendly and low-cost cement-bonded composites. MOC was used as binder as it showed lower incompatibility with wood. Moreover, CO_2 curing and SCMs were used to improve the water resistance of MOC. The microstructure characteristics were analyzed to reveal the mechanisms of CO_2 curing and SCMs improving the water resistance of MOC. Furthermore, the properties of wood-MOC composites, such as flexure strength, water resistance, water absorption and thickness swelling, high temperature resistance, impact noise reduction property, thermal conductivity and lifecycle assessment, were evaluated to validate the potential application.

Based on the study, the following conclusions can be drawn:

- MOC paste showed poor water resistance as the strength retention coefficient of the control MOC paste was only 8.2%. When using CO_2 curing method, this value was increased up to 40.4%. The amorphous phase generated during CO_2 curing process interlocked with the hydration products and protected the hydration products from decomposition.
- Adding SCMs could significantly improve the water resistance of MOC. The strength retention coefficient of MOC paste incorporating 30% of PFA or ISSA was 72.2% and 84.6% respectively. The improvement of water resistance was due to the reaction between MOC and SCMs, which produced an amorphous gel that was stable in water

and interlocked with the hydration products, thus protecting the hydration products from decomposition. CO_2 curing could further improve the water resistance of MOC paste incorporating SCMs. Besides, SCMs could significantly improve the volume stability of MOC mortar in water.

- The GP-blended MOC paste had lower water resistance compared to PFA-blended cement due to the lower content of amorphous phase generated during air curing. The amorphous phase was stable in water and protected the Phase 3 and Phase 5 from decomposition. Therefore, the MOC containing higher content of amorphous phase had higher water resistance. Among the three types of SCMs, ISSA showed the highest positive effect on enhancing the water resistance due to the highest amount of amorphous phase formed due to the reaction of MOC and amorphous SiO_2 in ISSA. The product generated due to the reaction between SCMs and MOC interspersed with Phase 5 and changed the morphology of Phase 5 from a needle-like shape to a lath-like shape. M-A-S-H gel was observed using TEM method. These two phases interlocked with each other and formed a stable structure in water which improved the water resistance of MOC.
- Wood-MOC paste produced new chemical bondings such as carboxylate. A new phase (dashkovaite) was observed in the wood-MOC paste. Wood fibre enhanced the volume stability of MOC mortar as a certain amount of voids induced during fibre incorporation could reduce the expansion due to the hydration of excess MgO in MOC. The wood MOC cement paste incorporated longer fibre showed higher flexural strength and volume stability in air curing.
- Wood-MOC board incorporating higher content of wood fibre showed higher flexural strength, sound insulation property, thermal insulation property. Even though the water resistance of wood-MOC board increased with the increase of wood fiber content, the

water absorption values of all the composites was considered to be low. Besides, the thickness swelling of all the wood-MOC boards meet the requirement of the standard. GHGs emission of wood-MOC board incorporating ISSA was much lower than that of plywood production and comparable to the resin-based particleboard. The human toxicity of wood-MOC board was much lower than that of resin-based particleboard production.

9.2 Recommendations for further studies

For the ISSA-blended samples, CO_2 curing was not used to reduce cost as they showed excellent water resistance. However, CO_2 curing was applied for PFA/GP-blended MOC paste. The high CO_2 pressure and concentration would increase the cost of production and limit the application in the construction industry. The atmospheric pressure and low concentration of CO_2 could be investigated and adopted to improve the water resistance of MOC.

The reaction between CO_2 and MOC should be further investigated. The amorphous phase generated during CO_2 curing process could be investigated using TEM method. The CO_2 uptake degree could be assessed by measuring the mass of sample before and after CO_2 curing.

The reason for SCMs increasing the expansion of MOC during air curing process should be further studied. It may be related to both the solid volume change and crystal growth processes at non-bonding interfaces, which need further research.

No consistent trend was found regarding the effect of fibre length on the water resistance of wood-MOC paste. This may be related to the pore structure of wood-MOC composites, which needs further investigation.

Other properties of wood-MOC paste can be further investigated, such as setting time, compressive strength, elasticity modulus, etc.